



UNIVERSITY  
OF TRENTO - Italy

Department of Materials Engineering  
and Industrial Technologies

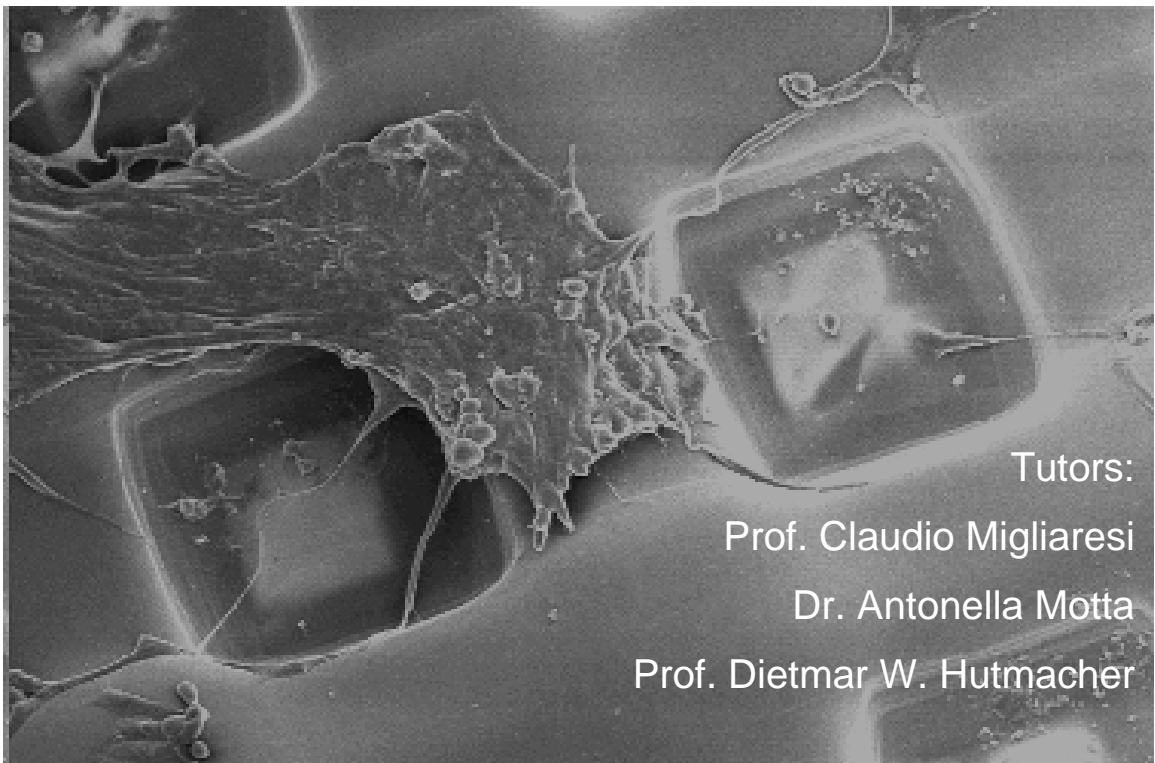
Doctorate School in Materials Engineering – XXI cycle

---

---

# 3D scaffolds for tissue engineering produced by microfabrication technology

Eleonora Carletti



Tutors:

Prof. Claudio Migliaresi

Dr. Antonella Motta

Prof. Dietmar W. Hutmacher

April 2009



---

# INDEX

<b>1</b>	<b>Aims of the thesis</b> .....	<b>11</b>
<b>2</b>	<b>Background</b> .....	<b>14</b>
2.1	Tissue engineering .....	14
2.2	Tissue engineering products .....	15
2.3	Scaffolds in tissue engineering .....	17
2.4	Polymers in tissue engineering .....	19
2.4.1	Natural polymers.....	19
2.4.2	Synthetic polymers.....	25
2.5	Degradation of Biodegradable Polymers.....	32
2.6	Process techniques.....	34
2.7	Solid Free Form fabrication techniques .....	37
2.7.1	Stereolithography (SLA).....	37
2.7.2	Selective laser sintering (SLS) .....	38
2.7.3	3D Printing (3DP).....	39
2.7.4	Shape deposition manufacturing (SDM) .....	39
2.7.5	Robotic microassembly .....	40
2.7.6	Microfabrication .....	40
2.7.7	Fused deposition modelling (FDM).....	41
2.8	Porous size and morphology for tissue regeneration .....	42
<b>3</b>	<b>Bibliography Chapter 2</b> .....	<b>48</b>
<b>4</b>	<b>Part 1: scaffold production by microfabrication</b> .....	<b>57</b>
4.1	Abstract.....	57
4.2	Introduction.....	58
4.3	Materials and Methods.....	61
4.3.1	Microfabrication System.....	61
4.3.2	Synthetic polymer materials: PDLA and PLGA.....	70
4.3.3	Natural polymer material: Chitosan .....	71
4.3.4	Gel Permeation Chromatography (GPC) .....	72
4.3.5	NMR.....	73
4.3.6	Rheological Tests .....	73
4.3.7	Attenuated Total Reflectance-Fourier Transform Infrared (ATR-FTIR).....	74

---

4.3.8	Differential Scanning Calorimetry (DSC).....	74
4.3.9	Thermo gravimetric analysis (TGA).....	75
4.3.10	Dynamical mechanical thermal analysis (DMTA).....	75
4.3.11	Preliminary in vitro culture studies.....	76
4.3.12	Atomic Force Microscopy (AFM) .....	76
4.3.13	Sample imaging .....	77
4.4	Results and Discussion: synthetic materials.....	78
4.4.1	Microfabricated scaffold.....	78
4.4.2	Rheological test on PDLA and PLGA solutions.....	81
4.4.3	Molecular weight distributions of PDLA and PLGA polymers.....	85
4.4.4	Differential scanning calorimetry (DSC) .....	89
4.4.5	Attenuated total reflection infrared spectroscopy (ATR- FTIR) 93	
4.4.6	Dynamic mechanical thermal analysis (DMTA) .....	94
4.4.7	Preliminary in vitro culture studies.....	98
4.5	Results and Discussion: microfabrication of chitosan scaffold 105	
4.5.1	Microfabrication of chitosan scaffold.....	105
4.5.2	Nuclear magnetic resonance (NMR).....	109
4.5.3	Rheological test on Chitosan solution.....	111
4.5.4	Differential scanning calorimetry (DSC) .....	114
4.5.5	Attenuated total reflection infrared spectroscopy (ATR- FTIR) 117	
4.5.6	Dynamic mechanical thermal analysis (DMTA) .....	118
4.5.7	Preliminary in vitro culture studies.....	121
4.6	Results and Discussion: microfabrication of chitosan ACP scaffolds.....	124
4.6.1	Microfabricated scaffold.....	126
4.6.2	Rheological tests .....	126
4.6.3	Thermogravimetric analysis (TGA).....	128
4.6.4	Preliminary in vitro culture studies.....	130
4.6.5	Energy dispersive spectroscopy (EDS) .....	131
4.6.6	Atomic Force Microscopy .....	135
<b>5</b>	<b>PART 2: fused deposition modelling scaffold for human osteoblasts cell cultures.....</b>	<b>139</b>
5.1	Abstract.....	139

---



---

5.2	Introduction.....	140
5.3	Materials and Method .....	142
5.3.1	FDM scaffolds .....	142
5.3.2	Cell culture .....	142
5.3.3	Proliferation assays .....	143
5.3.4	Scanning electron microscopy (SEM) .....	144
5.3.5	Cell staining and confocal laser microscopy imaging ..	145
5.4	Results and Discussion .....	146
5.4.1	Optical imaging.....	146
5.4.2	Confocal laser imaging: Phalloidin rhodamine and Dapi staining	148
5.4.3	Confocal laser imaging: fluorescein diacetate–propidium iodide (FDA–PI) .....	153
5.4.4	Scanning Electron Microscopy (SEM) .....	156
5.4.5	Proliferation Assay – PicoGreen™ .....	160
<b>6</b>	<b>Conclusions .....</b>	<b>161</b>
<b>7</b>	<b>Bibliography Chapter 4 and 5 .....</b>	<b>163</b>
<b>8</b>	<b>Acknowledgements.....</b>	<b>170</b>

---

## LIST OF FIGURES

Figure 2.1. Deacetylation of chitin by NaOH and chitosan formation.....	22
Figure 2.2. Chemical formula of PLA (A), PGA (B) and copolymer PLGA (C) .....	26
Figure 2.3. Chemical formula of PDS .....	29
Figure 2.4. Chemical formula of PCL.....	30
Figure 2.5. Chemical formula of polyurethane .....	31
Figure 2.6. Chemical formula of poly(ortho ester).....	31
Figure 2.7. Chemical formula of poly(anhydrides).....	32
Figure 2.8. Poly Amide 6 electrospun meshes <sup>51</sup> .....	36
Figure 2.9. Silk fibroin and PEG sponge (8 % fibroin, 10%w_PEG/w_fibroin) produced by salt leaching using NaCl (500 – 1180 nm granulometry) <sup>52</sup> ....	36
Figure 2.10. PCL scaffold obtain by solvent casting/phase inversion in ethanol/water solution <sup>53</sup> .....	36
Figure 2.11. Microfabrication system working principle.....	41
Figure 2.12. Scaffolds of mPCL:TCP (80:20) with a lay-down pattern 0/60/120° (adapted from D.W. Hutmacher et al.).....	42
Figure 2.13. FDM scheme <sup>68</sup> .....	42
Figure 2.14. Microfabricated chitosan scaffold seeded by human osteoblasts after 16 days of cells culture. A) SEM imaging B) confocal laser microscopy imaging after Phalloidin-Rhodamine/Dapi staining .....	45
Figure 2.15. FDM (mPCL:TCP, 80:20) scaffold seeded by human osteoblasts after 16 days of cells culture A) SEM imaging B) confocal laser microscopy imaging after Phalloidin-Rhodamine/Dapi staining (chapter 5.4.2).....	46
Figure 2.16. Electrospun mesh (2-5% PLLA-PDLLA in HFIF) seeded with prostate cancer cells (PC3K3s5, PSA overexpressed) after 21 days of cells	

---

culture A) SEM imaging B) confocal laser microscopy imaging after Phalloidin-Rhodamine/Dapi staining (D. W. Hutmacher et al., unpublished results) .....	46
Figure 2.17. FDM scaffold (mPCL:TCP, 80:20) seeded with prostate cancer cells (PC3K3s5, PSA overexpressed) after 21 days of cells culture. Confocal laser microscopy imaging after Phalloidin-Rhodamine/Dapi staining (D.W.Hutmacher et al., unpublished results) .....	47
Figure 4.1: Microfabrication system .....	61
Figure 4.2. Schematic representation of microfabrication system .....	62
Figure 4.3. Working principle of microfabrication system .....	62
Figure 4.4. A) microfabrication system platform; B) 90° needle point style .....	63
Figure 4.5. The micro-needle and scaffold microfabrication .....	64
Figure 4.6. LabVIEW front panels: A) and B) planar movements, C) vertical movement .....	66
Figure 4.7. LabVIEW block diagram of the vertical movement.....	66
Figure 4.8. LabVIEW block diagram of planar movements .....	68
Figure 4.9. Microfabricated chitosan scaffold .....	70
Figure 4.10. Optical (up) and scanning electron (down) microscopy images of a PDLA (left) and PLGA (right) scaffold .....	78
Figure 4.11. Optical images of a microfabricated scaffold with defects. A and B, PDLA; C and D, PLGA .....	79
Figure 4.12. PDLA microfabricated scaffold .....	80
Figure 4.13. Rheological test results for A) Viscosity of 20% PDLA solution in DCM:DMF (70:30) solvent, B) Viscosity of 20% PDLA solution in DCM:DMF (70:30) solvent obtained by three successive measurements ..	82

---

Figure 4.14. Rheological test results for A) Viscosity of 25% PLGA solution in DCM:DMF (70:30) solvent, B) Viscosity of 25% PLGA solution in DCM:DMF (70:30) solvent obtained by three successive measurements ..	83
Figure 4.15. Molecular weight distribution of PDLA based materials: base powder, cast film and microfabricated scaffold .....	86
Figure 4.16. Molecular weight distribution of PLGA based materials: base powder, cast film and microfabricated scaffold .....	87
Figure 4.17. Thermographs related to PDLA grains (A) and PDLA microfabricated scaffold (B).....	90
Figure 4.18. Thermographs of PLGA grains (A) and PLGA microfabricated scaffold (B) .....	91
Figure 4.19. ATR spectra of PDLA a) powder, b) film, c) microfabricated scaffold, d) DMF .....	93
Figure 4.20. ATR spectra of PLGA a) powder, b) film, c) microfabricated scaffold, d) DMF .....	94
Figure 4.21. Plots of storage modulus and loss factor for PDLA microfabricated scaffold (A) and cast film (B) as a function of temperature .....	96
Figure 4.22. Plots of storage modulus and loss factor for PLGA microfabricated scaffold (A) and cast film (B) as a function of temperature .....	97
Figure 4.23. SEM images of PDLA scaffold after 7 days (A and B) and 14 days (C and D) of osteoblast MG63 cell culture; the marker indicates 100 $\mu\text{m}$ .....	99
Figure 4.24. SEM images of PDLA scaffold after 7 days (A and B) and 14 days (C and D) of fibroblasts MRC5 cell culture; the marker indicates 100 $\mu\text{m}$ .....	100

---

---

Figure 4.25. SEM images of inner layers of PDLA microfabricated scaffold after osteoblasts MG63 cell seeding (7 days); (A) PDLA microfabricated scaffold before seeding, chapter 4.4.1, (B, C) different magnifications; markers indicate 30 $\mu\text{m}$ (B) and 100 $\mu\text{m}$ (C) .....	101
Figure 4.26. SEM images of inner layers of PDLA microfabricated scaffold after MRC5 cell seeding (7 days) ; (A) PDLA microfabricated scaffold before seeding, chapter 4.4.1, (B, C) different magnifications markers indicate 10 $\mu\text{m}$ (B), 30 $\mu\text{m}$ (C) and 100 $\mu\text{m}$ (D).....	102
Figure 4.27. SEM images of PLGA scaffold after 7 days (A and B, different magnifications) and 14 days (C and D, different magnifications) of osteoblasts (MG63) cell culture; in all the micrographs markers indicate 100 $\mu\text{m}$ .....	103
Figure 4.28. SEM images of PLGA scaffold after 7 days (A and B) and 14 days (C and D) of fibroblasts MRC5 cell culture; in all the micrographs markers indicate 100 $\mu\text{m}$ .....	104
Figure 4.29. Optical microscopy imaging of 80 layer chitosan scaffold ...	105
Figure 4.30. LV-SEM imaging of 90 layer chitosan scaffold at different magnifications.....	107
Figure 4.31. LV-SEM imaging of 20 layer chitosan scaffold at different magnifications after Na OH treatment.....	108
Figure 4.32. SEM imaging of chitosan scaffold without NaOH treatment after preliminary in vitro culture studies with osteoblast MG63 cell line after 7 days .....	109
Figure 4.33. $^{13}\text{C}$ CP-MAS NMR spectra of chitosan.....	110
Figure 4.34. Complex viscosity plotted over frequency. (A) average viscosity (B) solvent evaporation evaluation .....	113

---

---

Figure 4.35. Thermographs of Chitosan powder first run (B) and second run (A). Chitosan film first run (D) and second run (C). Chitosan microfabricated scaffold first run (F) and second run (E).....	116
Figure 4.36. ATR spectra of chitosan a) powder, b) film and c) microfabricated scaffold .....	118
Figure 4.37. DMTA thermographs of chitosan scaffold (A) and cast film (B) .....	120
Figure 4.38. SEM imaging of chitosan microfabricated scaffold after 4 days (A, C, E) and 10 days (B, D, F) cell seeding with MG63 cell line. A, B, C, D, E, F different magnifications .....	122
Figure 4.39. SEM imaging of chitosan microfabricated scaffold after 4 days (A, C, E) and 10 days (B, D, F) cell seeding with fibroblasts MRC5 cell line. A, B, C, D, E, F different magnifications .....	123
Figure 4.40. SEM images of Chitosan filled with ACP microfabricated scaffold .....	126
Figure 4.41. Comparison between viscosity of pure Chitosan solution and Chitosan filled with ACP particles solution .....	128
Figure 4.42. TGA thermograph related to pure chitosan, chitosan filled with ACP and pure ACP particles .....	129
Figure 4.43. SEM images of Chitosan filled with ACP microfabricated scaffolds after 4 days cell seeding with MG63.....	130
Figure 4.44. SEM images of Chitosan filled with ACP microfabricated scaffolds after 10 days cell seeding with MG63.....	131
Figure 4.45. E-SEM imaging of chitosan filled with ACP particles before NaOH washing treatment .....	132
Figure 4.46. EDS spectra and semi-quantitative analysis of chitosan/ACP scaffold surface non-washed by NaOH.....	133

---

---

Figure 4.47. E-SEM imaging of chitosan filled with ACP particles after NaOH washing treatment.....	133
Figure 4.48. EDS spectra and semi-quantitative analysis of chitosan/ACP scaffold surface washed by NaOH .....	134
Figure 4.49. EDS overlapped spectra of chitosan/ACP scaffold washed and non washed .....	135
Figure 4.50. AFM imaging of chitosan/ACP scaffold surface .....	136
Figure 4.51. AFM imaging of chitosan/ACP scaffold surface. Prewitt vertical filter applied.....	137
Figure 4.52. Three dimensional view of a 10 x 10 $\mu\text{m}$ square area analysed by AFM of a chitosan/ACP scaffold surface washed with NaOH .....	137
Figure 4.53. Topography of chitosan/ACP scaffold surface. The line indicates the selected area for the profile analysis .....	138
Figure 4.54. Surface height profile .....	138
Figure 5.1. Osteoblast cell sheet detaching from the 6 well-plate .....	143
Figure 5.2. Optical microscope images of mPCL:TCP scaffolds. The arrow indicates the bridging mechanism that cells use to grow in the corner of pores.....	146
Figure 5.3. Optical microscope images of PDLLA:TCP scaffolds. The arrow indicates the bridging mechanism that cells use to grow in the corner of pores.....	147
Figure 5.8. mPCL:TCP (80:20) scaffold cell seeded with human osteoblasts. fluorescein diacetate–propidium iodide (FDA–PI). The small images are the transmitted micrographs .....	154
Figure 5.9. PDLLA:TCP (90:10) scaffold cell seeded with human osteoblasts. fluorescein diacetate–propidium iodide (FDA–PI). The small images are the transmitted micrographs.....	155

---

---

Figure 5.10. SEM imaging of mPCL:TCP (80:20) scaffold cell seeded with human osteoblasts at different time points. The arrow indicates cells bridging mechanism at the matrix corners .....	157
Figure 5.11. SEM imaging of PDLLA:TCP (90:10) scaffold cell seeded with human osteoblasts at different time points.....	159
Figure 5.12. DNA amount profile as a function of culturing time.....	160



## 1 Aims of the thesis

This research work has been carried out in a tissue engineering context where the microfabrication system, developed and optimized in our laboratories and able to fabricate scaffolding supports of controlled geometry represents the core.

Our microfabrication technique makes use of polymeric solutions that are extruded over a platform moving on motorized slides along three mutually independent orthogonal directions and following a specific and predetermined trajectory chosen by the operator. LabVIEW software controls and moves the slides, thus allowing the deposition of the extruded polymer solution filament forming the desired geometry scaffold.

The system is innovative among all the tissue engineering solid free form (SFF) fabrication techniques already developed and studied, because it can fabricate reproducible three dimensional (3D) scaffolds with a well defined geometry and porosity at micro-scale level. This has been achieved by using 3 slides having a resolution up to 1  $\mu\text{m}$  and an extrusion syringe needle with inner diameter of 60  $\mu\text{m}$ .

Main processing parameters are polymer viscosity, slide velocity, and solution flow rate, and these, together with the environment conditions, greatly affect the fabrication process.

Using both synthetic and natural polymers microfabrication of different scaffold materials was performed.

Materials were characterized before and after scaffold fabrication to assess if any modification occurred; general processing parameters were defined according to the material utilized.

Furthermore, preliminary *in vitro* cell culture studies were performed on the microfabricated scaffolds and the relationship between cell types and the microstructure was then considered. In particular, cells attachment, proliferation, and migration inside the microporous matrix were evaluated.

The study was mainly conducted at the Department of Materials Engineering, University of Trento (Italy). Part of this activity was made in collaboration with Tugba Endogan, a PhD student from the METU - BIOMAT, Department of Polymer Science and Technology, Ankara (Turkey), who spent six months in our lab.

In addition to the above activity, during a six months stage with the Prof. Dietmar W. Hutmacher at the Queensland University of Technology, Brisbane (Australia), a different microfabrication technique was studied. Scaffolds made by Fused Deposition Modeling (FDM), were cell cultured over different time points with human osteoblasts. Cells attachment, growing and proliferation were measured by imaging analysis techniques and specific proliferation assays, respectively. Cell culture was performed by adding to the culture medium supplements; calcium phosphate synthesis and the formation of detachable osteoblast sheets were induced.

In general, the work aimed at investigating how the two techniques, able to produce tissue engineering scaffolds with ordered structure, could assist the cellular growth and tissue regeneration.

This thesis has been structured with an introduction where the state of the art of tissue engineering has been reviewed. In particular the relationship

## Aims of the thesis

---

between different scaffold structures and morphologies and tissue types has been considered.

After the introduction part, the core section is divided as:

- PART 1: Scaffold production by microfabrication
  - Microfabrication of synthetic polymers (PDLA, PLGA)
  - Microfabrication of natural polymer (Chitosan)
  - Microfabrication of chitosan filled with ACP particles
- PART 2: Fused deposition modelling scaffold for human osteoblasts cell culture

## 2 Background

### *2.1 Tissue engineering*

Tissue engineering refers to a field of therapeutic or diagnostic products and processes which are based upon the combination of living cells, engineering biomaterials and suitable biochemical factors, to restore, improve or maintain biological functions.

Tissue engineering can be defined as an interdisciplinary field combining bioengineering, life science and clinical sciences<sup>1</sup>.

MacArthur and Oreffo considered tissue engineering as "understanding the principles of tissue growth, and applying this to produce functional replacement tissue for clinical use"<sup>2</sup>. Further descriptions focus on the principle that the employment of natural biology of the system will allow for greater success in developing therapeutic strategies aimed at the replacement, repair, maintenance, and/or enhancement of tissue function.

In other words tissue engineering applies principles and methods of engineering and the life sciences to make clear the relationship between structure and function in normal and pathological mammalian tissues to finally develop biological substitutes to restore, maintain or improve function<sup>3</sup>.

Actually tissue engineering covers a broader range of applications and it is closely connected with other fields, i.e. cell transplantation that is transplantation of cells that perform a specific biochemical function (e.g., an artificial pancreas, or an artificial liver).

The term regenerative medicine is often used synonymously with tissue engineering, although those involved in regenerative medicine place more emphasis on the use of stem cells to produce tissues<sup>4</sup>.

Generally, tissue engineering revolves around the use of living cell and/or extracellular matrix (ECM) components in the development of implantable parts or devices and in particular one of the main target of tissue engineering concerns cell seeding on porous biodegradable 3-dimensional scaffolds, following by implantation of the scaffold into the injured area to provide regeneration.

### ***2.2 Tissue engineering products***

Based on the concept that each tissue is characterized by different functions and features the tissue-engineering products design strongly depends on material properties and on cellular response to the chosen biomaterials. In addition, the ability to shape into the suitable cellular level architecture has to be taken into account and the final architecture must be compatible with the desired tissue response.

The proper biomaterial selection is assisted by the development of methods and sophisticated modelling techniques that permit prediction of polymer properties and cellular response to the material. Such techniques allow a wide use of biodegradable polymers for tissue engineering applications. Tissue engineering products can be designed to conduct, induct or block tissues responses and architectures. Depending on the final purpose barriers (membranes or tubes), gels or matrices can be developed<sup>5</sup>.

Membranes are required where cell activity is needed on one surface of a device precluding transverse movement of surrounding cells onto that surface. For instance peripheral nerve regeneration needs an axonal growth

## Background

---

and at the same time preventing fibroblast activity that would produce neural-inhibiting connective tissue<sup>6</sup>. Furthermore, collagen membranes used in periodontal repairing provide the right environment for periodontal ligament regrowth and attachment but at the same time they avoid the epithelial ingrowth into the healing site<sup>7</sup>. Prevention of post-surgical adhesion obtained by using hyaluronic acid compounds is another example of barrier biomaterials.

Hydrogel biomaterials can encapsulate and represent a specialized environment for isolated cells. Collagen gels, for instance, can be used for the preservation and immunoprotection of xenograft and homograft cells, such as hepatocytes, chondrocytes, and islets of Langerhans, used for transplantation. Semipermeable gels can be a support for cells in systems where cell-cell communication and interaction with surrounding tissue has to be minimized as well as the movement of peptide factors and nutrients through the implant. Gels are particularly suitable in applications such as bone and cartilage tissue regeneration where the material has to be injectable and polymerization in situ is needed<sup>8</sup>.

Tissue engineering scaffolds or matrices are an important component for tissue development and their characteristics such as pore size and the structure, ordered and regular or randomly distributed, are fundamental in forming tissues with a proper cell morphology, orientation, arrangement of intercellular material, and the relationship between different cell types.

Besides several techniques have been developed to form well defined scaffolds using different kind of biomaterials and physical characteristics of the matrices can be varied to maximize cellular and tissue responses<sup>5,9,10</sup>.

### ***2.3 Scaffolds in tissue engineering***

The development of 3D scaffolds, support structures or matrices that induce cells to form functional tissues, is one of the main object of tissue engineering.

In particular by using scaffolds, transplanted cells can be delivered to a specific place in a tissue driving the growth of cells inside a desired anatomic site. Thus scaffolds represent the space available for the tissue to develop and a physical support for cells growth.

Three dimensionally (3D) porous matrices provide mechanical and adhesive support for seeded cells in culture and tissue in-growth allowing vascularisation and shape maintenance during the tissues regeneration.

Mechanical support against compressive or tensile forces present inside the physiological environmental system of the human body should be granted depending on the tissue the scaffold is designed for.

Enough mechanical strength and stiffness is needed to initially contrast wound contraction forces and later to guarantee a perfect reconstruction of the tissue. For this reason scaffold degradation profile must be designed so that it can support the tissue formation until neotissue (cells and extracellular matrix without vascularisation) is developed<sup>11</sup>.

Injecting cell suspension without scaffold has been sometime utilized as a technique<sup>12-14</sup> even if it presents the disadvantage that it is quite complicated to control the placement of transplanted cells and most of the mammalian cells reveal an anchorage-dependent behaviour and they difficult survive without a proper adhesion support.

Therefore the primary function of a scaffold is tissue conduction and thus it must allow cells attachment, migration onto or within the scaffold, cells

## Background

---

proliferation and differentiation. The morphology of the scaffold should be designed to be able to guide the formation of the new tissue in terms of pore size, shape and vascularisation.

Scaffold geometry should also define the space and the outer shape of the defect or lack to finally be properly adapted, also matching the healthy tissue stiffness and strength while maintaining an interconnected pore network for cell migration and nutrient transportation. It must also provide an environment in which cells can maintain their phenotype and synthesize proteins and molecules.

Compatibly to the structure of the tissue scaffolds should be designed to have high porosity, high surface area, fully interconnected geometry, structural strength and a specific three dimensional shape. Besides, scaffold materials should be biocompatible and biodegradable or resorbable so as to allow replacement by newly formed tissue in long term.

A porous structure is usually needed for two critical functions. First, pore channels provide ports of entry for migrating cells or for capillary suction of blood. Secondly, a large area is available for specific and numerous cell interactions.

In particular microporosity is fundamental for capillary ingrowth and cell-matrix interactions while macroporosity for nutrients supply and waste removal of cells grown on the scaffold.

It is important to underline that the ideal scaffold design does not exist but each tissue requires a specific matrix design with defined material properties.

Finally scaffolds should be manufactured in a reproducible, controlled and cost effective fashion with the possibility to include biological component, such as cells and grow factors.



The regeneration steps of a tissue are presented schematically as follow:

- Fabrication of a porous 3D scaffold of a well defined geometry and porosity
- Cell culture of porous scaffold; growth factors can be included
- Cell growing, proliferation and differentiation and tissue formation while scaffold is degrading
- Culturing and then implanting the scaffold into the defect part

It must be considered however, that for regulatory reasons and intrinsic difficulties associated with the above procedure, pre-seeded scaffolds use could be limited to specific applications and restricted to a few authorized institutions. This could favour the implant of tissue engineering scaffolds directly in the body without preseeded cells.

### ***2.4 Polymers in tissue engineering***

Various materials have been utilized to produce scaffolds for several applications. The most important one are natural and synthetic polymers. Ceramic materials are also used, particularly in combination with polymers especially in bone tissue applications, thus forming composite materials with improved mechanical and biological properties.

#### **2.4.1 Natural polymers**

Naturally-derived polymer materials<sup>15,16</sup>, such as collagen, fibrin, glycosaminoglycans (GAGs), chitosan, alginates and starch, can be extracted from plants, animals or human tissues; they exhibit good

biocompatibility, low toxicity and a low chronic inflammatory response but they can undergo to batch-to-batch variations, they show a short range of properties and difficult processing.

They can be combined into a composite with other natural materials or synthetic materials and can be degraded by naturally occurring enzymes. Disadvantages include poor mechanical properties and they often require chemical modification to increase strength such as cross-linking by dehydrative methods or chemical methods (glutaraldehyde).

### *2.4.1.1 Collagen*

An example of a commonly used natural material is collagen. Collagen is a major protein of the extracellular matrix, which is a component of connective tissues and can provide mechanical support; therefore it is a fibrous protein with a long, stiff, triple-stranded helical structure. There are three main collagen types: type I (in skin and bone), type II (cartilage), type III (blood vessels walls).

It is possible to built porous collagen scaffolds by freezing a dilute suspension and then inducing sublimation of the ice crystals by exposure to a low temperature vacuum.

Clinical applications of collagen scaffolds are highly relevant to otorhinolaryngological practice. These include the manufacture of sutures, haemostatic agents (powder, sponge, fleece), blood vessels (extruded collagen tubes) tendons and ligaments, dermal regeneration for burn treatment and peripheral nerve regeneration (porous collagen-GAG copolymer)<sup>7,15,17-20</sup>.

### 2.4.1.2 Chitosan

Chitosan is the N-deacetylated derivative of chitin, a natural polysaccharide commonly located in the exoskeleton of crustaceans and insects<sup>21,22</sup>.

It is a linear polysaccharide composed of  $\beta$  (1-4) linked D-glucosamine with randomly dispersed N-acetyl-D-glucosamine groups.

Chitosan can undergo degradation by enzymes such as chitosanase and lysozyme.

There is a big concern around this natural polymer in the tissue engineering field because it is a well-tolerant implant material, non-antigenic, biodegradable and it has good structural properties. Chitosan biodegradation rate depends on the amount of residual acetyl content, that is the deacetylation degree<sup>23</sup>. Molecular weight and deacetylation degree affect physical and mechanical properties of the polymer<sup>24,25</sup>.

Chitosan is insoluble above pH 7 and soluble below pH 5; it can be gelled into strong fibers when pH is high enough. Hydrogels can also be produced by either ionic bonding or covalent cross-linking, using cross-linking agents such as glutaraldehyde.

Chitosan can be formed into membranes and matrices for tissue engineering applications. Biological evaluations by culturing hepatocyte cells on chitosan scaffolds show how cells maintain their morphology once seeded; metabolic activities, such as albumin secretion and urea synthesis, are present as well.

Chitosan material has also been used to produce scaffolds for bone tissue regeneration and to support chondrocyte attachment and growth.

---

## Background

---

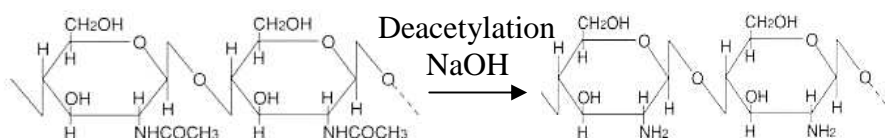


Figure 2.1. Deacetylation of chitin by NaOH and chitosan formation

### 2.4.1.3 Glycosaminoglycan

Glycosaminoglycan (GAGs) are glycoproteins widely present inside the ECM of the body; many studies have proved the success of combining GAG and collagen to form a nanofibrous scaffolds<sup>19,26</sup>.

GAGs are long chain not branched consisting of disaccharide units containing carboxylic and/or sulfate ester groups, that are functional groups able to bridge and link collagens to finally construct interpenetrating networks of extracellular matrix (ECM).

Hyaluronic acid is a fundamental compound of connective tissues in mammals and represents the most common GAG; it is an anionic polysaccharide with repeating disaccharide units of N-acetylglucosamine and glucuronic acid, with unbranched units ranging from 500 to several thousands.

It has a extremely high water-binding capacity and dilute solutions of hyluronic acid show high viscosity values.

Hyaluronan is naturally found in many tissues of the body, i.e. skin, cartilage and the vitreous humor and it is particularly used in biomedical applications according to these tissues. It has been used during eye surgery since 1976 and later to treat osteoarthritis of the knee<sup>27</sup>. In addition, in the form of gels and films it can be utilized to prevent postsurgical adhesion<sup>28</sup>.

Recent studies show how hyaluronic acid can be used as scaffold material to support chondrocyte growth<sup>29</sup>; similar applications for bone tissue regeneration have also been considered<sup>30</sup>.

Hyaluronic acid derives from natural sources, such as rooster combs, or from microbial fermentation and it is quite easy to isolate and modify.

#### *2.4.1.4 Silk Fibroin*

Silks are fibrous proteins having interesting properties produced in fiber form by silkworms and spiders. Sutures produced by silk fibers material have been widely used for centuries. Recently starting from regenerated silk solutions a variety of biomaterials, such as gels, sponges and films have been produced for medical applications.

In particular silks from silkworms (e.g., *Bombyx mori*) have been explored to evidence possible usages as biomaterials according to different applications<sup>31,32</sup>; furthermore several processing mechanisms have been developed.

In general silk fibroin materials exhibit a good biocompatibility able to support the growth of human cells.

#### *2.4.1.5 Agarose*

Agarose is a polysaccharide polymer extracted from algae and it is widely used in various fields of biomedical research, particularly in tissue culture systems because it permits cells to grow inside a three-dimensional suspension. Its molecular structure is composed by an alternating copolymer linkage of 1,4-linked, 3-6 anhydro- $\alpha$ -galactose and 1,3-linked- $\beta$ -D-galactose and due to its high amount of hydroxyl groups it results very soluble in

water. A double helix structure is formed by interaction of two agarose chains by hydrogen bonds. Agarose material undergoes to enzymatic degradation by agarases and properties of agarose gels, especially strength and permeability, depend on concentration of agarose.

Agarose gels are particularly important in the application of tissue engineering concepts as regard to cartilage repair because it supports the cartilage phenotype as well as nerve regeneration<sup>33</sup>.

### *2.4.1.6 Alginate*

Alginate is a naturally derived polysaccharide that is abundant in cell walls of brown algae. As for agarose it shows a very high solubility in water. It is a polyanion composed of two repeating monomer units:  $\beta$ -D-mannuronate (M) and  $\alpha$ -L-guluronate (G). Physical and mechanical properties of alginate are highly related to the guluronate block, in terms of chain length and proportions, that is present inside the polymer.

Alginate has an electrolytic nature and it has the exclusive property of being able to form a gel in the presence of certain divalent cations (e.g., calcium, strontium, or barium); for the same reason alginate gels can be solubilized when cations are removed.

Alginate has been used for tissue engineering scaffolding and different cell types have shown to keep their morphology once in contact with the material.

Alginate sponges have been used for fibroblasts cell culture<sup>34</sup> and cell adhesion was found to be non dependent on scaffold porosity; besides while chondrocytes could proliferate and express type II collagen once embedded in alginate matrix. Hepatocytes were also seeded on alginate porous

scaffolds where albumin was found to be secreted, a good index of cell functionality<sup>35</sup>.

## 2.4.2 Synthetic polymers

Biodegradable polymers which are chemically synthesized are widely used as scaffold materials in tissue engineering because they typically offer an high versatility, stable properties and good workability<sup>36</sup>.

Therefore tailing synthetic polymers is easier compared to natural polymers and a wider range of shape and properties can be obtained; furthermore the final result is more predictable and the scaffolds are more uniform<sup>5</sup>.

Degradation rate of scaffolds can be adapted to the specific applications by selecting specific polymers, copolymers or blends. Most of these polymers undergo to a simple hydrolytic degradation.

However, biocompatibility of synthetic polymers is generally lower than natural polymers. For acidic degradation products, high local concentrations of these products can affect cell growth on the scaffolds *in vitro* and cause inflammatory responses *in vivo*.

Among these bioresorbable polymers, the most used as scaffolds are poly(glycolic acid) (PGA), poly(lactic acid) (PLA) or their copolymers or blends as well as the aliphatic polyester polycaprolactone (PCL).

### 2.4.2.1 Poly(glycolic acid), poly(lactic acid) and copolymers

Poly ( $\alpha$ -hydroxyacids) are bioabsorbable synthetic polymers widely known, studied and successfully employed as tissue engineering scaffolds for cell transplantation and tissue regeneration. The homopolymers poly(glycolic

---

## Background

---

acid) (PGA) and poly (lactic acid) (PLA) and their copolymers (PLGA), are all poly ( $\alpha$ -hydroxyacids)<sup>1,5,37-40</sup>.

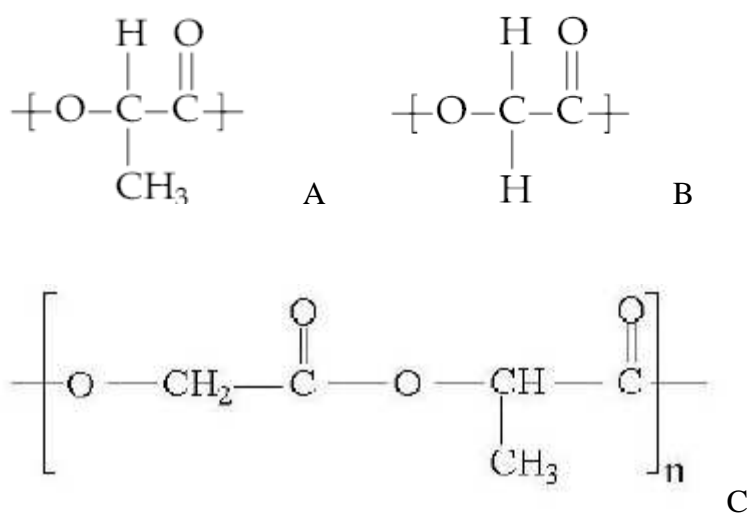


Figure 2.2. Chemical formula of PLA (A), PGA (B) and copolymer PLGA (C)

These linear aliphatic polyesters degrade by hydrolysis and the degradation rate of these polymers depends on configuration structure, initial molecular weight, exposed surface area, crystallinity, stresses, amount of residual monomer, site of implantation and, in the case of copolymers, the ratio of the hydroxy acid monomers.

The poly ( $\alpha$ -hydroxyacids) polymers have a modest range of mechanical properties but and being thermoplastics polymers they can easily be shaped into films, tubes and matrices using standard processing techniques as molding, extrusion, solvent casting and spin casting. Ordered fibers, meshes, and open-cell foams have been formed to fulfill the surface area and cellular requirements of a variety of tissue-engineering constructs.



## Background

---

PGA has the simplest chemical structure, thus it has an high degree of cristallinity, high melting point and low solubility in organic solvents. It has been widely used as surgical suture materials and since it has a very high affinity with water, mechanical strength of the sutures decreases rapidly within 4 weeks inside a biological environment.

As shown above (Figure 2.2 A and B), PLA, presents in its chemical structure an extra methyl group, thus resulting more hydrophobic than PGA. Since degradation is controlled by the degree of access that water molecules have to ester linkages in the polymer chains, PLA degrades at a much slower rate compared to PGA.

PLA is also more soluble in organic solvents than PGA.

Due to the chiral nature of lactic acid, two stereoisomeric forms are possible and distinct polymers can be obtained: the two stereoregular polymer D-PLA, L-PLA, and the D,L-PLA. Poly-L-lactide (PLLA) is the product resulting from the ring-opening polymerization of L-lactide; it presents a cristallinity of about 37% with glass transition temperature between 50°C and 80°C and fusion temperature between 180°C and 190°C. Poly-D-lactide (PDLA) is analogous to PLLA but it is derived from polymerization of D-lactide; it exists just at an experimental level without practical applications. Poly-D,L-lactide (PDLLA) is the racemic polymer obtained from a mixture of D- and L-lactic acids; it has an amorphous structure presenting a glass transition temperature at about 60°C.

The degree of cristallinity strongly affects the water uptake and the degradation kinetic; consequently, amorphous regions offer a better accessibility and mobility to water molecules and, degradation occurs at higher rate. The less crystalline racemic mixture D,L-PLA degrades at higher rate than L-PLA. Differences in cristallinity also influence the area of

applicability field of the polymers and for example amorphous polymers are usually more suitable for drug delivery applications where it is easier to homogeneously distribute the active species inside the supporting matrix while semicrystalline materials have better mechanical properties and they are chosen in applications where a structural support is needed.

Especially in bone tissue regeneration the combination of PLA, PGA and their copolymers together with ceramic materials such as Bioglass particles or hydroxyapatite has been considered. These fillers can induce bone regeneration and at the same time improve the mechanical properties of the material. Bioglass particles also have been shown an angiogenic character.

Biocompatibility plays an important role in the long and short term success of all implants; for biodegradable devices it is fundamental that both the implant and its degradation products are biocompatible and non-toxic. These issues have been widely studied for PLA, PGA and copolymers and several publications reported in-vitro and in-vivo studies of biocompatibility. Some complications have occasionally been reported following implantation of PLA-PGA biomaterials and some of these problems may be attributable to the release of acidic degradation products after material degradation. Nevertheless the majority of clinical studies citing complications in human due to PLA and PGA implants report only soft reactions and suggest non-specific foreign body reaction as the cause<sup>41</sup>.

### *2.4.2.2 Polydioxanone (PDS)*

Polydioxanone derives from a ring-opening polymerization of p-dioxanone. The products of its degradation are particularly non toxic in-vivo and it possesses a better flexibility if compared to PGA and PLA. PDS

degradation rate is comparable to that of PGA and is in general faster than PLA.

Often used combined with others polymers thus forming copolymers, PDS is used to produce suture filaments.

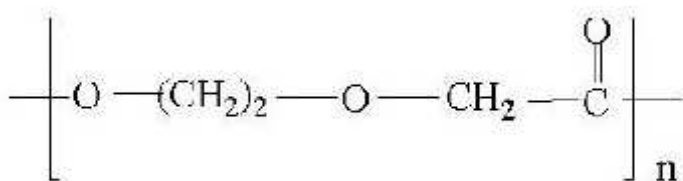


Figure 2.3. Chemical formula of PDS

#### 2.4.2.3 Poly( $\epsilon$ -caprolactone)

Poly( $\epsilon$ -caprolactone) is a biodegradable aliphatic polyester with important applications in the field of human therapy, due to its biocompatibility and bioresorbability. PCL has a low melting point at about 60°C, a glass transition temperature at -60°C, thus in a rubbery state at room temperature, and in general a quite high thermal stability (decomposition temperature occurs at 350°C). It is obtain by a ring-opening polymerization of  $\epsilon$ -caprolactone using a catalyst such as stannous octanoate.

PCL can be degraded by hydrolytic mechanism and therefore under physiological conditions<sup>42,43</sup>. Enzymatic degradation is also possible under certain conditions. In general degradation rate of PCL is slower than PGA and PLA thus resulting more suitable for long term implantable devices.

PCL can be combined with other biomaterials to form blends and  $\epsilon$ -caprolactone can be copolymerized together with other different monomers.

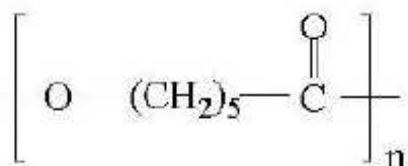


Figure 2.4. Chemical formula of PCL

#### 2.4.2.4 Polyurethanes

Polyurethane is a term that comprehend a wide family of thermosetting polymers in which the polymer chain contains urethanes bonds. Polyurethanes are produced by the reaction between a diisocyanate and a polyol; a segmented block copolymer is then obtained and low-glass transition temperature segments are combined with hard segments.

Polyurethanes possess excellent physical properties and good biocompatibility that make them a good choice for different biomedical applications.

Polyurethanes were first introduced to the medical device market in the earliest '50s for foam breast prosthesis and cardiovascular devices. Since then, a lot of work and development was done to improve their properties and biostability.

In general polyurethanes are used as biomaterials for different applications such as pacemaker, lead insulator, catheters, total artificial heart and heart valves.

To overcome the degradation of polyurethanes, several research groups have adopted strategies like varying the material chemistry that is altering the type and ratio of monomers; incorporation of additives is also possible. In particular biodegradable polyurethanes are made from diisocyanates such

---

## Background

---

as lysine-diisocyanate or hexamethylene diisocyanate that release non toxic degradation products instead of the conventional aromatic diisocyanates.

Biodegradable polyurethanes have been developed for tissue engineering applications such as for myocardial repair and vascular tissues<sup>44,45</sup>.

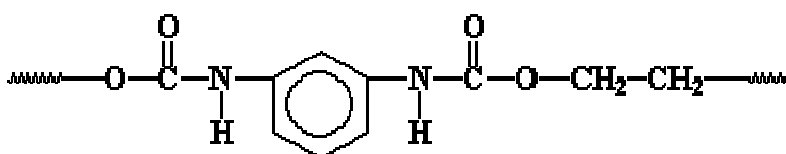


Figure 2.5. Chemical formula of polyurethane

### 2.4.2.5 Poly(ortho Ester)

Poly(ortho Ester) are biodegradable synthetic polymers that have the peculiarity to degrade by surface erosion, a mechanism by which the material is becoming thinner and thinner rather than breaking into pieces<sup>46</sup>. This property is quite interesting for drug-delivery applications where the release results in general more controlled.

Degradation of poly(ortho ester) is via hydrolysis and degradation rate increases with time because the acidic products work as catalysts for the degradation reaction.

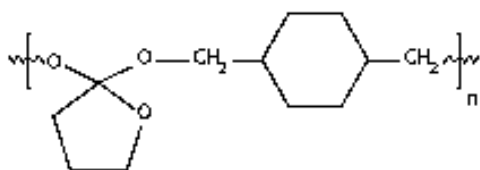


Figure 2.6. Chemical formula of poly(ortho ester)

### 2.4.2.6 Poly(anhydrides)

Poly(anhydrides) present a excellent *in-vivo* biocompatibility and they are widely used in drug-delivery applications<sup>47</sup>; in particular different types of drugs and proteins including insulin, bovine growth factors, angiogenesis inhibitors, enzymes and anesthetics have been incorporated inside poly(anhydrides) matrices. In particular delivery of chemotherapeutic agents has been highly investigated.

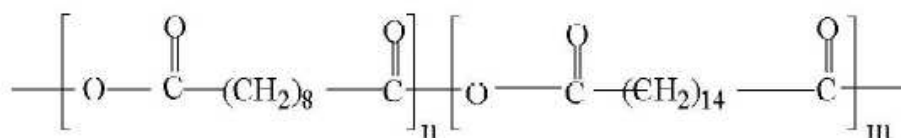


Figure 2.7. Chemical formula of poly(anhydrides)

## 2.5 Degradation of Biodegradable Polymers

Applications of biodegradable polymers in medicine comprise resorbable surgical sutures, matrices for the controlled release of drugs, tissue engineering scaffolds, resorbable orthopaedic devices such as pins, screws and plates.

The applicability of biomaterials refers to a broad field of interest and several possible applications can be possible.

For this reason the development and the choice of biomaterials requires an extensive evaluation, in terms of biocompatibility, mechanical properties and degradation behavior in order to determine whether a certain material is suitable for a particular application.

In particular, degradation behavior of biomaterials can follow several mechanisms and being controlled by different factors. Understanding the

## Background

---

degradation kinetics of biomaterials is necessary to optimize their possible usage.

Most biomedical applications require the usage of biomaterials with specific controlled and predictable degradations kinetics; this had led to research on the degradation behavior of a variety of biodegradable polymers.

The term biodegradation refers to a degradation occurring in a biological environment and maybe defined as the “gradual breakdown of a material mediated by a specific biological activity”<sup>48</sup>.

Since biodegradable polymers have a temporary function, degradation should occur as a controlled mechanism; degradation kinetics, evolution of mechanical properties and evaluation of degradation products has to be taken into account.

Particularly in drug delivery applications, the polymer is required to degrade following a well defined mass loss profile in order to release the encapsulated drugs at specific times.

The degradation of a polymer can occur at different stages depending on its preparation, processing and storage.

In fact during polymer processing and fabrication some degradation can occur affecting also the degradation behavior *in vivo*. If processing techniques involve high temperature or high shear stresses inside the material, this may cause degradation of the starting polymer; on the contrary, some chain orientation caused by some process could alter the degradation time of the polymer, being the material generally more resistant. Sterilization method may also have an effect on the material degradation causing crosslinking or polymer chain breakage depending on sterilization system and the polymer properties.

Regarding the degradation mechanisms occurring to materials when exposed to the body fluids the most important ones are oxidation and hydrolysis.

A biomaterial can degrade by chemical and enzymatic oxidation once in contact with the physiological environment<sup>48-50</sup>. During inflammatory response to foreign materials, inflammatory cells produce highly reactive oxygen species, such as superoxide ( $O_2^-$ ), hydrogen peroxide ( $H_2O_2$ ), nitric oxide (NO) and hypochlorous acid (HOCl), which can cause polymer chain scission leading to degradation.

On the other hand hydrolytic degradation is the scission of chemical bonds in the polymer backbone by the attack of water to form oligomers and monomers. Water attack is directed to water-labile bonds by either direct access to the polymer surface or by imbibitions into the polymer matrix followed by bond hydrolysis.

The hydrophilic or hydrophobic nature of polymeric materials influences their degradation rate, which is the chemical structure of the polymer: covalent bonds in the backbone and no hydrolysable groups require longer times to degrade.

Enzymes known as hydrolases, such as proteases, esterases, glycosidases and phosphatases, may catalyze hydrolysis reactions.

### ***2.6 Process techniques***

Traditional scaffold fabrication techniques have involved the production of porous polymeric matrices as substrate for cell support, adhesion, growth and subsequently proliferation and differentiation on or within their structure.



## Background

---

A big variety of matrices has been developed due to the large range of tissues to reproduce and the need to create cellular supports with different physical appearance, porosity, permeability, mechanical characteristics. The final purpose is to reproduce a micro- and a macro-environment that mimic the natural ECM features. Together with the development of advanced materials and process engineering 3D matrix formation and fabrication techniques have evolved considerably.

A wide variety of techniques commonly used in tissue engineering generate scaffolds with non-ordered structure with unpredictable pore sizes and reduced pore interconnections. Any variation in porosity within the 3D structure cannot be controlled, and mechanical strength, structural stability and reproducibility are generally low. Among these techniques solvent casting, freeze drying, phase inversion, fiber bonding, melt based technologies, high pressure based methods are the most used. Recently also electrospinning technique has widely investigated to produce meshes of nanometric fibres for different tissue engineering applications (Figure 2.8). To overcome the limits of these methods, more efficient technology to generate complex scaffold structures of desired features and solid free-form fabrication (SFF) or rapid prototyping (RP) techniques have been developed. These computer controlled techniques can generate biodegradable polymer scaffolds with designed architecture and shape complexity<sup>9</sup>.

## Background

---

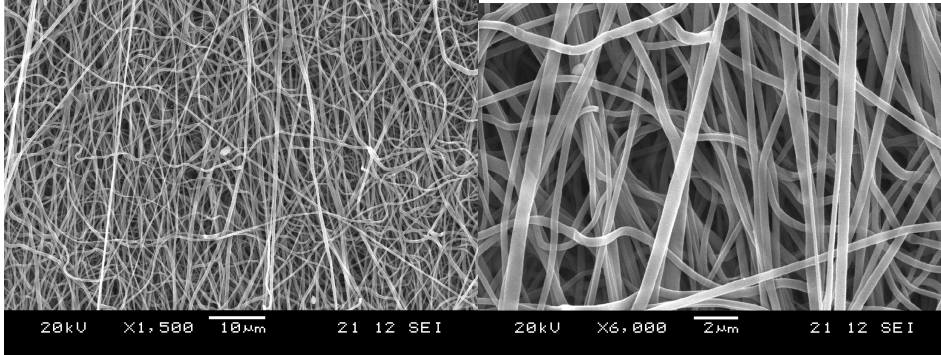


Figure 2.8. Poly Amide 6 electrospun meshes<sup>51</sup>

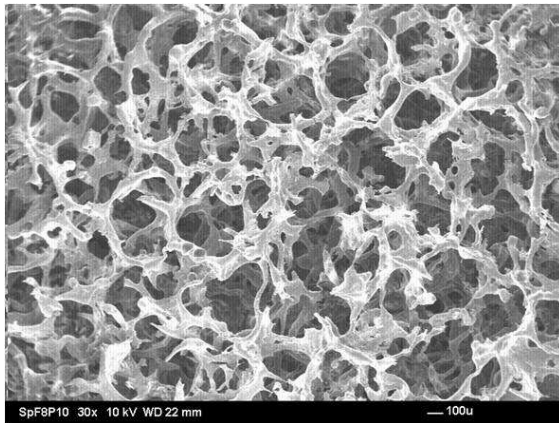


Figure 2.9. Silk fibroin and PEG sponge (8 % fibroin, 10% w\_PEG/w\_fibroin) produced by salt leaching using NaCl (500 – 1180 nm granulometry)<sup>52</sup>

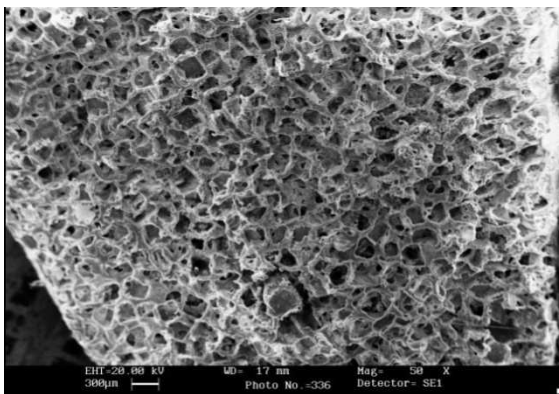


Figure 2.10. PCL scaffold obtain by solvent casting/phase inversion in ethanol/water solution<sup>53</sup>

Unlike the more traditional techniques, which involve constant removal of materials, SFF fabricates scaffolds by selectively adding materials, layer by layer, as specified by a computer software.

High resolution and reproducibility of the scaffold is gained by SFF techniques. Fused deposition modelling (FDM), three dimensional printing (3-DP), selective laser sintering (SLS) and stereolithography (SLA) are some example of rapid prototyping technique.

Novel robotic assembly and automated 3D cell encapsulation techniques have been also improved to have the possibility to add cells during the scaffold fabrication<sup>54,55</sup>.

As a result of these technologies, tissue-engineering constructs can be contain a controlled spatial distribution of cells, bioactive molecules and structural matrices. The combination of these components create a scaffold that promote repair and regeneration of the damaged and diseased tissue.

## ***2.7 Solid Free Form fabrication techniques***

### **2.7.1 Stereolithography (SLA)**

Maybe the precursor among all the RP techniques, SLA system makes use of a UV laser beam to polymerize selectively a photopolymerisable liquid polymer material. The polymer solidifies from the bath once in contact with the beam, at, and just below the surface of the bath. The solidification process takes place repeatedly layer over layer. Once the model is concluded the extra-resin is washed away and the product is cured in a UV oven and finished by smoothing the surface irregularities.

Nowadays SLA is used mainly to produce anatomical models for surgical planning and teaching.

The process, due to curing and shrinkage after post-processing, has a low resolution and, especially in small and intricate objects, deformation phenomena can occur<sup>56,57</sup>.

Furthermore only a small amount of biocompatible polymers can photopolymerise so being suitable to become a tissue engineering scaffold. Polyethylene glycol (PEG) acrylate, PEG methacrylate, polyvinyl alcohol (PVA), hyaluronic acid and dextran methacrylate are the most common.

Micrometric stereolithography can fabricate scaffolds with micrometric resolution.

### **2.7.2 Selective laser sintering (SLS)**

This technique applies the use of a CO<sub>2</sub> laser beam able to sinter thin layers of powdered polymeric materials. The beam can increase the local temperature of the polymer and particles can fuse to each other. The laser scans over the powder following the cross-sectional profiles taking by the slice data and subsequent layers are formed over the previous one introducing extra powder as the preceding layer is completed.

Simple and linear bulk components can be easily fabricated by SLS technique while sheet-like structures undergo to shrinkage.

Ultra high molecular weight polyethylene (UHMWPE) has been used to produce implants by SLS technique and it has been notice that degradation (breakage of molecular chains), oxidation and cross linking occurs during sintering if the starting polymer molecular weight is not high enough<sup>58</sup>.

Furthermore, calcium phosphate (CaP) material was used in combination with SLS technique to produce bone implants<sup>59</sup>.

### **2.7.3 3D Printing (3DP)**

During 3DP process a first layer of polymeric powder is spread over a deposition base while a inkjet print head deposits the binder solution over it; following, a new layer of powder is spread again on the previous one and the printing cycle continues; layers merge together when fresh binder is added. At the end of the process the not bonded extra powder is removed<sup>60,61</sup>.

The technique has been widely investigated in respect of tissue engineering applications and drug-delivery systems and the major advantage related to 3DP is the possibility to work inside an ambient environment.

Removing the extra powder from complicated shaped model is difficult so the technique is suitable for easier geometry without internal holes.

The printer resolution depends on nozzle size and on the degree of control allowed over the position controller that regulates the print head movement.

The layer thickness is determined by powder size and in general surface roughness and aggregation properties of the powdered materials affect the final resolution.

Natural biopolymers have been used in combination with water as a binder eliminating the problem to use organic solvents<sup>62</sup>. Further post processing step to waterproof the product is obviously necessary.

### **2.7.4 Shape deposition manufacturing (SDM)**

SDM technique makes use of clinical imaging data to control the fabrication of layered scaffolds by a computer-numerically-controlled cutting machine<sup>63</sup>. Addition of cells and growth factors during the three dimensional scaffold production is provided as well.

The technique was initially thought for bone tissue regeneration and represents one of the most interesting techniques among all the assembly technology-based systems. Osteogenic scaffolds produced by SDM based on blends of polycaprolactone (PCL) and poly-D,L-lactide-co-glycolide (PGLA) together with HA grains have been reported <sup>64</sup>. During the manufacturing process, the scaffolds were incrementally built up from thin, prefabricated cross-sectional layers of foams made by solvent-casting and salt-leaching process.

### **2.7.5 Robotic microassembly**

The robotic microassembly technique has been studied and developed at the National University of Singapore <sup>65</sup>. The principle which regulates the robotic microassembly technique is that the final scaffold structure is composed by small building block units having a different design and previously fabricated via lithography or other microfabrication techniques. The blocks are then assembled by using a specific precision robotic system having microgripping capabilities. Finally a scaffold having the desired material, chemical and physical properties is obtained.

### **2.7.6 Microfabrication**

The technique aims to produce scaffolds for tissue engineering applications having a micrometric resolution.

Starting from polymer solutions, the extrusion over a platform moving in the three main directions is operated by a micro-syringe.

Well ordered scaffolds can be produced following process parameters set through a computer platform and different biomaterials can be used.

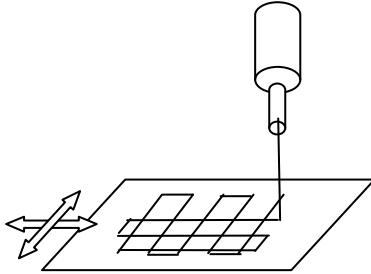


Figure 2.11. Microfabrication system working principle

### 2.7.7 Fused deposition modelling (FDM)

FDM is a heat-based manufacturing technology that has been applied toward the building of 3D scaffolds<sup>66,67</sup>.

The system includes a head-heated liquefier fixed to a carriage moving along the horizontal plane; the head can extrude the material pumping a filament of it through a nozzle directly on a platform following a previously programmed trajectory.

Such scaffolds are built up layer over layer in the vertical direction and the layer thickness depends on the nozzle inner diameter.

The technique is limited to thermoplastic polymers with proper viscous properties and cells cannot be included during the process.

Hutmacher and coworkers have used FDM to fabricate bioresorbable scaffolds of PCL also in combination with HA and TCP particles thus forming composite materials for bone tissue applications.

A variation of FDM is the so-called precision extruding deposition (PED) system which doesn't need the previous filament preparation but the material can be directly extruded.

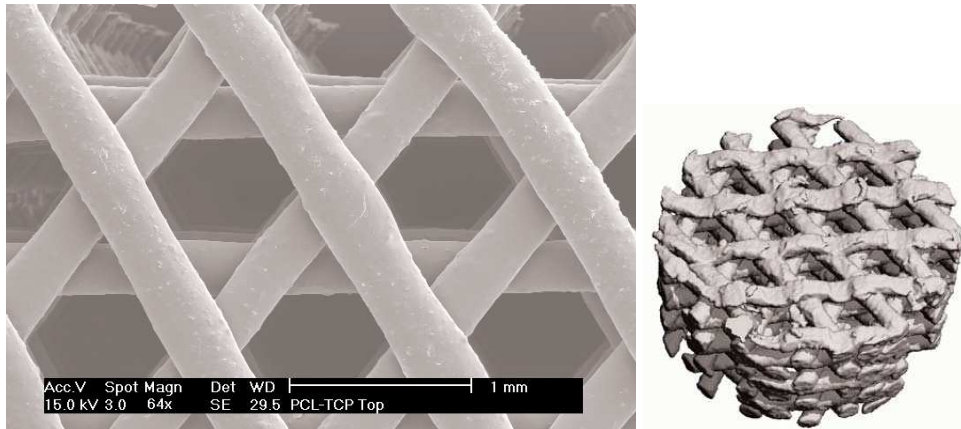


Figure 2.12. Scaffolds of mPCL:TCP (80:20) with a lay-down pattern 0/60/120° (adapted from D.W. Hutmacher et al.)

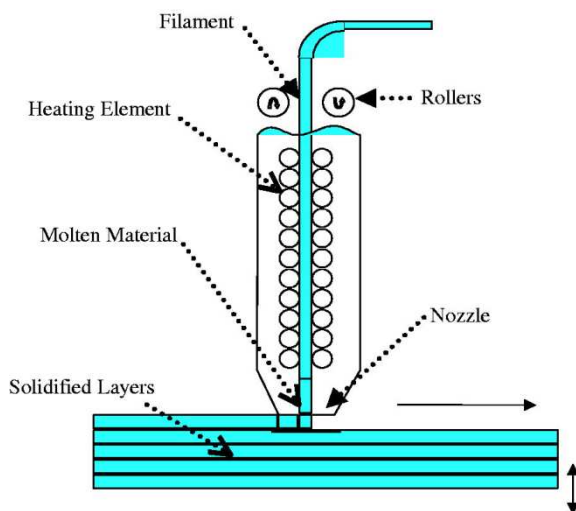


Figure 2.13. FDM scheme<sup>68</sup>

## **2.8 Porous size and morphology for tissue regeneration**

Three dimensional porous polymer scaffolds possess a high specific surface area for cell anchorage and a big volume fraction for cells growth,



migration, and effective fluid phase transport of nutrients. In addition to the size of the pores, the morphology can significantly resolve the performance of an implanted matrix, including the rate of tissue ingrowth.

Biological activity of a scaffold is theoretically affected by ligands density, i.e. scaffolds site at which specific cell binding occurs.

Scaffold composition and porous fraction, that is the total surface of the structure exposed to cells, determine the ligand density.

Several research works have demonstrated that pores need to be large enough to favour cellular migration into the structure, where they eventually bound to ligands expressed on the scaffold surface; furthermore, good vascular induction and easy diffusion of waste products is favoured; but conversely, pores should be small enough to reach a sufficiently high specific surface for a maximal ligand density in order to have an efficient binding of a critical number of cells.

The optimum porosity is strictly connected to the tissue type and diverse nature tissue architectures can be associated to a different microenvironment to reproduce. Cell dimension, together with cell activity behaviour, phenotypic expression and ECM production has also to be taken into account when designing a scaffold for tissue regeneration.

In bone tissue regeneration, for instance, the minimum pore size required is considered to be about 100  $\mu\text{m}$  due to cell size, migration conditions and transport. However, pore sizes bigger than 300  $\mu\text{m}$  are recommended, to improve new bone formation and to develop a net of capillaries<sup>69</sup>.

The investigation over two model cell types, fibroblast and endothelial cells, in respect of a range of defined pore features from 5 to 90  $\mu\text{m}$  in scaffolds fabricated by photolithographic technique, demonstrates how fibroblasts, using a bridging mechanism, can spread over neighbour cells being able to

## Background

---

fill even large pores while endothelial cells cannot use this bridging system and they prefer pore size close to their dimensions <sup>70</sup>.

In PLLA scaffolds, vascular smooth muscle specifically bind to one range of pore sizes (63 – 150  $\mu\text{m}$ ) while fibroblast, for their ability to form bridge connections, to a wider range (38 - 150  $\mu\text{m}$ ) <sup>70,71</sup>.

MC3T3-E1 mouse clonal osteogenic cells cultures on four different scaffolds, with variable specific surface areas, confirm a linear relationship between cell attachment and specific surface area. Over the range of pore sizes studied (95.9 – 150.5  $\mu\text{m}$ ) short-term cell viability was determined by the specific surface area available for binding <sup>18</sup>.

The rate of degradation is also strictly connected to the degree of porosity. For instance in polyester scaffold materials, a high porosity can reduce the accumulation of acidic degradation products thus reducing any possible reaction.

Moreover, scaffold heterogeneity has been shown to produce variability in cell adhesion and uniform distribution of extracellular matrix proteins is not easily obtained <sup>71</sup>. Tissues produced from a non-uniform pore architecture also show inferior biomechanical properties if compared with tissues derived from scaffold having a uniform pore structures <sup>72</sup>. Generally cells tend to follow the scaffold geometry: if pores are equiaxed, they distribute forming a spherical structure while in the case of elongated pores they also align along the pore main axis<sup>73</sup>.

Figure 2.14, Figure 2.15, Figure 2.16 and Figure 2.17 show some examples of different scaffolding structures cultured *in vitro* with different cell types.

In particular, Figure 2.14 shows human osteoblast cell culture on microfabricated chitosan scaffolds after 16 days of cell seeding. The

## Background

---

micrometric pore structure revealed to be suitable in term of size for osteoblasts growing: cells were able to easily migrate inside the structure and pores were quickly filled. The same cell culture was performed on FDM scaffolds (mPCL:TCP, 80:20) (Figure 2.15); after 16 days of cell culture cells started to form bridge connections at the corners of the structure.

Figure 2.16 and Figure 2.17 show prostate cancer cell culture (PC3K3s5, Kallikrein3 overexpressed modified serine amino acid; derived from bone metastatic site) after 21 days on 2-5% PLLA-PDLLA in HFIF electrospun mesh and mPCL:TCP (80:20) FDM scaffold, respectively.

Prostate cancer cells show a round shaped morphology. The electrospun mesh works as a barrier for cells while FDM scaffolds pores are definitely big compare to cells dimensions.

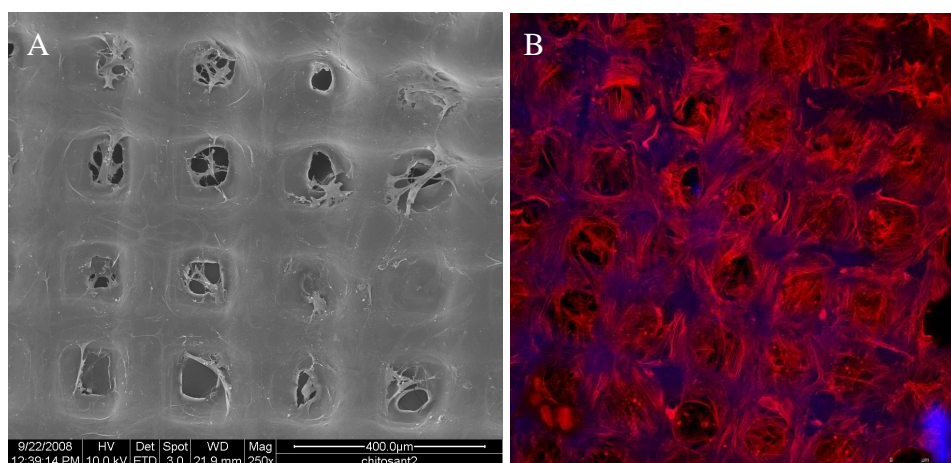


Figure 2.14. Microfabricated chitosan scaffold seeded by human osteoblasts after 16 days of cells culture. A) SEM imaging B) confocal laser microscopy imaging after Phalloidin-Rhodamine/Dapi staining

## Background

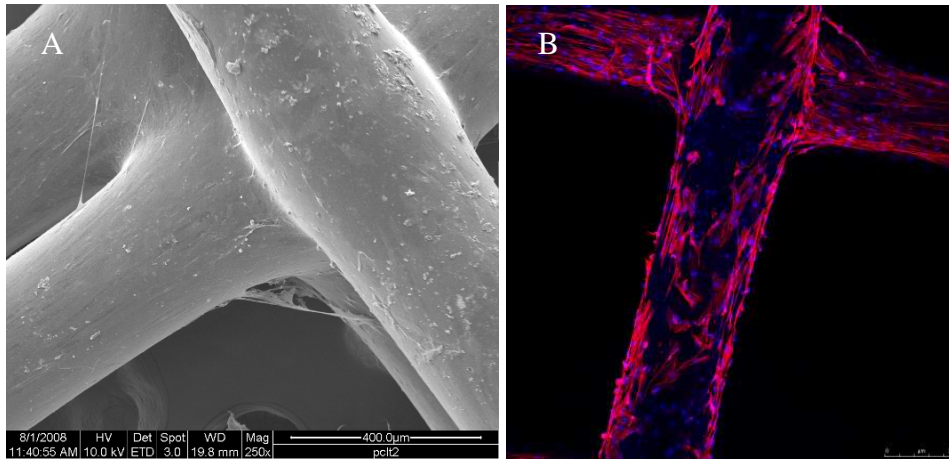


Figure 2.15. FDM (mPCL:TCP, 80:20) scaffold seeded by human osteoblasts after 16 days of cells culture A) SEM imaging B) confocal laser microscopy imaging after Phalloidin-Rhodamine/Dapi staining (chapter 5.4.2)

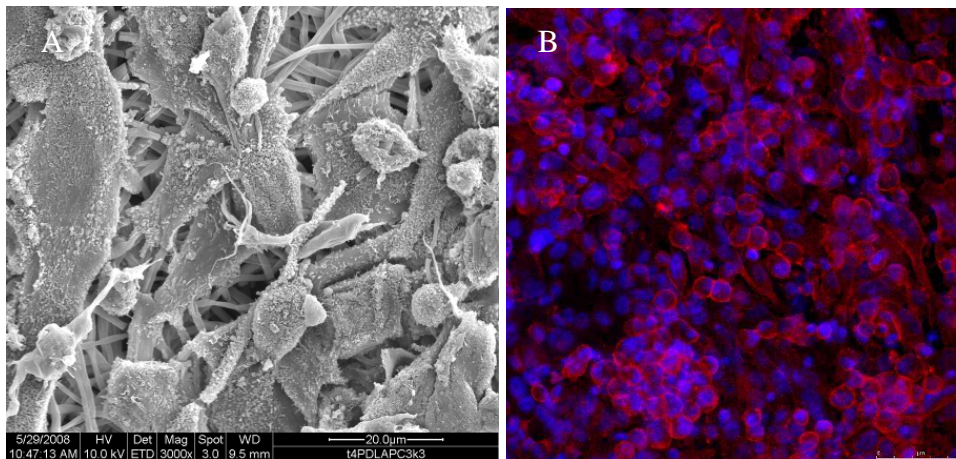


Figure 2.16. Electrospun mesh (2-5% PLLA-PDLLA in HFIF) seeded with prostate cancer cells (PC3K3s5, PSA overexpressed) after 21 days of cells culture A) SEM imaging B) confocal laser microscopy imaging after Phalloidin-Rhodamine/Dapi staining (D. W. Hutmacher et al., unpublished results)

## Background

---

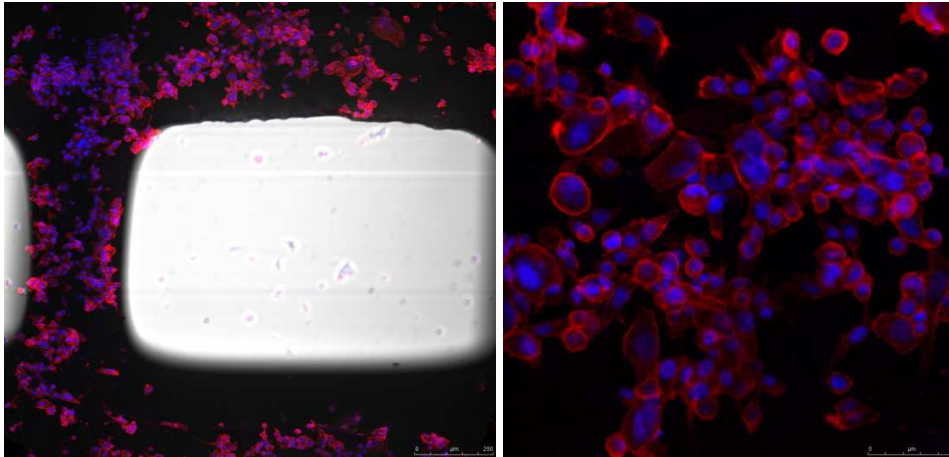


Figure 2.17. FDM scaffold (mPCL:TCP, 80:20) seeded with prostate cancer cells (PC3K3s5, PSA overexpressed) after 21 days of cells culture. Confocal laser microscopy imaging after Phalloidin-Rhodamine/Dapi staining (D.W.Hutmacher et al., unpublished results)

### 3 Bibliography Chapter 2

1. Langer, R. & Vacanti, J. P. *Tissue Engineering* (Science, 1993).
2. MacArthur, B. D. & Oreffo, R. O. C. Bridging the gap. *Nature* **433**, 19 (2005).
3. Nerem, R. M. & Sambanis, A. Tissue Engineering: From Biology to Biological Substitutes. *Tissue Engineering* **1**, 3-13 (1995).
4. Ringe, J., Kaps, C., Burmester, G. & Sittinger, M. Stem cells for regenerative medicine: advances in the engineering of tissues and organs. *Naturwissenschaften* **89**, 338-351 (2002).
5. Vacanti, J. P. & Langer, R. *Synthetic Biodegradable Polymer Scaffolds* (ed. Anthony Atala, D. J. M.) (1997).
6. Fawcett, J. W. & Keynes, R. J. Peripheral Nerve Regeneration. *Annual Review of Neuroscience* **13**, 43-60 (1990).
7. Pitaru, S., Tal, H., Soldinger, M., Grosskopf, A. & Noff, M. Partial regeneration of periodontal tissues using collagen barriers. Initial observations in the canine. *Periodontol* **59**, 380-386 (1988).
8. Drury, J. L. & Mooney, D. J. Hydrogels for tissue engineering: scaffold design variables and applications. *Biomaterials Synthesis of Biomimetic Polymers* **24**, 4337-4351 (2003).
9. Hutmacher, D. W., Sittinger, M. & Risbud, M. V. Scaffold-based tissue engineering: rationale for computer-aided design and solid free-form fabrication systems. *Trends in Biotechnology* **22**, 354-362 (2004).

---

Bibliography Chapter 2

---

10. Vats, A., Tolley, N. S., Polak, J. M. & Gough, J. E. Scaffolds and biomaterials for tissue engineering: a review of clinical applications. *Clinical Otolaryngology & Allied Sciences* **28**, 165-172 (2002).
11. Hutmacher, D. W. Scaffolds in tissue engineering bone and cartilage. *Biomaterials* **21**, 2529-2543 (2000).
12. Britberg, M. Articular Cartilage Repair in the Knee Joint with Autologous Chondrocytes and Periosteal Graft. *Orthopedics and Traumatology* **9**, 185-194 (2001).
13. Matas, A. J. et al. Hepatocellular transplantation for metabolic deficiencies: Decrease of plasma bilirubin in Gunn rats. *Science* **192**, 892-894 (1976).
14. Ponder, K. P. et al. Mouse hepatocytes migrate to liver parenchyma and function indefinitely after intrasplenic transplantation. *Proc Natl Acad Sci USA* **88**, 1217-1221 (1991).
15. Lee, C. H., Singla, A. & Lee, Y. Biomedical applications of collagen. *Int J Pharm* **221**, 1-22 (2001).
16. Bensaid, W., Triffitt, J. T. & Blanchat, C. A biodegradable fibrin scaffold for mesenchymal stem cell transplantation. *Biomaterials* **24**, 2497-502 (2003).
17. Negri, S., Fila, C., Farinato, S., Bellomi, A. & Pagliaro, P. P. Tissue engineering: chondrocyte culture on type 1 collagen support. Cytohistological and immunohistochemical study. *Journal of Tissue Engineering and Regenerative Medicine* **1**, 158-159 (2007).
18. O'Brien, F. J., Harley, B. A., Yannas, I. V. & Gibson, L. J. The effect of pore size on cell adhesion in collagen-GAG scaffolds. *Biomaterials* **26**, 433-441 (2005).

19. Zhong, S. P. et al. Development of a novel collagen-GAG nanofibrous scaffold via electrospinning. *Materials Science and Engineering: C Symposium A: Advanced Biomaterials International Conference on Materials for Advanced Technologies (ICMAT 2005)* **27**, 262-266 (2007).
20. Flanagan, T. C. et al. A collagen-glycosaminoglycan co-culture model for heart valve tissue engineering applications. *Biomaterials* **27**, 2233-2246 (2006).
21. Di Martino, A., Sittinger, M. & Risbud, M. V. Chitosan: A versatile biopolymer for orthopaedic tissue-engineering. *Biomaterials* **26**, 5983-5990 (2005).
22. Chun, H. J., Kim, G. W. & Kim, C. H. Fabrication of porous chitosan scaffold in order to improve biocompatibility. *Journal of Physics and Chemistry of Solids* **69**, 1573-1576 (2008).
23. Duarte, M. L., Ferreira, M. C., Marvão, M. R. & Rocha, J. Determination of the degree of acetylation of chitin materials by <sup>13</sup>C CP/MAS NMR spectroscopy. *Biological Macromolecules* **28**, 359-363 (2001).
24. Zhou, H. Y. et al. Effect of molecular weight and degree of chitosan deacetylation on the preparation and characteristics of chitosan thermosensitive hydrogel as a delivery system. *Carbohydrate Polymers* **73**, 265-273 (2008).
25. Hsu, S. H. et al. Chitosan as Scaffold Materials: Effects of Molecular Weight and Degree of Deacetylation. *Journal of Polymer Research* **11**, 141-147 (2004).



## Bibliography Chapter 2

---

26. Birk, D. E., Lande, M. A. & Fernandez-Madrid, F. R. Collagen and glycosaminoglycan synthesis in aging human keratocyte cultures. *Experimental Eye Research* **32**, 331-339 (1981).
27. Weiss, C., Balazs, E. A., St. Onge, R. & Denlinger, J. L. Clinical studies of the intraarticular injection of HealonR (sodium hyaluronate) in the treatment of osteoarthritis of human knees. *Seminars in Arthritis and Rheumatism* **11**, 143-144 (1981).
28. Holzman, S. & Connolly, R. J. Effect of Hyaluronic Acid Solution on Healing of Bowel Anastomoses. *Journal of Investigative Surgery* **7**, 431 - 437 (1994).
29. Grigolo, B. et al. Evidence for re-differentiation of human chondrocytes seeded on a hyaluronan derivative scaffold. *Arthritis Res* **3**, P7 (2001).
30. Giordano, C., Sanginario, V., Ambrosio, L., Silvio, L. D. & Santin, M. Chemical-Physical Characterization and in vitro Preliminary Biological Assessment of Hyaluronic Acid Benzyl Ester-Hydroxyapatite Composite. *J Biomater Appl* **20**, 237-252 (2006).
31. Motta, A., Migliaresi, C., Lloyd, A. W., Denyer, S. P. & Santin, M. Serum protein adsorption on silk fibroin fibres and membranes: surface opsonization and binding strength. *Journal of bioactive and compatible polymers* **17**, 23-35 (2002).
32. Motta, A., Fambri, L. & Migliaresi, C. Regenerated silk fibroin films: Thermal and dynamic mechanical analysis. *Macromolecular Chemistry Physics* **203** (2002).
33. Rahfoth, B. et al. Transplantation of allograft chondrocytes embedded in agarose gel into cartilage defects of rabbits. *Osteoarthritis Cartilage* **6**, 50-65 (1998).

34. Shapiro, L. & Cohen, S. Novel alginate sponges for cell culture and transplantation. *Biomaterials* **18**, 583-590 (1997).
35. Dvir-Ginzberg, M., Gamlieli-Bonshtein, I., Agbaria, R. & Cohen, S. Liver Tissue Engineering within Alginate Scaffolds: Effects of Cell-Seeding Density on Hepatocyte Viability, Morphology, and Function. *Tissue Engineering* **9**, 757-766 (2003).
36. Gunatillake, P. A. & Adhikari, R. Biodegradable synthetic polymer for tissue engineering. *European Cells and Materials* **5**, 1-16 (2003).
37. Athanasiou, K. A., Niederauer, G. G. & Agrawal, C. M. Sterilization, toxicity, biocompatibility and clinical applications of polylactic acid/ polyglycolic acid copolymers. *Biomaterials Polymer Scaffolding and Hard Tissue Engineering* **17**, 93-102 (1996).
38. Mooney, D. J., Baldwin, D. F., P., S. N., Vacanti, J. P. & Langer, R. Novel approach to fabricate porous sponges of poly(D,L-lactic-co-glycolic acid) without the use of organic solvents. *Biomaterials* **17**, 1417-1422 (1996).
39. Schieker, M., Seitz, H., Drosse, I., Seitz, S. & Mutschler, W. Biomaterials as Scaffold for Bone Tissue Engineering. *European Journal of Trauma* **32**, 114-124 (2006).
40. Yang, F. et al. Poly(1,l-lactide-co-glycolide)/tricalcium phosphate composite scaffold and its various changes during degradation in vitro. *Polymer Degradation and Stability* **91**, 3065-3073 (2006).
41. Bostman, O., Partio, E., Hirvensalo, E. & Rokkanen, P. Foreign-body reactions to polyglycolide screws. *Acta Orthopaedica* **63**, 173 - 176 (1992).
42. Jenkins, M. J. & Harrison, K. L. The effect of crystalline morphology on the degradation of polycaprolactone in a solution of

- phosphate buffer and lipase. *Polymers for Advanced Technologies* **19**, 1901-1906 (2008).
43. Hongfan, S., Lin, M., Cunxian, S., Xiumin, C. & Pengyan, W. The in vivo degradation, absorption and excretion of PCL-based implant. *Biomaterials* **27**, 1735-1740 (2006).
44. McDevitt, T. C., Woodhouse, K. A., Hauschka, S. D., Murry, C. E. & Stayton, P. S. Spatially organized layers of cardiomyocytes on biodegradable polyurethane films for myocardial repair. *Biomed Mater Res A* **66**, 586-595 (2003).
45. Stankus, J. J., Guan, J. & Wagner, W. R. Fabrication of biodegradable elastomeric scaffolds with sub-micron morphologies. *Journal of Biomedical Materials Research Part A* **70A**, 603-614 (2004).
46. Heller, J. et al. Poly(ortho esters) : their development and some recent applications. *European journal of pharmaceutics and biopharmaceutics* **50**, 121-128 (2000).
47. Chasin, M. & Langer, R. in *Biodegradable polymers as drug delivery systems*.
48. Williams, D. F. & Zhong, S. P. Biodeterioration/biodegradation of polymeric medical devices in situ. *Int. Biodeter. Biodegrad.* **95** (1994).
49. Labow, R. S., Tang, Y., McCloskey, C. B. & Santerre, J. P. The effect of oxidation on the enzyme-catalyzed hydrolytic biodegradation of poly(urethane)s. *Journal of Biomaterials Science, Polymer Edition* **13**, 651-665 (2002).
50. Coleman, J. W. Nitric oxide in immunity inflammation. *Int. Immunopharm* **1**, 1397 (2001).
-

## Bibliography Chapter 2

---

51. Volpato, F. Z., Ramos, S. L. F., Belfiore, L. A. & Migliaresi, C. in *NanoTech 2009* (Houston (Texas), 2009).
52. Motta, A. et al. in *TERMIS 2008* (Porto (Portugal), 2008).
53. Ciapetti, G. et al. Osteoblast growth and function in porous poly [var epsilon]-caprolactone matrices for bone repair: a preliminary study. *Biomaterials* **24**, 3815-3824 (2003).
54. Mironov, V., Boland, T., Trusk, T., Forgacs, G. & Markwald, R. R. Organ printing: computer-aided jet-based 3D tissue engineering. *Trends in Biotechnology* **21**, 157-161 (2003).
55. Fedorovich, N. E. et al. Hydrogels as extracellular matrices for skeletal tissue engineering: state-of-the-art and novel application in organ printing. *Tissue Engineering* **13**, 1905-1925 (2007).
56. Harris, R. A., Hague, R. J. M. & Dickens, P. M. Crystallinity control in parts produced from stereolithography injection mould tooling. *Proceedings of the I MECH E Part L Journal of Materials: Design and Applications* **217**, 269-276.
57. Wang, W. L., Cheah, C. M., Fuh, J. Y. H. & Lu, L. Influence of process parameters on stereolithography part shrinkage. *Materials and Design* **17**, 205-213.
58. Rimell, J. T. & Marquis, P. M. Selective laser sintering of ultra high molecular weight polyethylene for clinical applications. *Journal of Biomedical Materials Research* **53**, 414-420 (2000).
59. Vail, N. K. et al. in *Solid Freeform fabrication proceedings* 621-628 (1998).
60. Curodeau, A., Sachs, E. & Caldarise, S. Design and fabrication of cast orthopedic implants with freeform surface textures from 3-D

- printed ceramic shell. *Journal of Biomedical Materials Research* **53**, 525-535 (2000).
61. Giordano, C. et al. Mechanical properties of dense polylactic acid structures fabricated by three dimensional printing. *Biomaterials Science* **8**, 63-75 (1997).
62. Lam, C. X. F., Mo, X. M., Teoh, S. H. & Hutmacher, D. W. Scaffold development using 3D printing with a starch-based polymer. *Materials science & engineering C. Biomimetic and supramolecular systems* **20**, 49-56 (2002).
63. Sachs, E. M., Haggerty, J. S., Cima, M. J. & Williams, P. A. (U.S., 1989).
64. Marra, K. G., Szem, J. W., Kumta, P. N., DiMilla, P. A. & L., W. In Vitro analysis of biodegradable polymer blend/hydroxyapatite composites for bone tissue engineering. *Biomed Mater Res A* **47**, 324-335 (1999).
65. Hutmacher, D. W. Polymeric scaffolds in tissue engineering bone and cartilage. *Biomaterials* **21**, 2529-2543 (2000).
66. Zein, I., Hutmacher, D. W., Tan, K. C. & Teoh, S. H. Fused deposition modeling of novel scaffold architectures for tissue engineering applications. *Biomaterials* **23**, 1169-1185 (2002).
67. Comb, J. W., Priedeman, W. R. & Turley, P. W. in *Proc. of the Solid Freeform Fabrication Symposium* (ed. Marcus, H. L. e. a.) 42-49 (1994).
68. Masood, S. H. Application of fused deposition modelling in controlled drug delivery devices. *Assembly Automation* **27** (2007).
69. Karageorgiou, V. & Kaplan, D. Porosity of 3D biomaterial scaffolds and osteogenesis. *Biomaterials* **26**, 5474-5491 (2005).

## Bibliography Chapter 2

---

70. Salem, A. K. et al. Interactions of 3T3 fibroblasts and endothelial cells with defined pore features. *Journal of Biomedical Materials Research* **61**, 212-217 (2002).
71. Zeltinger, J., Sherwood, J. K., Graham, D. A., Mueller, R. & Griffith, L. G. Effect of Pore Size and Void Fraction on Cellular Adhesion, Proliferation, and Matrix Deposition. *Tissue Engineering* **7**, 557-572 (2001).
72. Hollister, S. J., Maddox, R. D. & Taboas, J. M. Optimal design and fabrication of scaffolds to mimic tissue properties and satisfy biological constraints. *Biomaterials* **23**, 4095-4103 (2002).
73. Zhou, Y., Hutmacher, D. W., Varawan, S. L. & Lim, T. M. Effect of Collagen-I Modified Composites on Proliferation and Differentiation of human Alveolar Osteoblasts. *Aust. J. Chem* **59**, 571-578 (2006).

## **4 Part 1: scaffold production by microfabrication**

### **4.1 Abstract**

Rapid prototyping techniques (RP) hold great promise for designing 3-dimensional (3-D) regular and ordered scaffolds. With these techniques, good architecture reproducibility as well as porosity control of the structure can be obtained.

This work dealt with the fabrication of tissue engineering scaffolds with regular micrometric geometry by using an in-house built microfabrication system.

Poly(D,L-lactic acid) (PDLA), poly(D,L-lactic-co-glycolic acid) (PLGA) and chitosan scaffolds presenting homogeneously distributed 100  $\mu\text{m}$  size pores have been fabricated. Fabrication consisted in a layer by layer deposition of filaments of PDLA and PLGA dichloro methane/dimethylformamide (DMC/DMF) solutions and chitosan acetic acid solutions, respectively, on a plate moving with micrometric precision in the x,y,z directions.

Additional chitosan scaffolds filled with amorphous calcium phosphate (ACP) particles were also microfabricated, considering the possibility to take advantage of the osteoconductive character of ACP for bone tissue regeneration applications.

The in-house built system utilizes highly accurate 3-D micro-positioning slides having a resolution up to 1  $\mu\text{m}$ . Through a microsyringe equipped with a micro-needle having 60  $\mu\text{m}$  inner diameter, an automatic pumping

system extrudes a filament of the selected solution on a plate. The plate is connected to three slides moving independently in the x,y,z directions. A computer controls the slides movement so that the filament that deposits on the plate builds layer by layer scaffolds of designed geometry.

Rheological tests have been used to characterize the polymer solution viscosities while thermal analysis (DSC), ATR-FTIR and dynamic mechanical tests (DMTA) have characterized the produced scaffold. Cast films from the same polymer solutions were used as control. Preliminary biological evaluations were done by seeding on the scaffolds osteoblasts (MG63) and fibroblasts (MRC5) cell lines.

SEM and LV-SEM imaging evidenced scaffold morphology and cell adhesion and growth behavior.

In addition, surface topography of ACP filled chitosan scaffolds has been determined by atomic force microscopy (AFM) and their surface elemental composition evaluated by energy dispersive spectroscopy (EDS).

## **4.2 Introduction**

Tissue engineering is a challenging field that aims at restoring or replacing deteriorating or aging biological structures such as tissues or organs. It involves the use of living cells and extracellular components, either natural or synthetic, to develop implantable parts<sup>1</sup>. In particular tissue engineering uses a combination of living cells and a porous support structure called scaffold on/in which cell attach, grow and proliferate<sup>2,3</sup>.

Since tissue engineering scaffold will be implanted in the human body, the scaffold materials should meet specific characteristics; in particular the used material should be non-antigenic, non-carcinogenic, non-toxic, and possess



high cell/tissue biocompatibility so that they will not give rise to any unfavourable cellular/tissue reactions after implantation. Moreover, the scaffold should have an interconnected porosity with pores large enough to permit cell penetration and, at the same time, vascularisation, nutrients transport and removal of metabolic waste. However, pore size should not be too large, in order to offer to cells a structural support for extracellular matrix formation with a morphology resembling the one of the target biological tissue. Mechanical properties of the produced scaffold have also to be considered in relation to the specific tissue that the scaffold is thought of<sup>2-5</sup>.

A wide variety of techniques commonly used in tissue engineering produce scaffolds having non-ordered structures with reduced pore interconnections, poor mechanical strength and reproducibility; moreover, most of these techniques can't control any variation in porosity within the 3-D structure. Among these techniques, solvent casting, freeze drying, phase inversion, fiber bonding, melt based technologies, high pressure based methods are the most used. To overcome the limits and the lacks of these methods, solid free-form fabrication (SFF) or rapid prototyping (RP) techniques have been introduced in order to computer control architecture and shape of the scaffolds<sup>6-9</sup>. Scaffold with high resolution and reproducibility can be fabricated by SFF techniques. Fused deposition modelling (FDM), three dimensional printing (3-DP), selective laser sintering (SLS) and stereolithography apparatus (SLA) are some examples of rapid prototyping techniques<sup>7</sup>. Some in-house built systems have also been used to fabricate ordered and reproducible scaffolds<sup>9</sup>.

Microfabrication aims at producing scaffolds of proper morphology/geometry with a micro-resolution.

Many synthetic and natural polymers, are suitable for the fabrication of biodegradable scaffolds.

Members of poly ( $\alpha$ -hydroxyl acids) family, such as poly(glycolic acid) (PGA), poly(lactic acid) (PLA), and poly(D,L-lactic-co-glycolic acid) (PLGA) have been widely used in tissue engineering applications<sup>10-13</sup>. They are considered to be biocompatible with degradation products, lactic acid and glycolic acid, that can enter into normal metabolic pathways<sup>14,15</sup>.

Among natural polymers, chitosan is a well-tolerated, non-antigenic, biodegradable<sup>16-19</sup>. Chitosan is the N-deacetylated derivative of chitin, a very abundant natural polysaccharide commonly located in crustaceans and insects. The biodegradation time of chitosan is determined by the amount of residual acetyl content<sup>20-22</sup>.

Polymer based composite materials are often used to obtain scaffolds with increased properties. In particular, with the use of ceramic fillers, scaffolds with better mechanical properties can be obtained. The added value of some ceramics is their osteogenic potential, very important for applications for bone repair and regeneration.

This work describes the use of a made-in-house microfabrication system to produce scaffolds from different materials having a microresolution and a well-defined ordered structure. Several physical tests were performed to evaluate the starting materials and the produced scaffolds. Preliminary biological tests allowed to evaluate cells attachment and penetration.

## **4.3 Materials and Methods**

### **4.3.1 Microfabrication System**

The microfabrication system picture is reported below, Figure 4.1. Three independent slides (National Instrument, Austin, Texas, US), computer controlled by a labVIEW platform, can independently move in the x,y,z directions with a 1  $\mu\text{m}$  resolution.

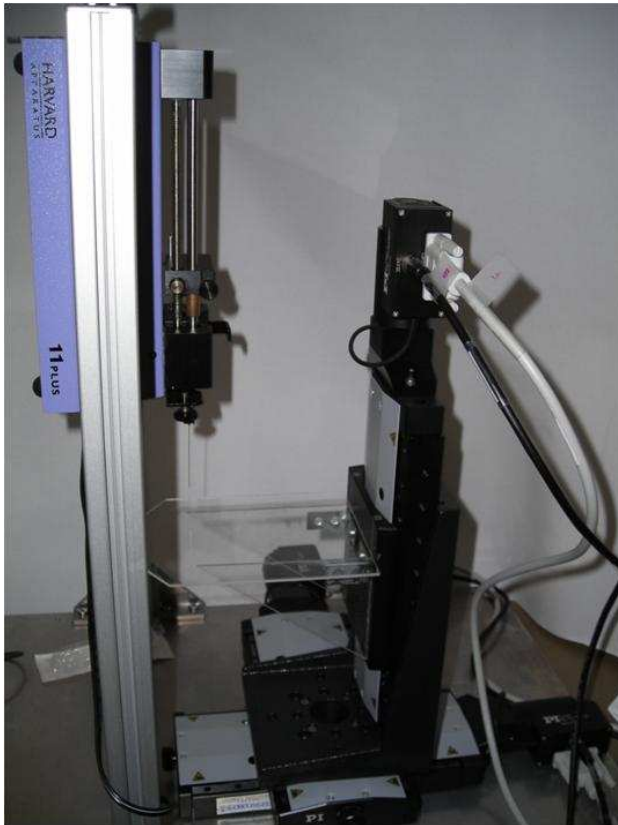


Figure 4.1: Microfabrication system

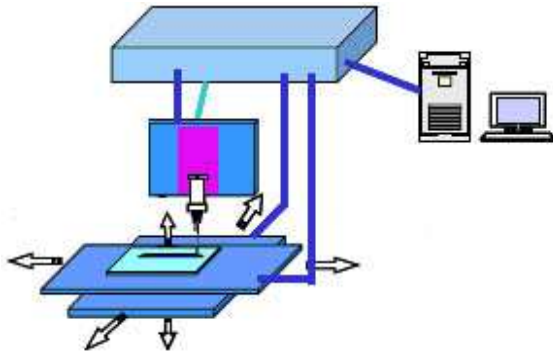


Figure 4.2. Schematic representation of microfabrication system

Each slide is connected to a DC motor which can impose a 15 mm/sec maximum velocity. The process parameters set by the LabVIEW front panels are sent to the axis through a controller which can also receive possible limit switch signals back from the slides.

Figure 4.2 and Figure 4.3 show the schematic representation of the microfabrication system and its working principle, respectively

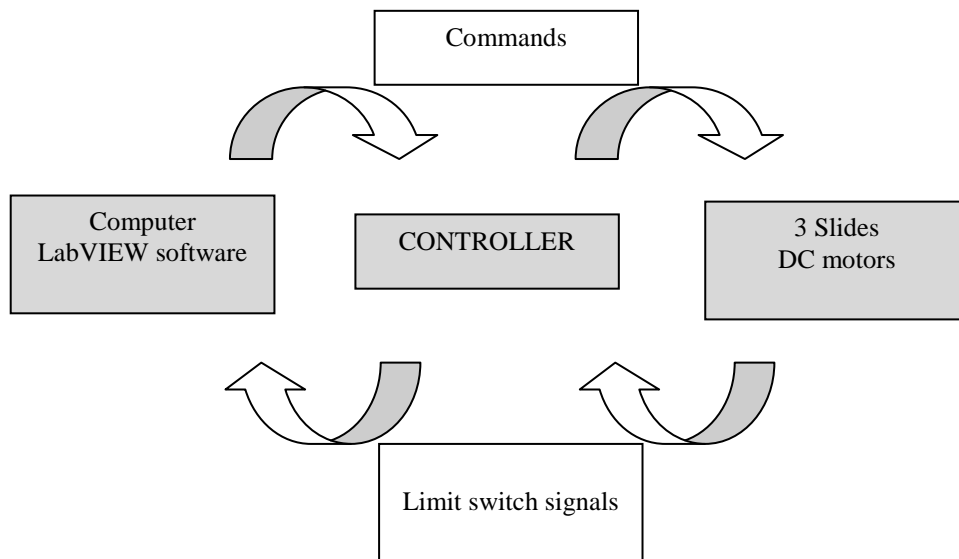


Figure 4.3. Working principle of microfabrication system

---

## Part 1: scaffold production by microfabrication

---

The slides, having a movement range up to 100 mm, move a platform where the polymer solution is extruded and the scaffold is built on. The extrusion system is composed by a glass syringe fixed up on an automatic pumping system (11 Plus, Harvard Apparatus, Massachusetts, US) (Figure 4.4) by which it is possible to set the proper flow rate; a metal micro-needle (Hamilton™, 34 gauge – 60 microns inner diameter; 1 cm length, 90° point style) is connected to the glass syringe by a luer-lock mechanism.

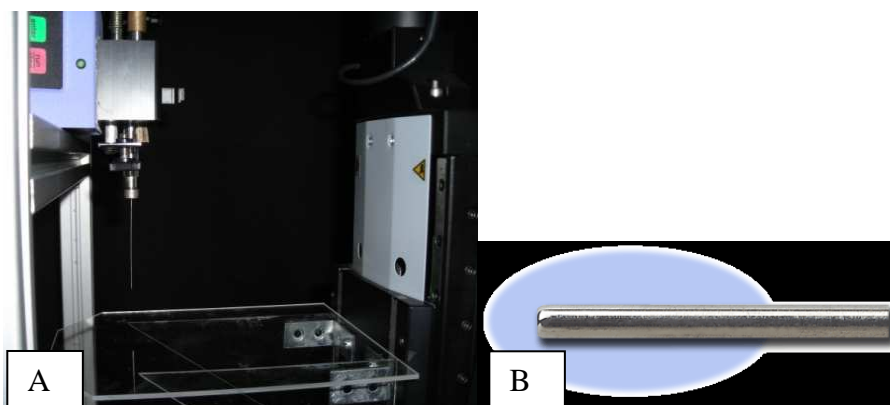


Figure 4.4. A) microfabrication system platform; B) 90° needle point style

Since the process strongly depends on environmental variables (such as temperature and humidity), a protective glass box encloses the whole system, to ensure constant conditions for the deposition.

The polymer solution is deposited from the needle of the glass syringe with a constant flow rate on a polyethylene terephthalate (PET) platform (Figure 4.5).

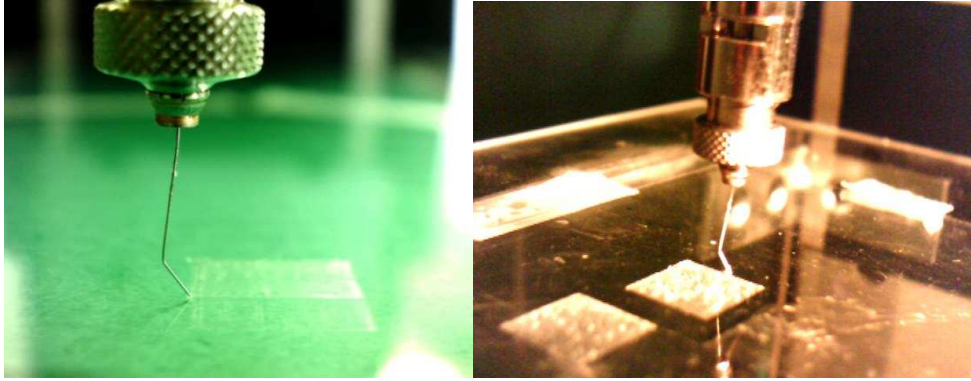


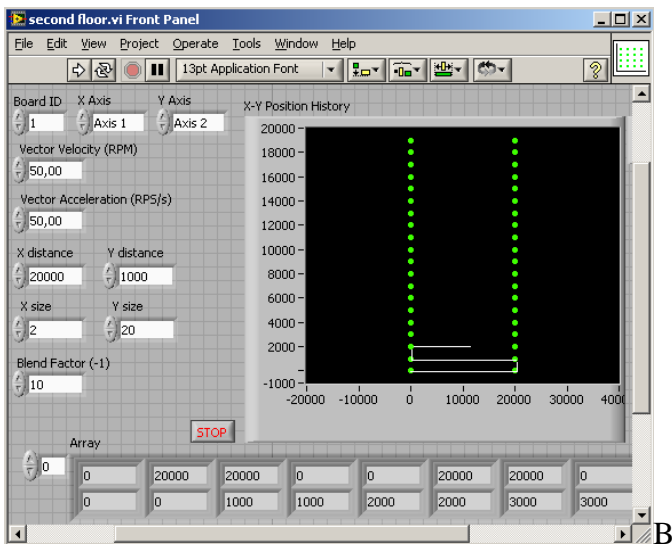
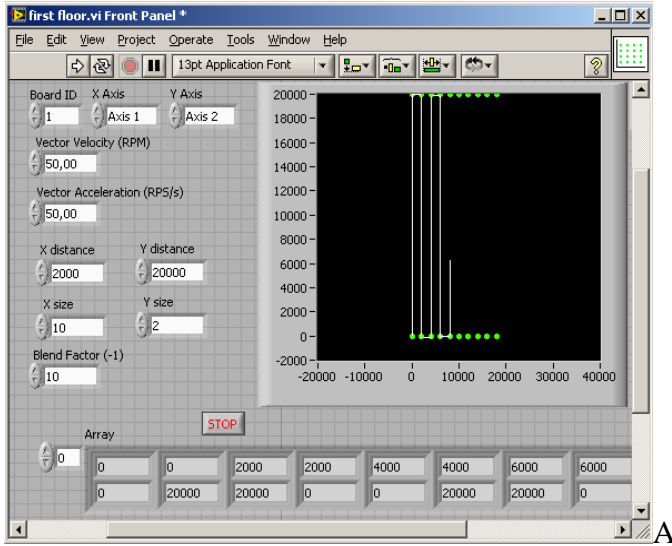
Figure 4.5. The micro-needle and scaffold microfabrication

Scaffold is built on layer by layer in the vertical direction. Each layer is composed by a series of parallel fibers, deposited by the syringe through a back-and-forward movement. The distance between the fibers, which influences the properties of the scaffold, is a parameter that the operator inserts in the control panel of the software. Once a layer is completed, the support moves down by an amount corresponding to the height of the deposited fibers, such that the distance between the needle and the deposition plane is constant. Then, another layer is deposited, whose fibers are perpendicular to those of the previous one, thus resulting in a scaffold with interconnected porosity. The number of iterations of this sequence determines the number of layers composing the scaffold, while fibers dimension depends on the pressure applied to the syringe, the viscosity of the solution, the motor speed and the dimensions of the needle.

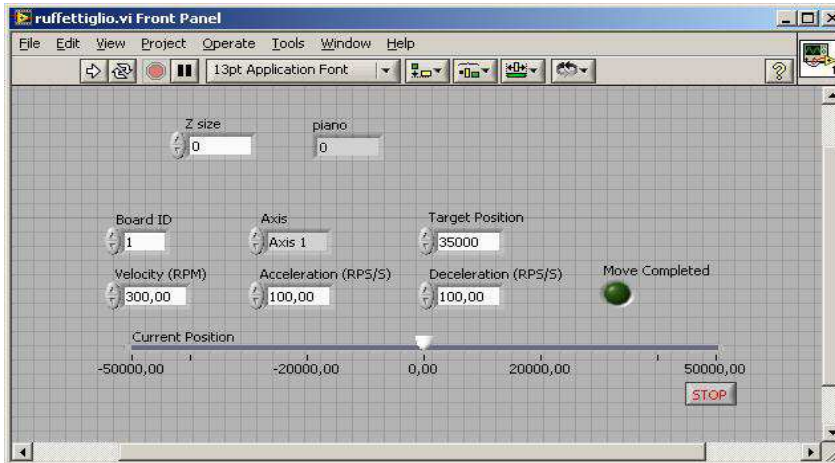
The process parameters which can be controlled through the LabVIEW front panels are the following: slide velocity and acceleration, the distance between fibers, the number of layers and the vertical displacement of the platform between the depositions of two subsequent layers. Figure 4.6

## Part 1: scaffold production by microfabrication

shows the graphical user interface of the labVIEW front panels.



Part 1: scaffold production by microfabrication



C

Figure 4.6. LabVIEW front panels: A) and B) planar movements, C) vertical movement

Figure 4.7 and Figure 4.8 are the LabVIEW block diagrams associated to the graphical user interfaces. In particular, Figure 4.7 shows the block diagram that regulates the vertical movement of the platform.

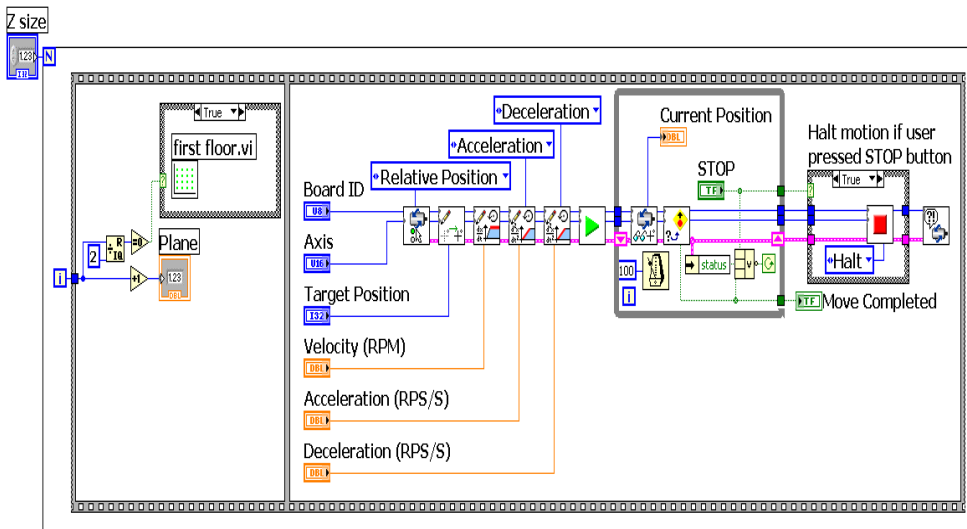
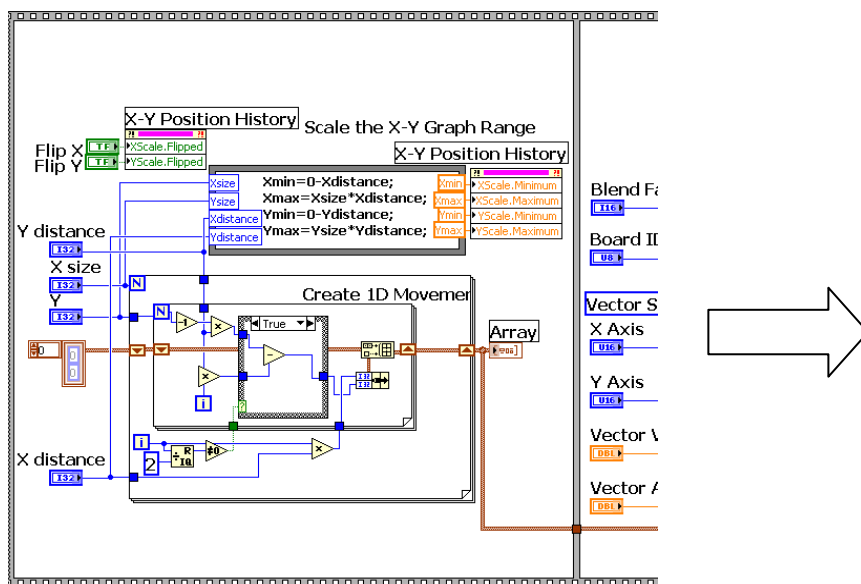


Figure 4.7. LabVIEW block diagram of the vertical movement



## Part 1: scaffold production by microfabrication

The program is essentially composed of a “For Loop”, that repeats a number of time corresponding to the number of layers the scaffold will be composed of. The program uses an incremental number to enumerate the cycles; this variable is used to distinguish between odd-numbered and even-numbered layers. Depending on that, the program executes alternatively two sub-programs, which differs on fibers orientation. In that way, odd-numbered layers are composed of fibers oriented perpendicularly respect to the ones of even-numbered layers. The second part of this block diagram represents the vertical displacement, executed after each of the two sub-programs that determines in-plane movements. The input values inserted are read by the program which actuates the movement.



---

Part 1: scaffold production by microfabrication

---

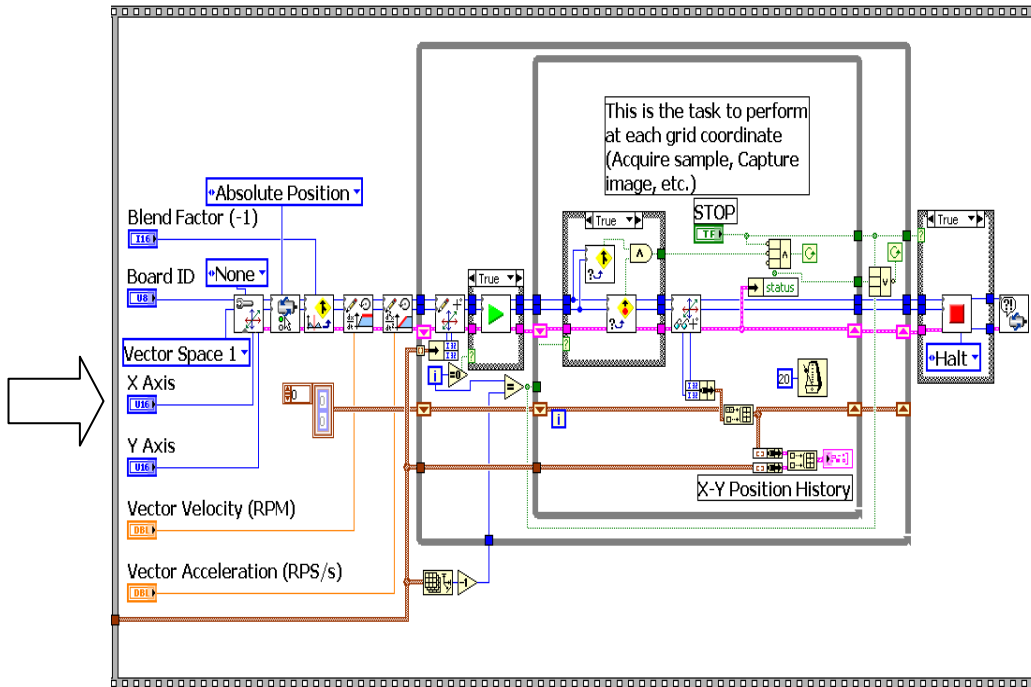


Figure 4.8. LabVIEW block diagram of planar movements

Figure 4.8 is the block diagram related to the planar movement and finally associated to the layers formation. It can be divided into two parts: the first one represents the creation of an array, that is the instructions for the platform to move, forming the grid. Practically, the array corresponds to the geometrical parameters of the scaffold. The formed array is then used in the second part of this block diagram, where the instructions for the movements are taken as input values and used to move the slides.

The needle path to obtain the desired scaffold geometry is described by a set of spatial coordinates, which, basically, represent the boundaries of each

layer of the scaffold. The back-and-forward movement passing through these points determines the fibers deposition. Figure 4.6 shows the graphical user interface associated to the subprograms related to the layer formation (with two different orientation, A and B in the figure) and to the vertical movement (C) of the deposition platform.

All the process parameters were set from the LabVIEW front panels exclusive of flow rate that is controlled directly from the automatic pumping system.

Flow rate, velocity, target position (distance between layers) are strictly related to each other and dependent on polymer solution viscosity and scaffold geometric features. In the tested solutions the process parameters combination related to a specific and pre-determined solution viscosity, were fixed as follow:

- Flow rate: 1  $\mu\text{L}/\text{min}$
- Slide velocity: 4.6 mm/sec
- Distance between layer: 25  $\mu\text{m}$

Each square scaffold, (generally either 1 cm x 1 cm or 2 cm x 2 cm dimensions were chosen), is composed of about 100  $\mu\text{m}$  equidistance rows. Synthetic polymer scaffolds were formed by 30 layers while the chitosan polymer scaffolds by 80 layers. The final thickness of the synthetic scaffolds was approximately 350  $\mu\text{m}$  while natural polymer matrices had a total thickness not bigger than 100  $\mu\text{m}$ .

Figure 4.9 represents a natural polymer scaffold 2 cm x 2 cm produced by microfabrication technique.

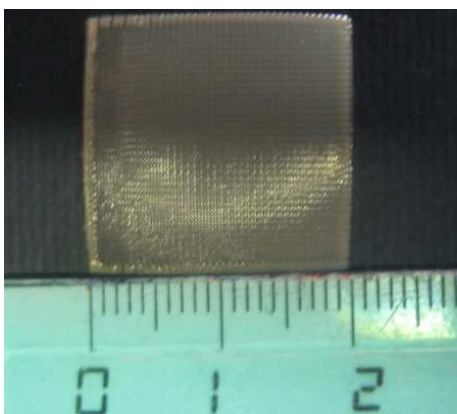


Figure 4.9. Microfabricated chitosan scaffold

### 4.3.2 Synthetic polymer materials: PDLA and PLGA

Poly(D,L-lactic acid) (PDLA, type RESOMER<sup>®</sup> 207, MW= 252 kDa) poly(D,L-lactic-co-glycolic acid) (PLGA, type RESOMER<sup>®</sup> 503, 50:50 molar ratio D,L-lactide:glycolide, MW= 39 kDa) were purchased from Boehringer Ingelheim, Germany. The polymers were used without further purification.

Dichloromethane (DCM) and dimethylformamide (DMF) were obtained from BDH Chemicals (UK) and J.T.Baker (Holland), respectively.

PDLA and PLGA were dissolved in dichloromethane:dimethyl formamide (70:30 v/v) to prepare 20% (w/v) and 25% (w/v) solutions, respectively. Before being used inside the microfabrication system, the solutions were

---

## Part 1: scaffold production by microfabrication

---

magnetically stirred at 40°C for 18 hours, then filtered with Millipore Nylon Net filter having 20 µm pore size.

The specifications of the solvents are given in the Table 4.1.

Table 4.1. properties of solvents

	Density [g/ml]	Boiling Temp [°C]	Viscosity [cP]	Firm	Purity [%]	Water [%]
DCM	1.325	40	0.44	BDH (UK)	99.5	0.05
DMF	0.944	153	0.91	J.T.Baker (Holland)	99	0.05

Films obtained by casting the solutions in Petri dishes were used as control. The solvent was allowed to evaporate gently in order to avoid bubble formation. The resulting polymer films were dried under vacuum for 1 day at room temperature to produce 0.2 mm thick PDLA and PLGA films.

### 4.3.3 Natural polymer material: Chitosan

Chitosan (low viscosity, 78% deacetylated) and acetic acid were purchased from Fluka (Missouri, US).

Chitosan was used without further purification. Sodium hydroxide (NaOH) was obtained from J.T. Baker (Holland).

Chitosan was dissolved in 5% (v/v) acetic acid to prepare 3% (w/v) chitosan solution. Polymer solution was then filtered through Millipore Nylon Net filter with 20 µm pore size.

After microfabrication, chitosan scaffolds were treated with 1 M NaOH for one hour and then washed with distilled water until neutrality.

The specifications of the solvents are given in the Table 4.2.

---

## Part 1: scaffold production by microfabrication

---

Table 4.2. Properties of solvent

	Density [g/ml]	Boiling Temp [°C]	Viscosity [cP]	Firm	Purity [%]
Acetic Acid	1.049	118.1	1.22	Fluka (MO, US)	99

Additional chitosan scaffolds filled with amorphous calcium phosphate (ACP) particles were fabricated. A solution was prepared dissolving 2.6% (w/v) chitosan and 0.4% (w/v) ACP in 5% (v/v) acetic acid solution.

The particles were synthesized via sol-gel process, which was previously described by Skirtic et al.<sup>23</sup>. The particles mean diameter was kept as  $2.17 \pm 2.07$   $\mu\text{m}$ . The precursors  $\text{Ca}(\text{NO}_3)_2 \cdot 4\text{H}_2\text{O}$ ,  $\text{Na}_2\text{HPO}_4 \cdot 2\text{H}_2\text{O}$  and  $\text{Na}_4\text{P}_2\text{O}_7 \cdot 10\text{H}_2\text{O}$  used in the synthesis of amorphous calcium phosphate (ACP) particles were supplied by Sigma-Aldrich (St. Louis, MO – US).

Films obtained by casting the solutions in Petri dishes were used as control. The solvent was allowed to evaporate gently in order to avoid bubble formation. The resulting polymer films were dried under vacuum for 1 day at room temperature to produce 0.2 mm thick chitosan films.

### 4.3.4 Gel Permeation Chromatography (GPC)

Weight average molecular weight of the used synthetic polymers used was determined by gel permeation chromatography (GPC, Spectra System

P1500) by using a Shodex K-804 column (Shodex, Tokyo, Japan) and a KG pre-column.

Chloroform was used as solvent for the polymers and 1 mL/min eluent constant flux was applied.

The Universal Calibration method with polystyrene standards was used to obtain a calibration curve.

#### **4.3.5 NMR**

$^{13}\text{C}$  CP MAS NMR spectroscopy was used to determine the average degree of acetylation of chitosan.

Solid State NMR experiments were carried out on a Bruker Avance 400 WB spectrometer, operating at 100.613 MHz for  $^{13}\text{C}$ . Samples were packed in 4 mm diameter zirconia rotors which were spun at 9 kHz under air flow. The experiment was performed at  $^{13}\text{C}$  SP-MAS, operating conditions were 3.5  $\mu\text{s}$  for 90° pulse and 5.3  $\mu\text{s}$  for decoupling pulse both at -1.7 dB of power level, 10 s for recycle delay. Adamantane was used as external shift scale reference.

#### **4.3.6 Rheological Tests**

For rheological measurements on the solutions, a rotational rheometer (Advanced Rheometric Expansion System - ARES – TA Instrument, New Castle, DE – US) was used. A cone-plate configuration (50 mm plate diameter, 0.04 rad cone angle, 0.050 mm initial gap between cone and plate) and a dynamic frequency sweep test mode (strain control, 3% strain, 1 rad/sec initial frequency, 22°C working temperature) were employed.

To prevent solvent evaporation during the experiments, a humidity chamber enclosing the cone-plate apparatus and lined with a solvent soaked sponge was used. Complex viscosity over frequency range between 1 and 100 rad/sec was measured and efficiency of humidity chamber was tested by sequentially running the rheometric measurements on the same sample.

#### **4.3.7 Attenuated Total Reflectance-Fourier Transform Infrared (ATR-FTIR)**

Infrared spectroscopy analysis (Spectrum One Spectrometer – PerkinElmer, Germany) was utilized to evaluate possible material modifications due to the process or solvent retention. Films from the same polymer solution were used as control.

All the spectra were analyzed after ATR and baseline correction.

#### **4.3.8 Differential Scanning Calorimetry (DSC)**

Differential scanning calorimetry (DSC) (DSC 30 Mettler-Toledo, USA) was performed on polymers before and after microfabrication to investigate possible modifications due to the fabrication procedure. Approximately 5-10 mg samples were placed in aluminum DSC pans. Every sample underwent two heating scans from -20°C to 120°C in the case of PLGA and PDLA; for chitosan the first scan was from 0°C to 200°C while the second one from 0°C to 300°C; heating rate was fixed at 10°Cmin<sup>-1</sup> and cooling rate at 100°Cmin<sup>-1</sup> under a nitrogen flux of 10 mLmin<sup>-1</sup>.

Evaluations on the obtained graphs were performed by STARe – Thermal analysis software.



Second order phase transition, that is glass transition temperature ( $T_g$ ) and first order phase transition endothermic and exothermic peaks were detected.

#### **4.3.9 Thermo gravimetric analysis (TGA)**

Mettler TG50 thermogravimetric balance connected to a Mettler TC10A processor was used to measure weight loss as a function of temperature of chitosan polymer, chitosan polymer filled with ACP particles and ACP particles.

A temperature range between  $0^\circ\text{C}$  and  $800^\circ\text{C}$  was evaluated under a nitrogen flux of 200 ml/min.

#### **4.3.10 Dynamical mechanical thermal analysis (DMTA)**

Dynamic mechanical thermal analysis (DMTA) was performed by DMTA Mk II (tensile mode) of Polymer Laboratories Scientific Firm.

The analysis were conducted by keeping the frequency constant (1 Hz) and varying the temperature at a heating rate of  $3^\circ\text{C}/\text{min}$  from  $-60^\circ\text{C}$  to  $100^\circ\text{C}$  in the case of PLGA and PDLA and from  $-60^\circ\text{C}$  to  $200^\circ\text{C}$  in the case of chitosan material.

Cast films  $40\ \mu\text{m}$  thick were produced and used as a control.

Storage modulus ( $E'$ ) and loss factor ( $\tan\delta$ ) were plotted over temperature.

### **4.3.11 Preliminary in vitro culture studies**

Human osteosarcoma derived osteoblasts MG63 and human embryonal lung origin fibroblast MRC5 cell line were seeded on the produced PDLA, PLGA and chitosan, plain and ACP filled, scaffolds

Cells were incubated at 37°C in a 5% CO<sub>2</sub> atmosphere incubator, and when reached the confluence stage they were harvested by trypsinization followed by the addition of fresh culture medium to create a cell suspension. Minimum essential medium (MEM) supplemented with 10% Fetal Bovine Serum (FBS), 1% penicillin, 1% Glutamax, 1% Vitamine, 1% non essential amino acids was used for MG63 cell line media; 1% Sodium Piruvate in addition to these ingredients was used for MRC5 cell line media.

All of the scaffold samples were sterilized by immersion in 70% ethanol followed by washing with distilled water and were seeded with a cell suspension of  $5 \times 10^5$  cell/mL concentration in 48 well plates. The density of cells was determined by a glass hemacytometer. For each well 0.5 ml of cell suspension was added. Medium was changed every 2 days. At chosen times, scaffolds were removed, cells were fixed and the morphology of the cells was examined by SEM and LV-SEM imaging analysis.

### **4.3.12 Atomic Force Microscopy (AFM)**

Topography of ACP filled chitosan scaffolds was evaluated by AFM analysis.

Topography was analyzed by AFM (NT-MDT Solver AFM) in contact mode, collecting topography profiles maps with silicon contact tips (conical shape, angle < 22 deg., typical curvature 10 nm radius, Kel = 0.01 N/m). Measurements were carried out in air at room temperature, by a scanning

head of  $90 \mu\text{m}^2$  of  $10 \times 10 \mu\text{m}$  scan area; the scan frequency was kept between 1.0 Hz and 1.2 Hz.

#### **4.3.13 Sample imaging**

Morphological observations were performed with optical microscopy, scanning electron microscopy (SEM) (Cambridge Stereoscan 200 – operating mode: high vacuum, secondary electron SE detector) and Environmental-SEM (ESEM TMP FEI – operating mode: low vacuum, gaseous secondary electron GSE detector).

Before imaging, biological samples were fixed by using a glutaraldehyde solution (25% glutaraldehyde in cacodylic buffer solution 0.1 M, pH=7.2) to preserve the structure of living tissues. Then the samples were dehydrated by dipping in a series of aqueous ethanol solutions at increasing concentrations. Prior to SEM imaging, samples were sputter coated (SEM Coating Unit PS3, Assing S.p.A., Rome, Italy) with a thin layer of gold in argon atmosphere (20 mA at  $5 \times 10^{-7}$  Pa for 30 sec).

Energy dispersive spectroscopy (EDS, EDAX – Ametek) was used to determine the surface elemental composition of chitosan/ACP composite scaffolds before and after NaOH washing treatment.

## 4.4 Results and Discussion: synthetic materials

### 4.4.1 Microfabricated scaffold

Scaffolds of PLGA and PDLA were obtained by the superposition of 25 sequential orthogonal layers. Their optical and SEM images are reported in Figure 4.10.

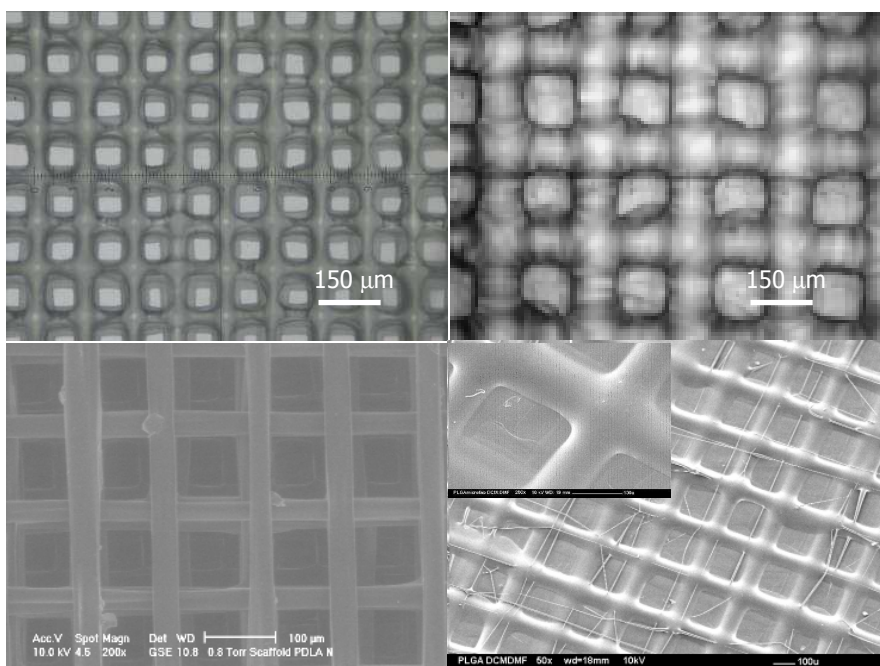


Figure 4.10. Optical (up) and scanning electron (down) microscopy images of a PDLA (left) and PLGA (right) scaffold

Setting the proper combination of process parameters was very important to produce homogeneous and regular scaffolds. Wrong setting of the machine combined with an improper polymer solution viscosity resulted in defects being created in the final scaffold structure. Solution viscosity and solvent

---

Part 1: scaffold production by microfabrication

---

evaporation rate are the main parameters controlling spinning of the solution and filament deposition.

Low-boiling temperature solvents evaporated too fast, even on the needle tip, causing the polymer solution to flow discontinuously and to stuck at the tip. Similar results were observed when the solution concentration was too high. Non-continuous flow created defects in the scaffold such as big droplets; moreover, fibers did not bind each other (Figure 4.11, A and B). High boiling temperature solvents, on the contrary, were difficult to remove from the material, so that the polymer spread on the collecting platform and following layers collapsed one over the others. The same effect was observed when the polymer concentration was too low (Figure 4.11, C and D).

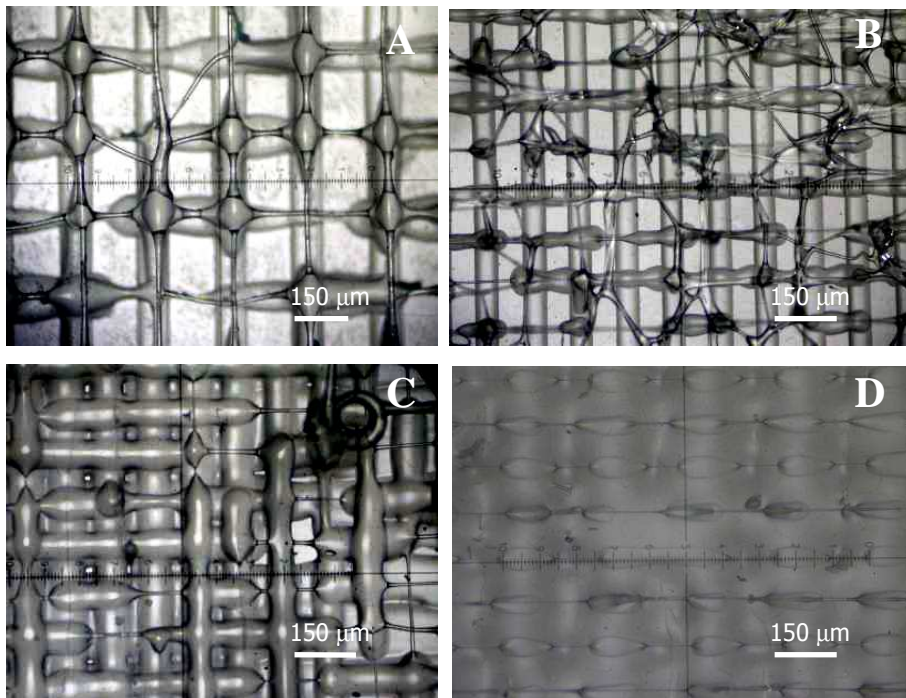


Figure 4.11. Optical images of a microfabricated scaffold with defects. A and B, PDLA; C and D, PLGA

Pores size and shape could varied depending on spinning parameters. For instance, for PDLA, at higher x,y slide velocity (4.6 mm/sec) pores were square shaped sizing about 100  $\mu\text{m}$  (Figure 4.12 A), while more elongated smaller pores (Figure 4.12 B) were obtained at slower slide velocity (4 mm/sec).

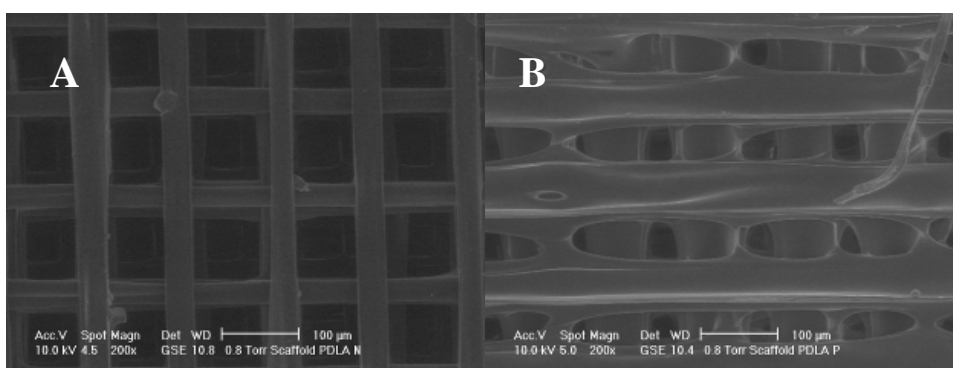


Figure 4.12. PDLA microfabricated scaffold

For PGLA, SEM imaging showed a regular structure with 100  $\mu\text{m}$  thick polymer rows and about 130  $\mu\text{m}$  side square holes (Figure 4.10).

PLGA scaffolds were produced by 25 overlapping layers; morphological evaluation by imaging analysis (SEM) showed a regular structure with 100  $\mu\text{m}$  polymer rows and about 130  $\mu\text{m}$  square holes (Figure 4.10).

Due to the lower solution viscosity (see chapter 4.3.6), in general the PLGA scaffolds were more difficult to process than PLDA and a three-dimensional structure was hardly obtained. Attempts made to microfabricate PLGA scaffolds starting from more concentrated polymer solutions were not successful due to the gelification of the solution in the syringe.

Proper solution concentration was the most important process parameter to set for PLGA scaffolds microfabrication. At low polymer concentration (15% w/v), the solution flowed out easily through the needle, however once

it was extruded on the substrate the solvent evaporated too slowly and the scaffold spread and collapsed. At 30 % w/v PLGA concentration, the unstirred solution behaved as a gel. A 25% (w/v) PLGA solution concentration resulted to be the optimal as regards the easiness of the process and the quality of the obtained scaffolds.

#### **4.4.2 Rheological test on PDLA and PLGA solutions**

Flow behaviour of polymer solutions is an important process parameter to consider during microfabrication process.

For this reason rheological test on the polymer solutions were performed in order to evaluate in which viscosity range the solutions were extruded during the microfabrication process.

Characterization of polymer solutions flow behaviour and selection of the proper viscosity working range in respect to microfabrication process were thus evaluated.

Both PDLA and PLGA solutions, at the concentration value that resulted to be optimal during the microfabrication process, were tested by using a rotational rheometer by a dynamic frequency sweep test: in this way complex viscosity was measured over a frequency range between 1 and 100 rad/s.

According to the Cox-Merz rule<sup>24</sup>, the complex viscosity as a function of the frequency corresponds to the shear viscosity as a function of shear rate. In addition, the effect of evaporation phenomena was evaluated by performing three measurements on the same sample one after one.

---

Part 1: scaffold production by microfabrication

---

Figure 4.13 and Figure 4.14 show the graphs resulting from the rheological tests on PDLA and PGLA solutions respectively.

Table 4.3 reports the viscosity values at fixed frequencies in order to evidence the effect of the three following runs for the two polymers.

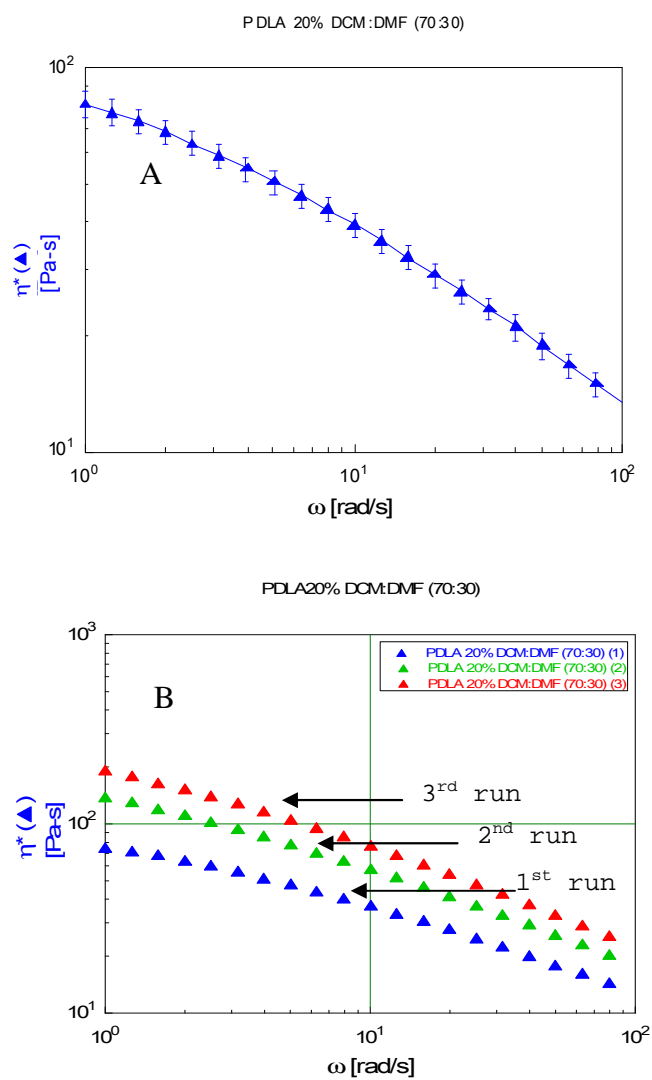


Figure 4.13. Rheological test results for A) Viscosity of 20% PDLA solution in DCM:DMF (70:30) solvent, B) Viscosity of 20% PDLA solution in DCM:DMF (70:30) solvent obtained by three successive measurements



Part 1: scaffold production by microfabrication

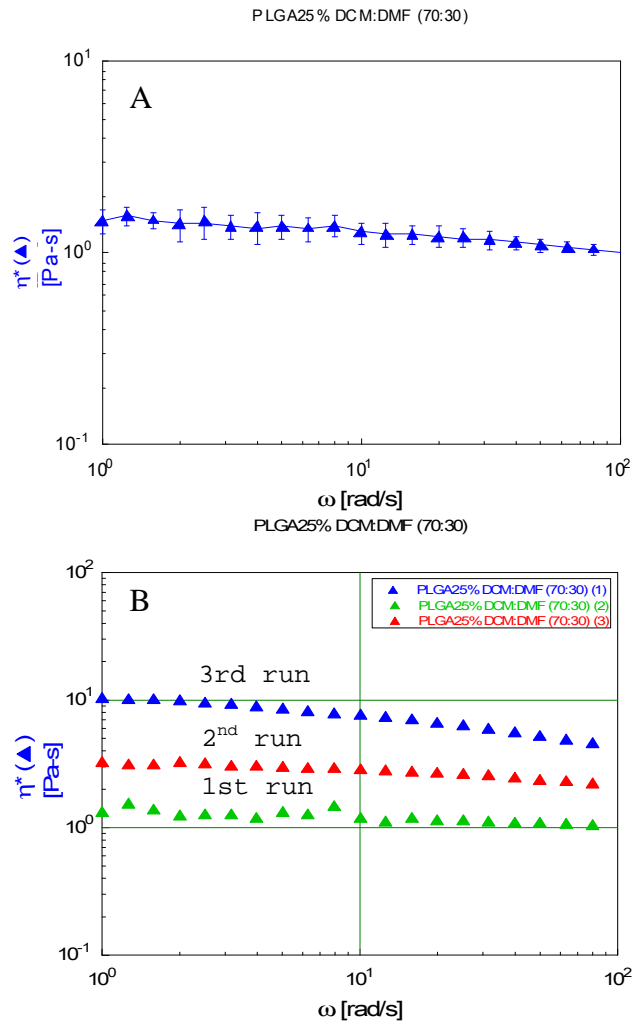


Figure 4.14. Rheological test results for A) Viscosity of 25% PLGA solution in DCM:DMF (70:30) solvent, B) Viscosity of 25% PLGA solution in DCM:DMF (70:30) solvent obtained by three successive measurements

---

Part 1: scaffold production by microfabrication

---

Table 4.3. Complex viscosity, expressed in PA.s, of PDLA solutions at fixed frequencies. The numbers between the round brackets indicate the relative change in comparison to the viscosity measured in the first run

$\omega$ [rad/s]	1	10	100
1 <sup>st</sup> run	76.45	36.65	14.26
2 <sup>nd</sup> run	137.93 (+80%)	57.61 (+57%)	17.87 (+25%)
3 <sup>rd</sup> run	190.78 (+150%)	76.25 (+108%)	22.20 (+56%)

Table 4.4. Complex viscosity, expressed in PA.s, of PLGA solutions at fixed frequencies. The numbers between the round brackets indicate the relative change in comparison to the viscosity measured in the first run

$\omega$ [rad/s]	1	10	100
1 <sup>st</sup> run	1.30	1.18	1.00
2 <sup>nd</sup> run	3.23 (+148%)	2.84 (+140%)	2.09 (+109%)
3 <sup>rd</sup> run	10.38 (+698%)	7.59 (+543%)	4.17 (+317%)

PDLA solution complex viscosity presents the typical polymer solution trend, that is a non-Newtonian pseudoplastic behaviour: the viscosity decreases at increasing frequencies.

Instead, PLGA solutions in the considered frequency present an almost Newtonian behaviour.

In view of the fact that the polymers chemical structures are quite similar the viscosity value is highly dependent on the polymer molecular weight<sup>24</sup> and for this reason the measured complex viscosity of of the lower concentration PDLA solution is higher than PLGA.

Besides, comparison between the increasing values of viscosities of PDLA and PLGA polymer solutions after successive tests reveals that evaporation was more pronounced in PLGA solution. As a result, PLGA solution was therefore more unstable to be processed inside the microfabrication system and the whole scaffold production process was less reproducible. This problem was technically verified during the microfabrication process: unfortunately it was not possible to solve it by increasing the polymer solution concentration because the solution quickly converted into a gelly state as the concentration was increased.

Furthermore it is important to underline that the results obtained by the rheological tests performed on the solutions are related to the flow viscosity (shear stresses). However, especially in small capillary and in non-Newtonian fluids (such as polymer solutions), the contribution of extensional viscosity is also present. Extensional viscosity (or elongational viscosity) is the resistance to flow in a stretching deformation. It is independent of shear viscosity for non-Newtonian fluids and can be hundred times larger<sup>24,25</sup>.

#### **4.4.3 Molecular weight distributions of PDLA and PLGA polymers**

Molecular weight distribution of PDLA and PGLA base powders, cast films and microfabricated scaffolds was evaluated in order to identify any possible material modification induced by the process.

Processes where polymer solutions undergo to shear stresses were occasionally reported to induce polymer degradation phenomena which are evidenced as a reduction of the molecular weight<sup>26-28</sup>.

---

Part 1: scaffold production by microfabrication

---

The results of the GPC analyses are presented in Figure 4.15 and Figure 4.16, which show the molecular weight distributions of PDLA and PLGA based materials, respectively, and in Table 4.5, which contains the calculated weight average molecular weight and polydispersity index for each tested material.

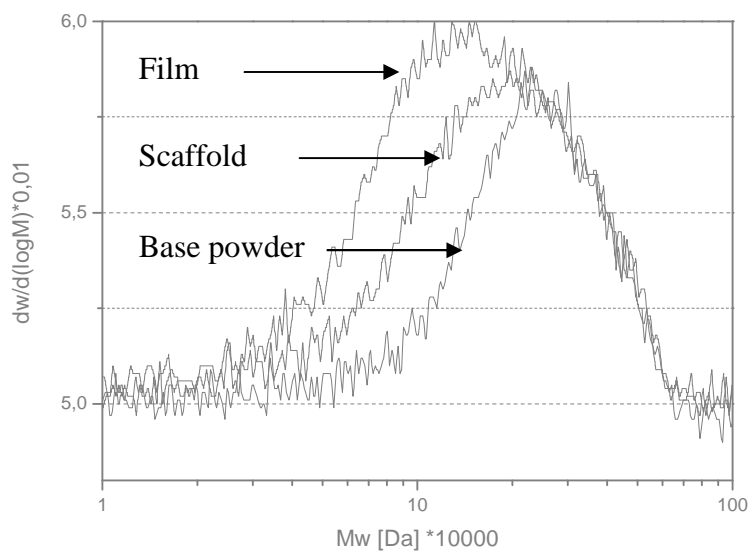


Figure 4.15. Molecular weight distribution of PDLA based materials: base powder, cast film and microfabricated scaffold

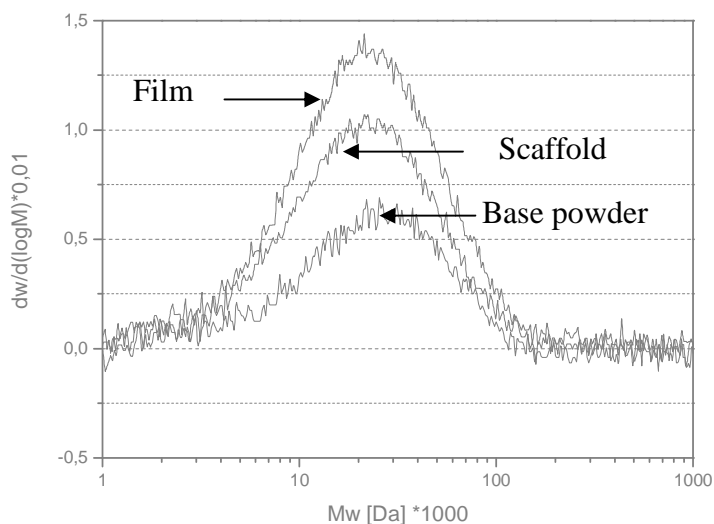


Figure 4.16. Molecular weight distribution of PLGA based materials: base powder, cast film and microfabricated scaffold

Table 4.5. Weight average molecular weight and polydispersity index for PDLA and PLGA based materials

	Mw [kDa]	pdi
PDLA powder	252	2.03
PDLA microfabricated	206	1.83
PDLA film	177	1.88
PLGA powder	39.4	4.20
PLGA microfabricated	<b>28.6</b>	2.19
PLGA film	<b>29.3</b>	2.45

Figure 4.15 evidences as the molecular weight distributions of the cast film and the microfabricated scaffold of PDLA and PLGA shift to lower values in comparison to the base powder of both the polymers: this fact corresponds to lower weight average molecular weights observed in Table 4.5. In particular the decrease is more evident for PDLA cast film compared to PDLA scaffold. Moreover, the polydispersity index results to be lower in

the case of the cast film and the microfabricated scaffold: this fact corresponds to a narrowing of the molecular weight distribution evidenced in Figure 4.15 and Figure 4.16.

These degradation phenomena could be attributed to the hydrolytic degradation typical for poly( $\alpha$ -hydroxyacids)<sup>29-34</sup>. Being the DMF solvent highly hygroscopic<sup>35</sup>, some water could be present and contribute to easily degrade the polymer. In fact, after processing, as proved by the ATR-FTIR spectra (chapter 4.4.5), DMF is still present inside the products, scaffolds and films. Removing of DMF from scaffolds and film resulted complicated and evaporation after process was ineffective because of the high boiling temperature of DMF.

Reduction of glass transition temperatures (T<sub>g</sub>), noticed in the DSC thermograms also cooperates to confirm the DMF presence after processing (chapter 4.4.4).

On the other hand, the presence of the solvent resulted not to have consequences on biological evaluations performed *in vitro*: washing with ethanol and distilled water before usage in culture tests was enough to remove the DMF and the degradation of the polymer is negligible if tests are carried out immediately.

Difference in weight average molecular weight between PDLA scaffold and film could be caused by the slower evaporation in the film. Evaporation process is dependent on surface area and bulk thickness thus being faster in scaffolds than in films.

The fact that degradation occurred in both film and scaffold, states that the shear stresses applied to the polymer solution during spinning were not high enough to induce chain breaking. The observed degradation phenomena is attributable to hydrolysis of the poly ( $\alpha$ -hydroxyacids) chains.

#### 4.4.4 Differential scanning calorimetry (DSC)

Thermal properties of PDLA and PLGA polymers, before and after microfabrication process, were evaluated by differential scanning calorimetry (DSC) analysis in order to investigate possible material modifications due to the process.

As comparison, cast films obtained from the same solutions were analysed as well.

The resulted thermographs are shown in Figure 4.17 and in Figure 4.18. Table 4.6 shows the evaluations results.

A first heating scan from 0°C to 100°C was made to remove solvent traces. PDLA and PLGA are amorphous polymers and the base powders show a second order phase transition, i.e. glass transition temperature (T<sub>g</sub>) at 57,36°C and 46,49°C, respectively.

T<sub>g</sub> of microfabricated scaffold and film is lower. During the first heating scan the decrease is due to residual solvent inside the material acting as a plasticizer for the polymer<sup>36</sup>, lowering down the T<sub>g</sub>. Infrared spectroscopy analysis (chapter 4.4.5) confirmed the presence of DMF solvent.

Considering the second heating scan curves, T<sub>g</sub>s drop in the microfabricated polymers from 57,36 to 54,80°C, and from 46,49 to 42,72°C, for PDLA and PLGA polymers respectively.

These results are consistent with the already presented molecular weight findings (chapter 4.4.3), which have shown a degradation of the polymers in the microfabricated scaffolds.

Similar considerations can clarify cast film results at the same way.

Part 1: scaffold production by microfabrication

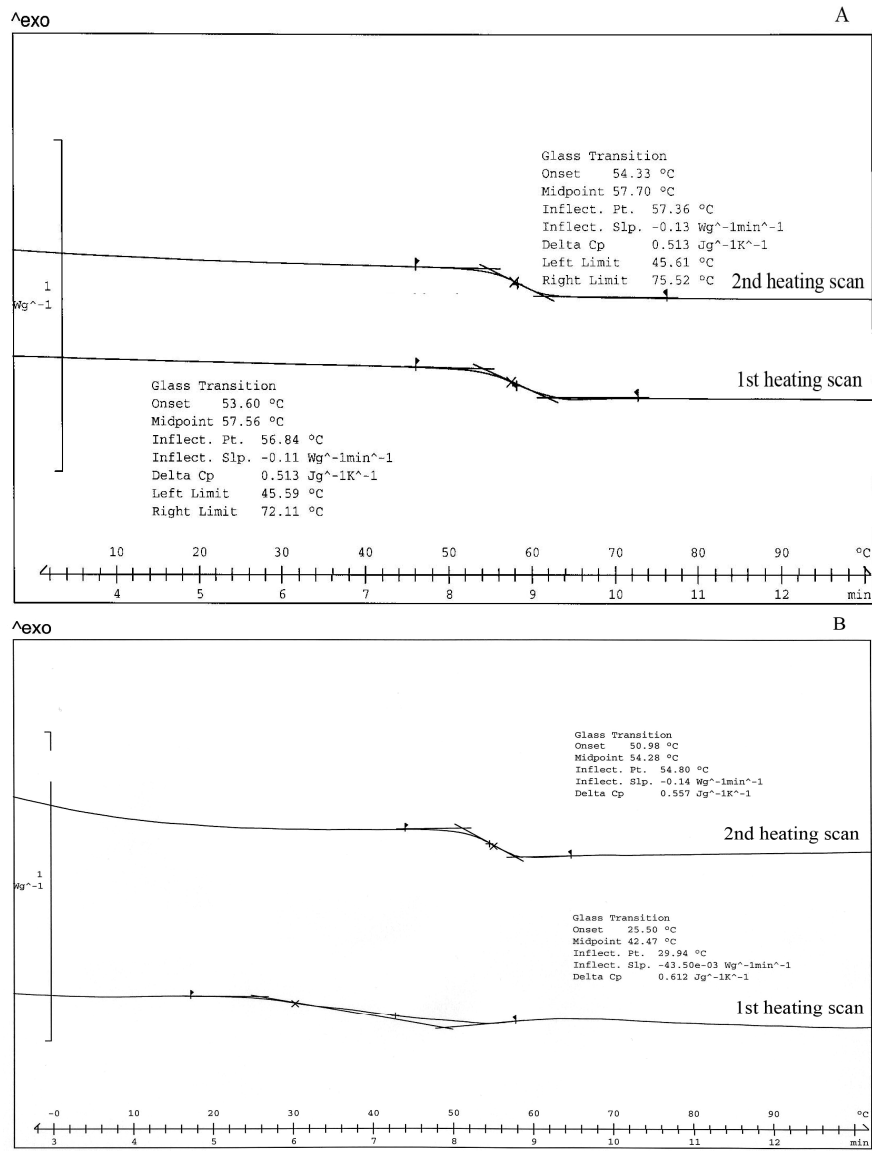


Figure 4.17. Thermographs related to PDLA grains (A) and PDLA microfabricated scaffold (B)



Part 1: scaffold production by microfabrication

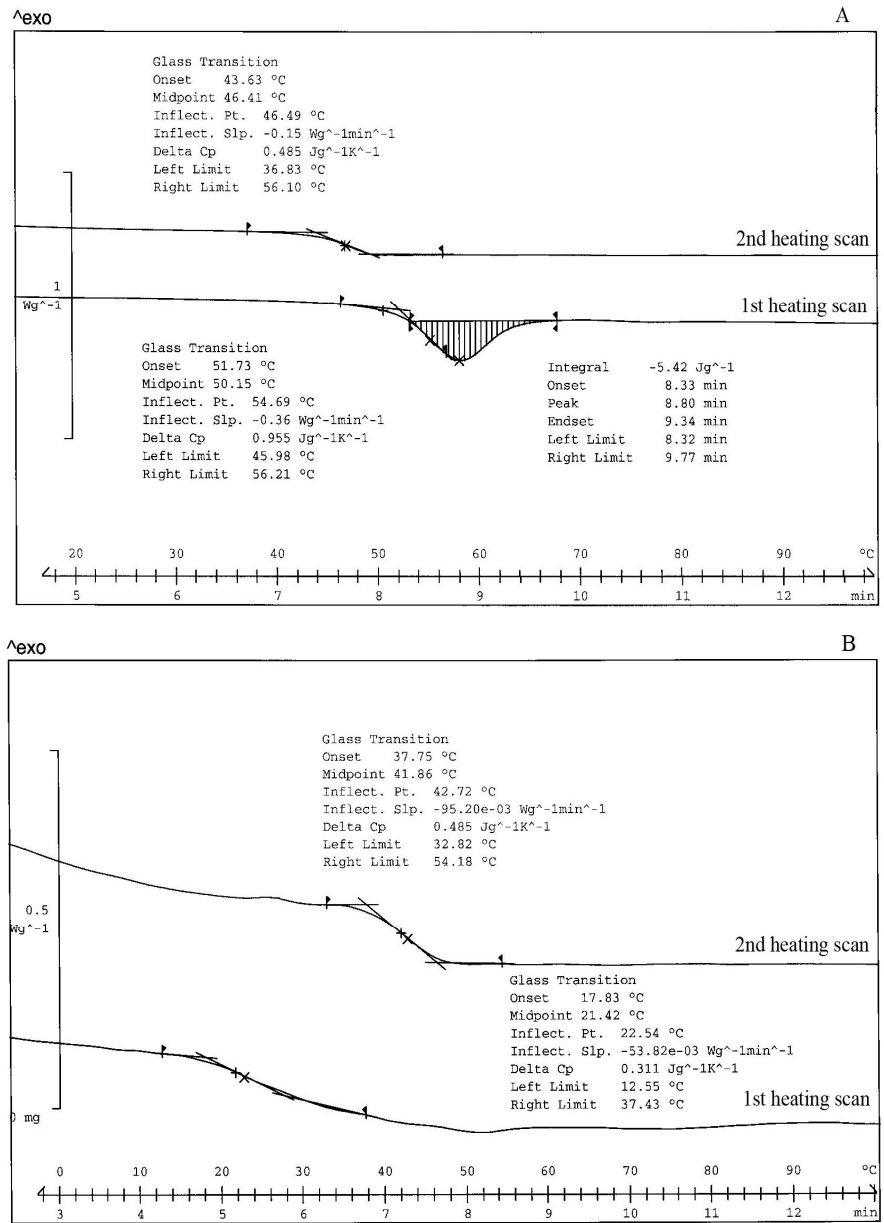


Figure 4.18. Thermographs of PLGA grains (A) and PLGA microfabricated scaffold (B)

Part 1: scaffold production by microfabrication

Table 4.6. DSC results for PDLA and PLGA grains, film and microfabricated scaffold

		1 <sup>st</sup> scan	2 <sup>nd</sup> scan
<b>PDLA</b> <b>raw</b> <b>material</b>	Tg	57.56°C	57,70°C
<b>PDLA</b> <b>Film</b>	Tg	36.72°C	46.47°C
<b>PDLA</b> <b>scaffold</b>	Tg	29.94°C	54.80°C
<b>PLGA</b> <b>raw</b> <b>material</b>	Tg	54.69°C	46.49°C
<b>PLGA</b> <b>Film</b>	Tg	7.66°C	14.73°C
<b>PLGA</b> <b>scaffold</b>	Tg	22.54°C	43.72°C

PLGA based grains during the first heating scan showed a first-order phase transition, i.e. an endothermic peak (Figure 4.18, A), just after Tg. This peak corresponds to the enthalpy involved in the relaxation of the more mobile polymer chains after Tg due to densification occurred during the polymer cooling but also storage. Densification reduces free volume and hence mobility of the glassy domains: the sudden increase in free volume at Tg enables the polymer chains relaxation if energy is furnished. This phenomenon is not present in the polymers second scan, being aging related, neither in the scaffold or cast film materials, due to the plasticizing effect of the residual solvent<sup>37</sup>.

#### 4.4.5 Attenuated total reflection infrared spectroscopy (ATR-FTIR)

Attenuated total reflection infrared (ATR-IR) spectroscopy analysis was used to identify spectra associated to the polymers before and after microfabrication process to evidence any possible variation inside the starting polymer chemical structure due to the process. Cast films from the same polymer solutions were analysed as well.

Both PDLA and PLGA spectra are reported in Figure 4.19 and Figure 4.20, respectively. The spectrum relative to DMF solvent is added.

Absorption peak near  $1670\text{ cm}^{-1}$ , typical for Amide I stretching vibration and characteristic for DMF solvent, reveals the presence of trapped solvent (DMF) inside the microfabricated scaffolds and cast film as previously shown by thermal analysis.

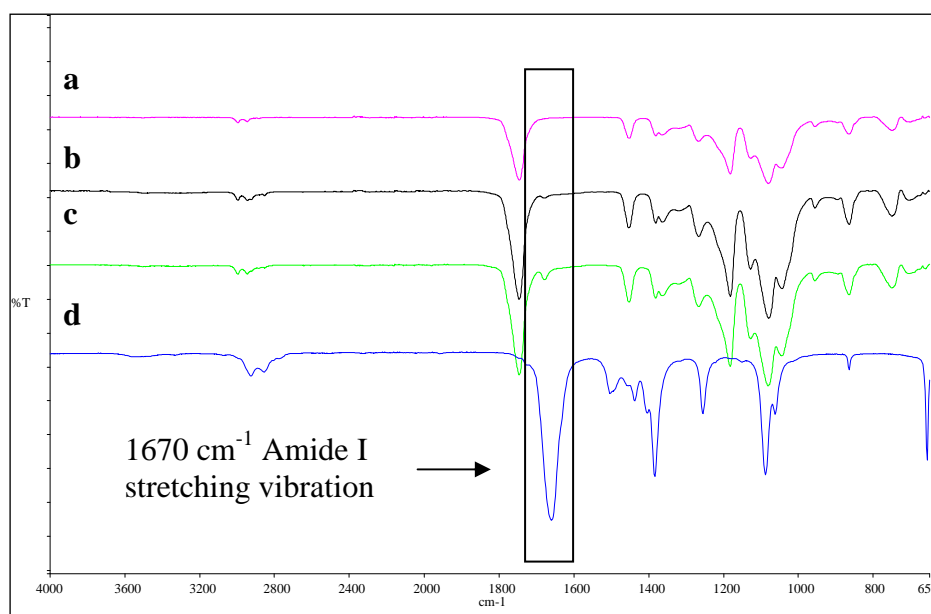


Figure 4.19. ATR spectra of PDLA a) powder, b) film, c) microfabricated scaffold, d) DMF

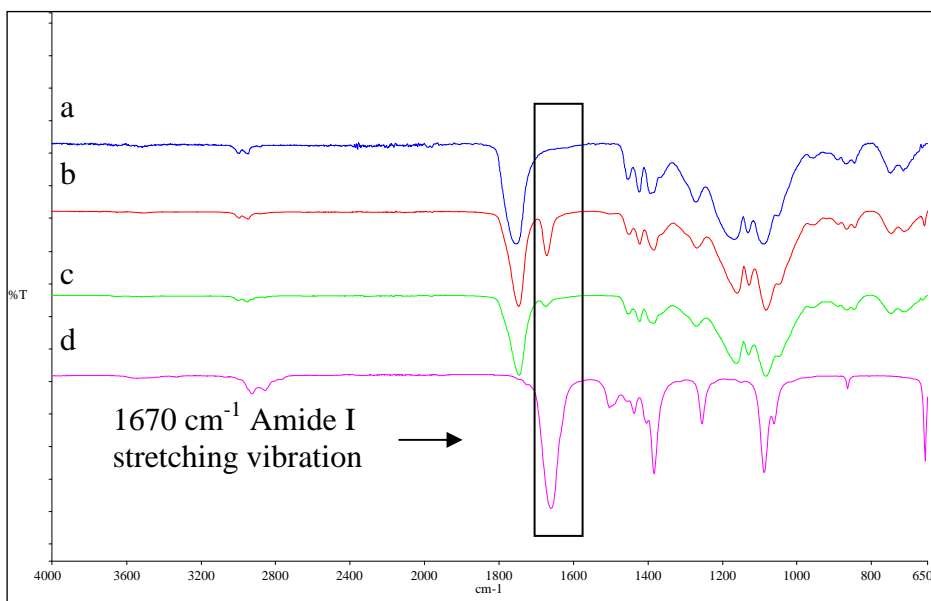


Figure 4.20. ATR spectra of PLGA a) powder, b) film, c) microfabricated scaffold, d) DMF

#### 4.4.6 Dynamic mechanical thermal analysis (DMTA)

Dynamic mechanical thermal analysis (DMTA) on PDLA and PLGA scaffold and cast film was performed to characterize the thermomechanical behavior of the polymeric products and to reveal differences in transition temperatures.

This practice is intended to provide means of determining the transition temperatures, elastic and loss moduli of the microfabricated scaffolds and films over the chosen range of temperatures at a specific frequency.

Plots of the storage modulus and loss factor are indicative of the viscoelastic characteristics of the polymer. These moduli are functions of temperature or frequency in polymers and change rapidly at particular temperatures or

frequencies. The regions of rapid modulus change are normally referred to as transition regions.

Figure 4.21 and Figure 4.22 show the storage modulus and loss factor as a function of temperature for PDLA and PLGA, microfabricated scaffolds and cast films, respectively.

In general microfabricated scaffold storage modulus for both polymers is quite low if compared with cast films, but this is simply due to the fact that in microfabricated scaffolds the resisting cross section is lower than the nominal one.

Decreasing of the storage modulus, which corresponds to a peak in the loss factor trend, indicates the glass transition temperature of the amorphous polymers. The value is particularly low because of the residual solvent still present inside the polymer, as stated before (chapter 4.4.5) which acts as a plasticizer thus reducing the  $T_g$  value.  $T_g$  values obtained by this characterization are lower than DSC, this fact being due to the lower heating rate in the DMTA.

In Figure 4.21 (B), the modulus  $E'$  of PDLA sharply decreases when temperature approaches the glass transition at about  $20^\circ\text{C}$ . Parallel to this, the loss factor increases until reaching a maximum value at about  $30^\circ\text{C}$ , that is identified as the glass transition temperature.

Notwithstanding, the loss factor doesn't evidence a sharp peak as in the case of the other materials because of technical problems.

PLGA scaffold storage modulus is extremely low, near the lower limit of the sensitivity of the apparatus and the first range of values at lower temperatures has to be neglected (Figure 4.22).

Around  $30^\circ\text{C}$ , the  $E'$  shows for the PLGA sample a peak just before the drop due to the glass-rubber transition ( $T_g$ ). This small peak reflects some

stiffening of the PLGA material preceding the  $T_g$ . This effect can be observed mostly in an amorphous material, and it has the origin in relaxation of internal stresses frozen during melt quenching<sup>38-41</sup>.

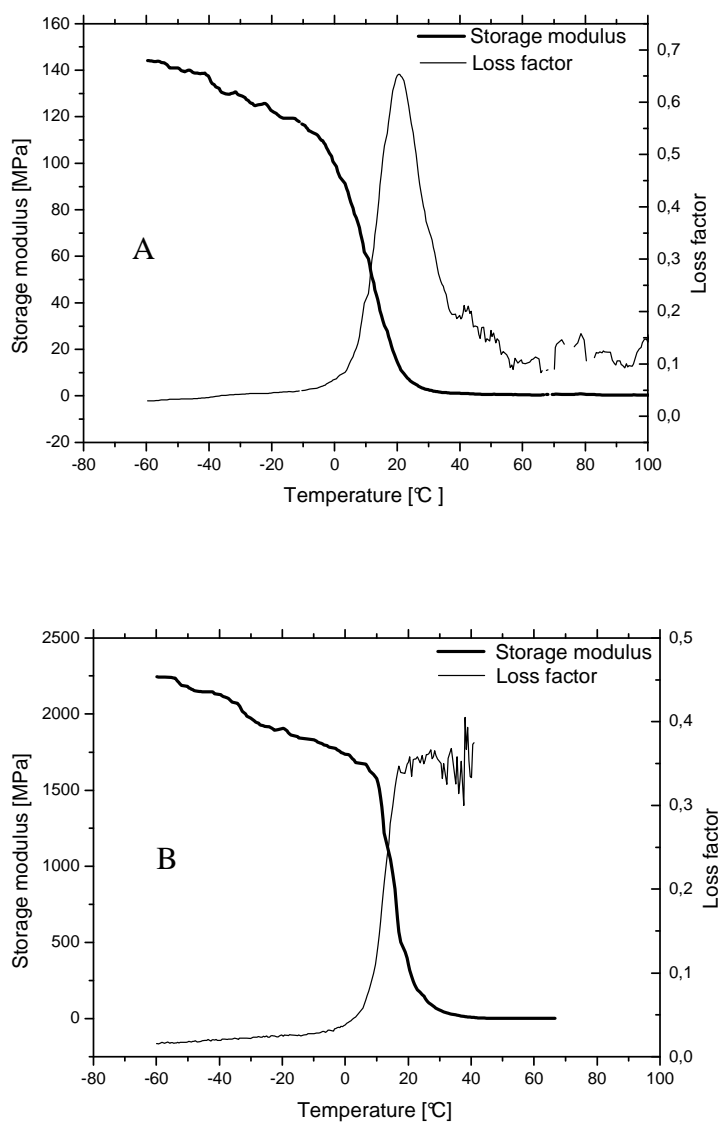


Figure 4.21. Plots of storage modulus and loss factor for PDLA microfabricated scaffold (A) and cast film (B) as a function of temperature

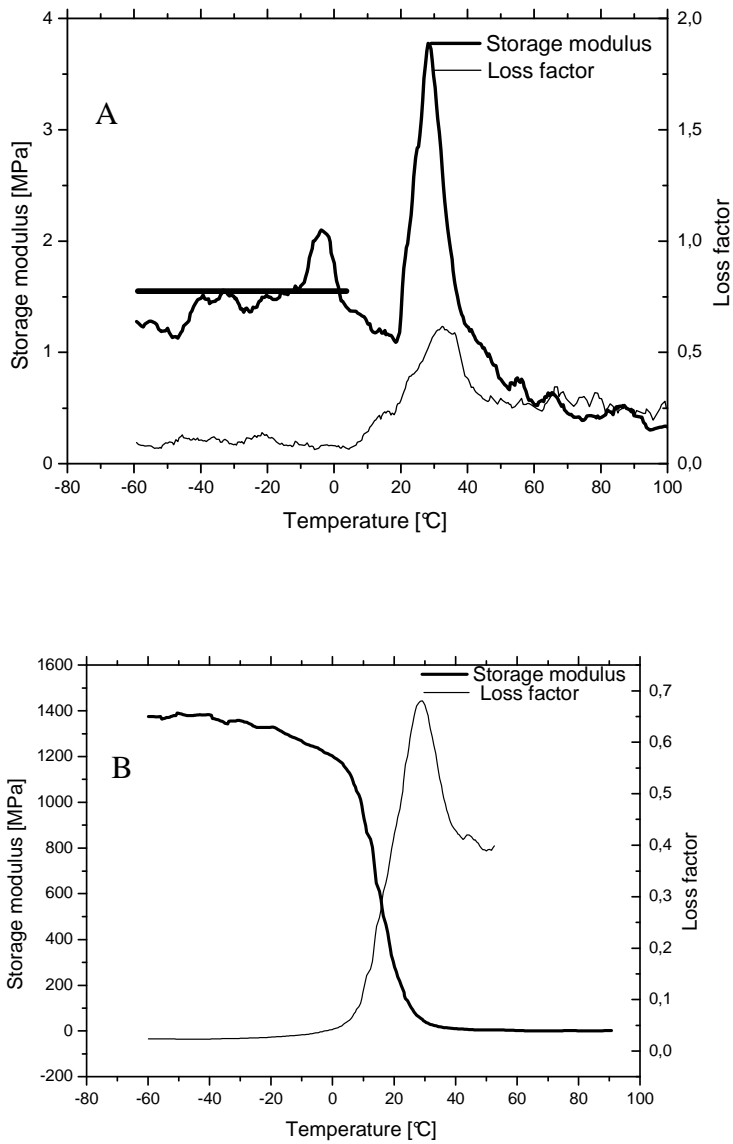


Figure 4.22. Plots of storage modulus and loss factor for PLGA microfabricated scaffold (A) and cast film (B) as a function of temperature

#### **4.4.7 Preliminary in vitro culture studies**

Human osteosarcoma derived osteoblasts (MG63) and human embryonal lung origin fibroblasts (MRC5) cell lines were seeded on microfabricated PDLA and PLGA scaffolds.

Cell attachment, growth and distribution over the chosen micro structured matrices, at two time points, was evaluated by SEM imaging.

In particular cells adhesion and their ability to enter into pores and proliferate also inside the micro structure was evaluated.



**PDLA microfabricated scaffolds:**

Figure 4.23 shows SEM imaging of an osteoblast (MG63) cell line culture on PDLA microfabricated scaffold after 7 days (A and B) and 14 days (C and D) of cell culture.

Osteoblast (MG63) grew extremely fast and after 7 days they were able to entirely cover the PDLA structure.

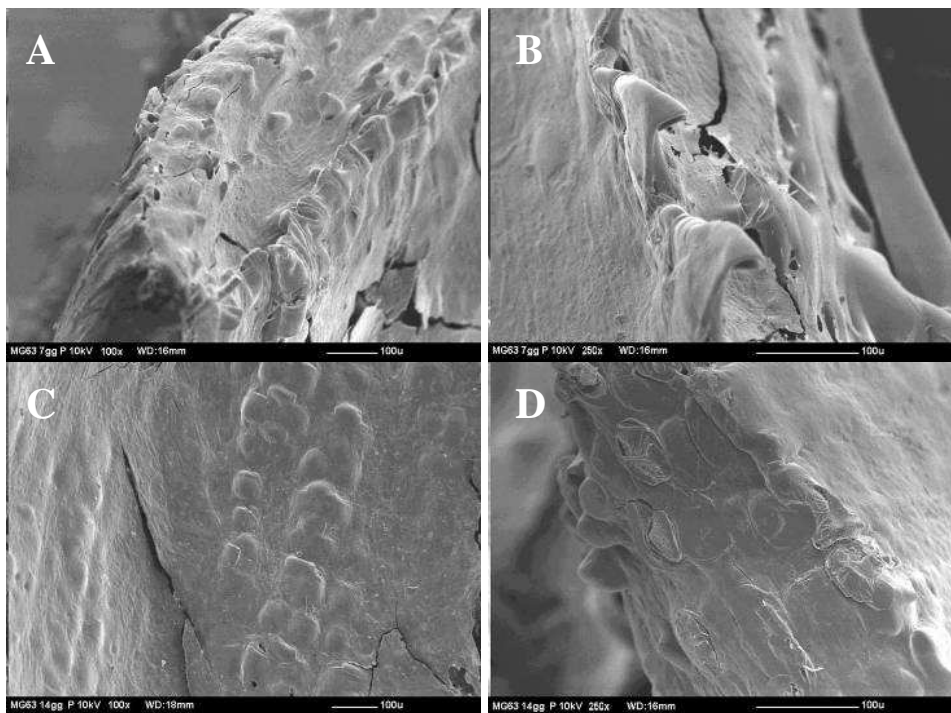


Figure 4.23. SEM images of PDLA scaffold after 7 days (A and B) and 14 days (C and D) of osteoblast MG63 cell culture; the marker indicates 100  $\mu\text{m}$

---

Part 1: scaffold production by microfabrication

---

Figure 4.24 reports the SEM imaging of fibroblasts (MRC5) cell culture on PDLA microfabricated scaffold after 7 days (A and B) and 14 days (C and D) of cell culture.

Growing for fibroblasts was slower, with part of the PDLA scaffold still uncovered after 7 days culture.

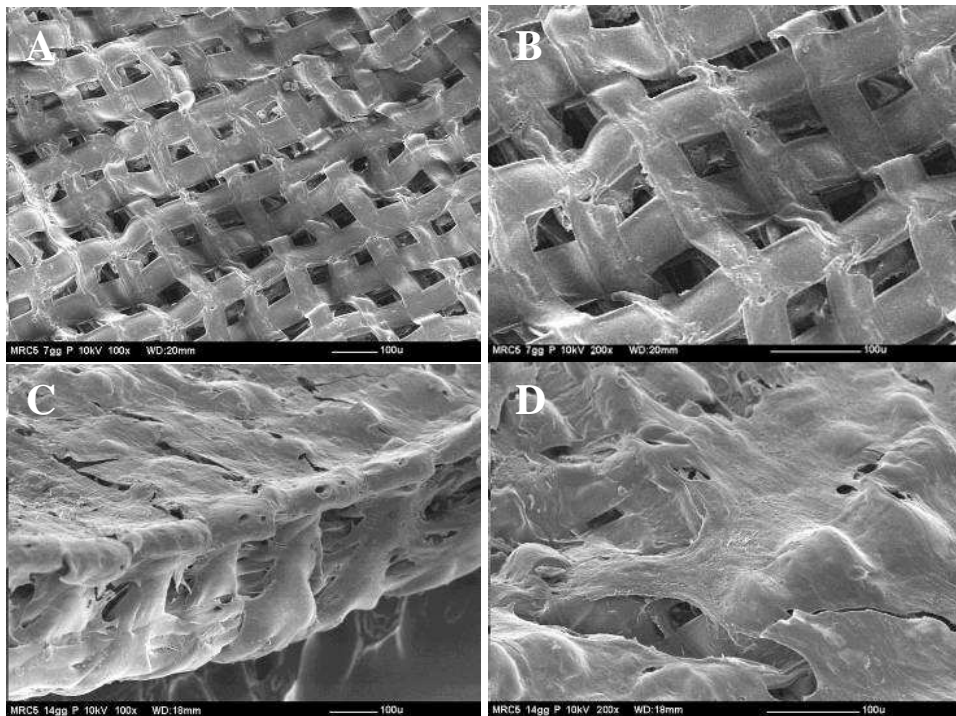


Figure 4.24. SEM images of PDLA scaffold after 7 days (A and B) and 14 days (C and D) of fibroblasts MRC5 cell culture; the marker indicates 100  $\mu\text{m}$

To evidence the ability of cells to grow also inside the three dimensional structure were unfolded and SEM imaging of the inner part were taken.

Figure 4.25 and Figure 4.26 show the internal part of a scaffold seeded with osteoblasts (MG63) and fibroblasts (MRC5), respectively.

---

## Part 1: scaffold production by microfabrication

---

In both cases, osteoblasts and fibroblasts could invade the inner part of the scaffolds, with cells adhering to single filaments or bridging between different filaments of the pore walls. In general, osteoblasts penetrated the scaffolds more than fibroblasts, confirming their faster growth as observed on the scaffold external surfaces. No modifications of the scaffold geometry and integrity were detectable after 14 days of cells culture.

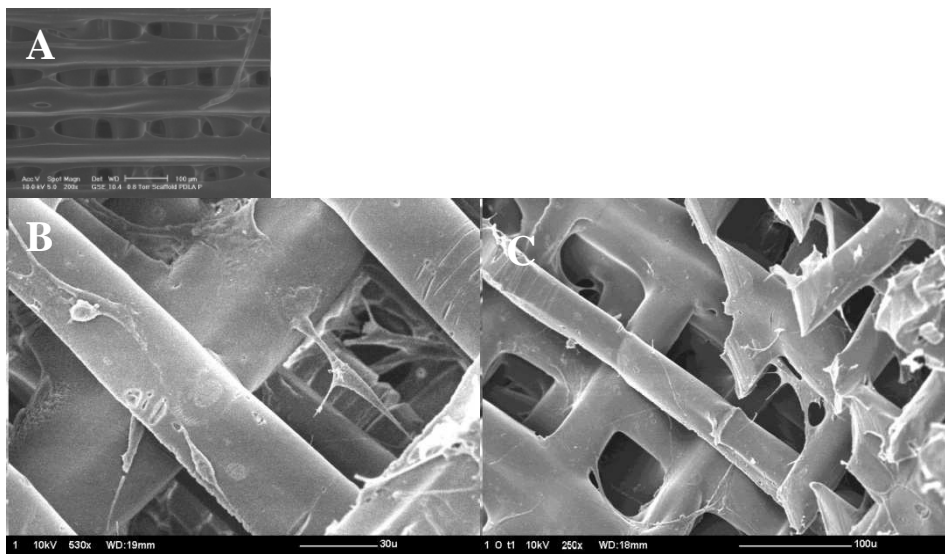


Figure 4.25. SEM images of inner layers of PDLA microfabricated scaffold after osteoblasts MG63 cell seeding (7 days); (A) PDLA microfabricated scaffold before seeding, chapter 4.4.1, (B, C) different magnifications; markers indicate 30  $\mu\text{m}$  (B) and 100  $\mu\text{m}$  (C)

Part 1: scaffold production by microfabrication

---

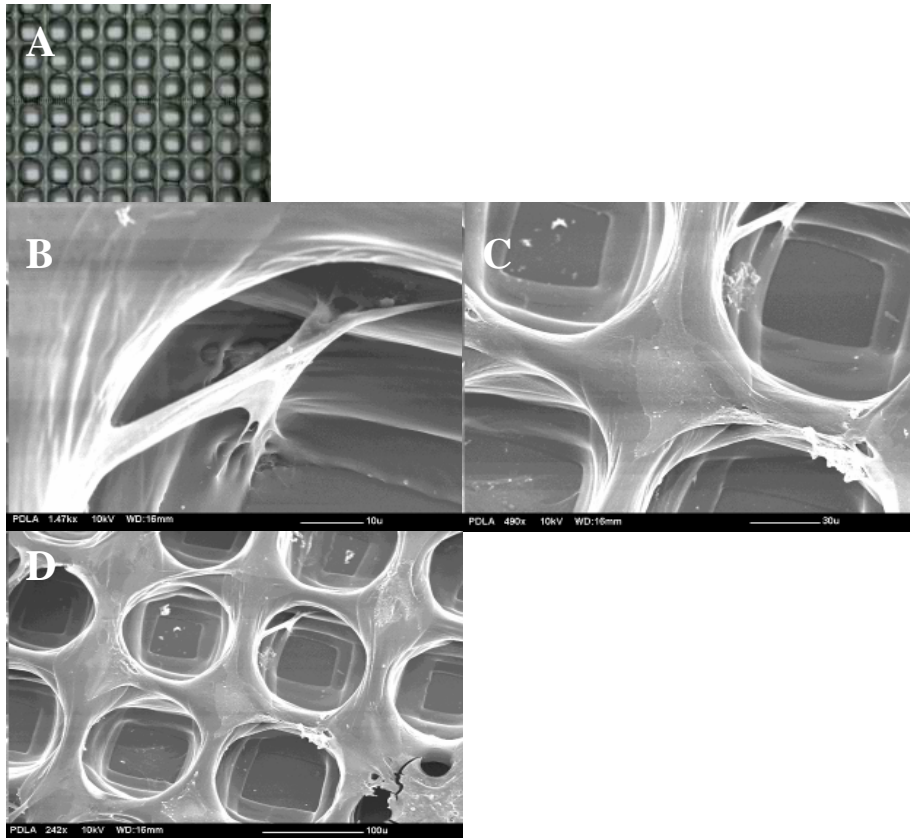


Figure 4.26. SEM images of inner layers of PDLA microfabricated scaffold after MRC5 cell seeding (7 days) ; (A) PDLA microfabricated scaffold before seeding, chapter 4.4.1, (B, C) different magnifications markers indicate 10 μm (B), 30 μm (C) and 100 μm (D)

**PLGA microfabricated scaffolds:**

Cell culture tests on PLGA microfabricated scaffold were performed and SEM imaging evaluation was done at day 7 and 14.

Figure 4.27 and Figure 4.28 show the SEM imaging results for osteoblasts and fibroblasts cell culture, respectively.

PLGA scaffolds were fully covered by a cell layer that was quite denser in the case of osteoblasts.

No evidence of cell migration inside the scaffold could be detected, this being however due to the more compact structure of the PLGA scaffolds with respect to the PLDA. After 14 days culture, evident signals of degradation were visible.

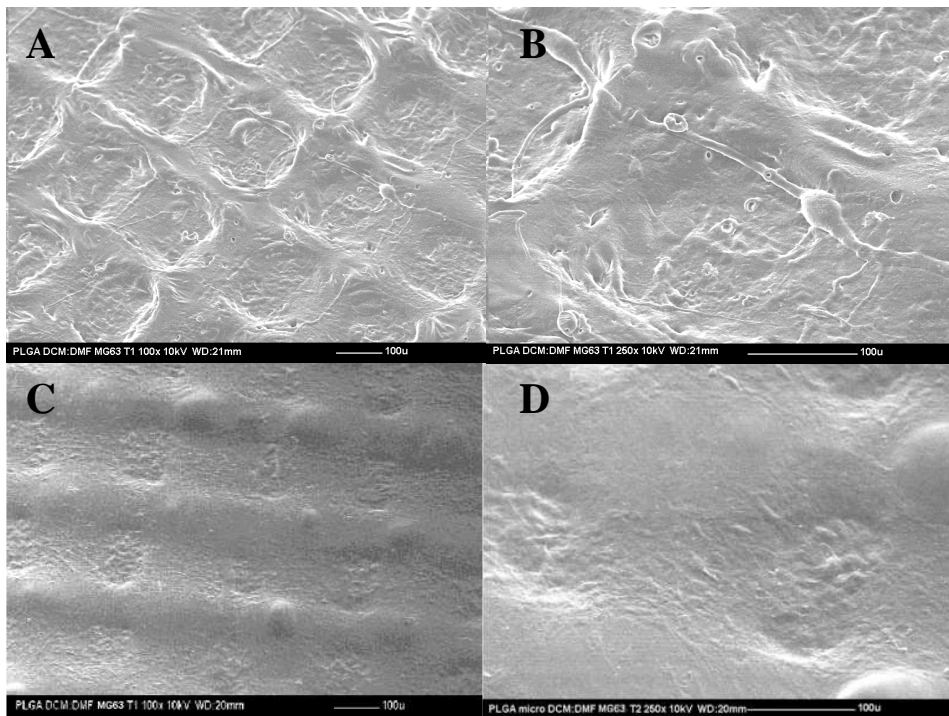


Figure 4.27. SEM images of PLGA scaffold after 7 days (A and B, different magnifications) and 14 days (C and D, different magnifications) of osteoblasts (MG63) cell culture; in all the micrographs markers indicate 100 μm

Part 1: scaffold production by microfabrication

---

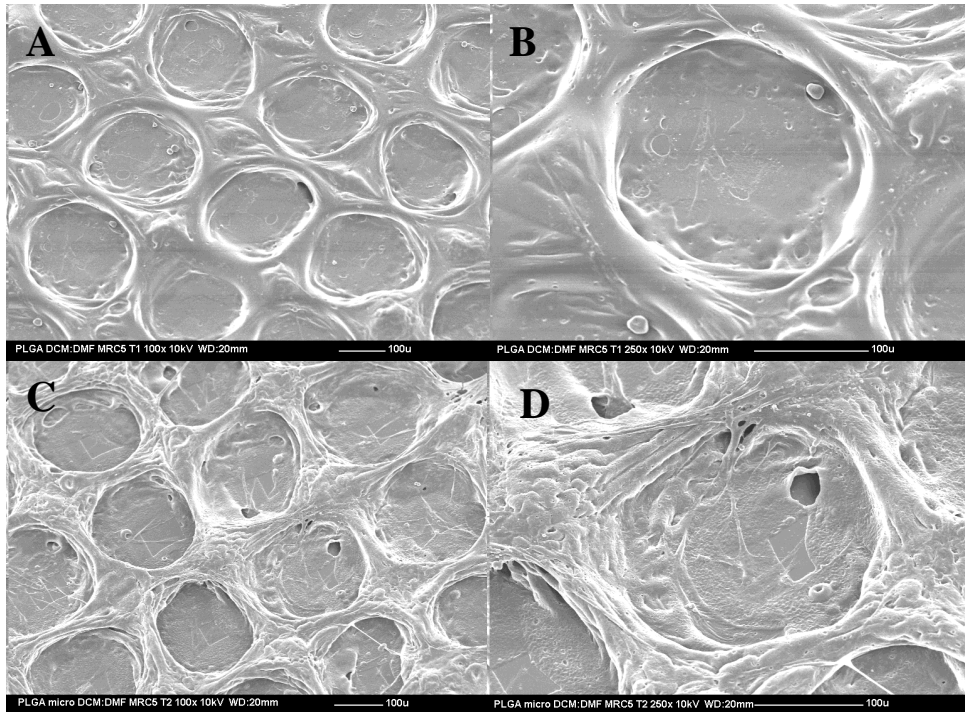


Figure 4.28. SEM images of PLGA scaffold after 7 days (A and B) and 14 days (C and D) of fibroblasts MRC5 cell culture; in all the micrographs markers indicate 100  $\mu$ m

## **4.5 Results and Discussion: microfabrication of chitosan scaffold**

### **4.5.1 Microfabrication of chitosan scaffold**

Microfabrication of chitosan scaffold was conducted starting from 3% (w/v) chitosan solution.

The final matrix is composed by 80 overlapped layers resulting in a well ordered geometry structure having 170  $\mu\text{m}$  large square holes and thickness of about 100  $\mu\text{m}$ .

Figure 4.29 shows the optical microscope imaging of a microfabricated scaffold.

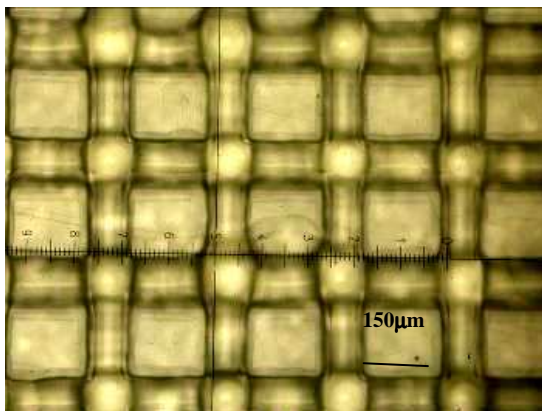


Figure 4.29. Optical microscopy imaging of 80 layer chitosan scaffold

The usage of chitosan material in robotic dispensing systems (RPBOD) but at a different scale level compared to the microfabrication technique has been widely studied by other research groups<sup>42</sup>.

These studies revealed the necessity to use sodium hydroxide (NaOH) as a dispensing medium to neutralize chitosan thus forming a gel-like precipitate.

In our first attempts we tried to microfabricate chitosan scaffolds extruding the polymer solution directly into a sodium hydroxide-ethanol solution but the micrometric fibres couldn't attach to each other forming the final scaffold. Comparing the microfabrication technique with other RP systems, the extruded filament has reduced micrometric dimensions and fibres floated in the medium. On the other side, the high evaporation of the solvent did not require precipitating the extruded filament in sodium hydroxide to make it solid.

Chitosan scaffolds were thus prepared by microfabrication on a PET sheet and later on treated with NaOH instead of using a coagulation medium.

Figure 4.30 shows LV-SEM imaging of microfabricated chitosan scaffolds. The final matrix resulted very thin even after 80 layers of deposition, with a film shape appearance; this is due to the low concentration of the starting chitosan solution.



---

Part 1: scaffold production by microfabrication

---

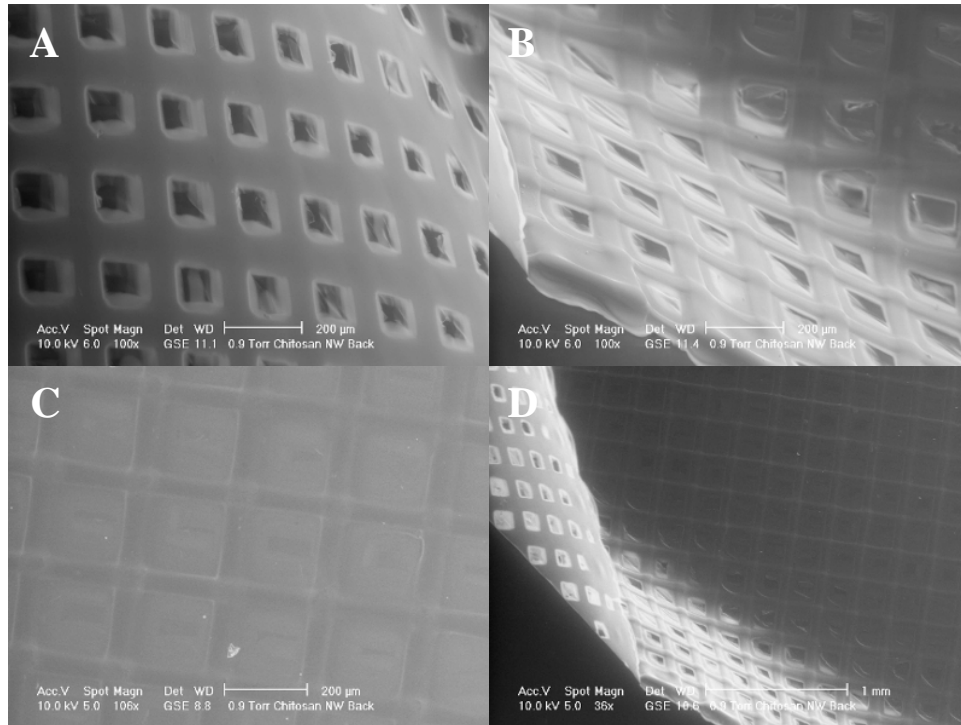


Figure 4.30. LV-SEM imaging of 90 layer chitosan scaffold at different magnifications

In general, the produced chitosan scaffold was kept in 1 M NaOH for one hour to neutralize the acetic acid and then washed with distilled water

After the neutralization and washing steps, the samples were examined with LV-SEM and the photographs are presented in Figure 4.31.

It can be observed that chitosan scaffolds, even after few deposited layers (20 in this specific case), maintained their shape and a regular structure after NaOH treatment. As the previous one, the layers stuck to each other forming a membrane structure.

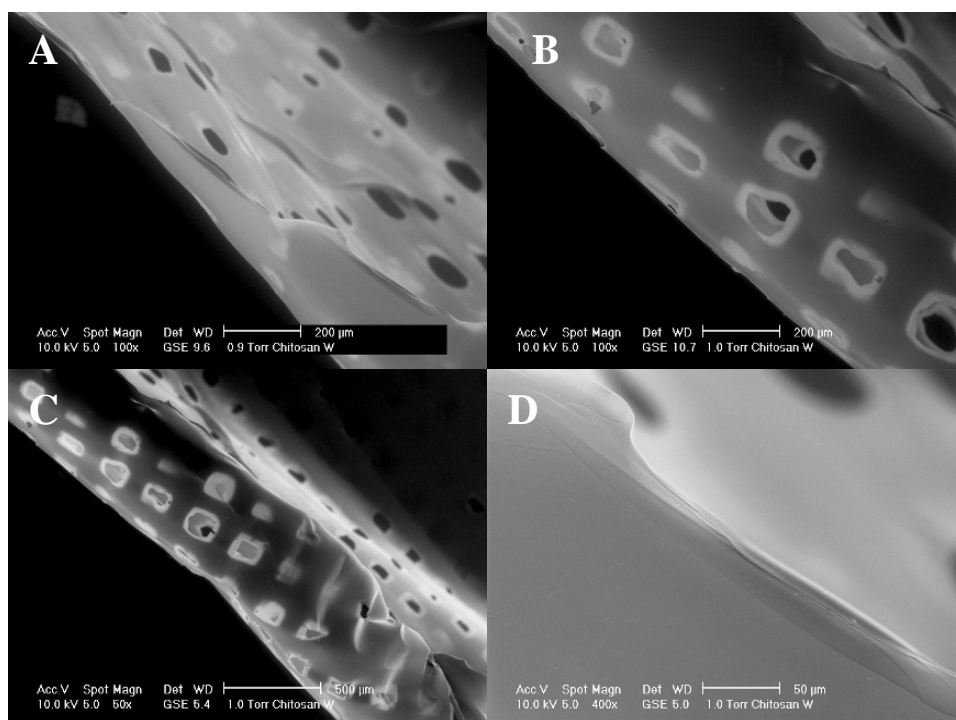


Figure 4.31. LV-SEM imaging of 20 layer chitosan scaffold at different magnifications after Na OH treatment

Preliminary *in vitro* cultures studies with osteoblasts MG63 cell line were conducted on microfabricated chitosan scaffolds.

Chitosan scaffolds, which were not treated with NaOH, broke into pieces after 7 days of cell seeding as shown in Figure 4.32.

Without NaOH washing the non neutralized material resulted to be not stable. Furthermore cells were not present on the scaffold surface owing to acetic acid still present inside the material and not completely washed away; this made the material not biocompatible and suitable for cells adhesion.

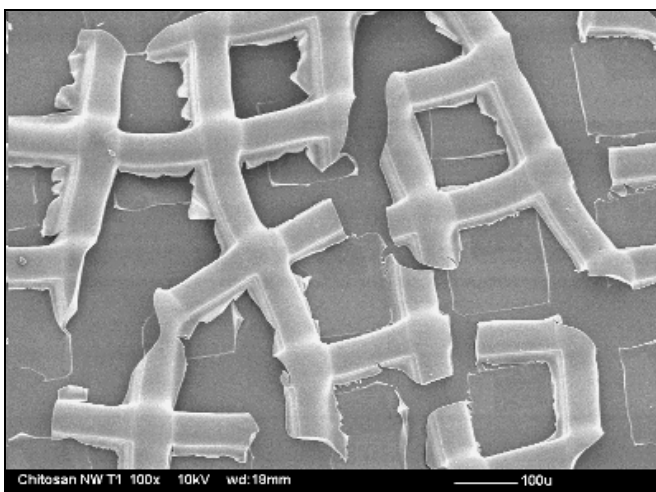


Figure 4.32. SEM imaging of chitosan scaffold without NaOH treatment after preliminary in vitro culture studies with osteoblast MG63 cell line after 7 days

#### 4.5.2 Nuclear magnetic resonance (NMR)

$^{13}\text{C}$  CP-MAS NMR spectroscopy has been revealed to be a good method to identify the degree of acetylation of chitin and chitosan<sup>43</sup>.

The chemical behaviour of chitin and related materials strongly depends on the degree of acetylation (DA), a parameter defined as the mole fraction of acetylated units in the polymer chain<sup>20</sup>.

Among all the available techniques commonly used to determine the DA value<sup>21,43</sup>,  $^{13}\text{C}$  nuclear magnetic resonance (NMR) spectroscopy is one of the most powerful, allowing a direct determination of DA of both soluble and non-soluble samples; no specific sample preparation is needed.

$^{13}\text{C}$  CP-MAS spectrum of chitosan powder is given in Figure 4.33.

---

Part 1: scaffold production by microfabrication

---

At 105.033 ppm, the resonance of the anomeric carbon C(1) of the glucosamine unit is observed. The resonances at 174.555 ppm and 23.735 ppm are attributable respectively to the carbonyl C(7) and to the methyl C(8) of N-acetylglucosamine units while the resonances at 61.147 ppm and 58.284 ppm to C(6) and C(2) correspondingly. At 75.553 ppm, a set of overlapped resonances is due both to C(3) and C(5). C(4) resonates at 82.698 ppm.

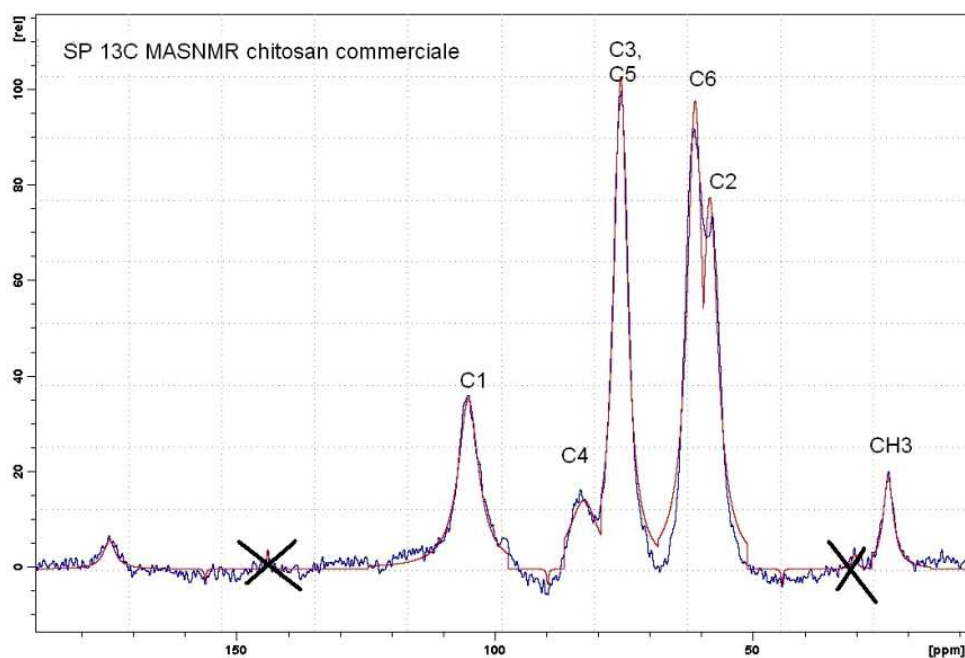


Figure 4.33. <sup>13</sup>C CP-MAS NMR spectra of chitosan

Chemical shifts of chitosan are given in Table 4.7.

Table 4.7. Chemical shifts of chitosan obtained by  $^{13}\text{C}$  CP-MAS NMR

<b>Functional group</b>	<b>Chemical shift</b>
C=O	174.555
C1	105.033
C4	82.698
C3	75.553
C6	61.147
C2	58.284
CH <sub>3</sub>	23.735

$^{13}\text{C}$  solid-state NMR appears to be the most reliable for the evaluation of the acetyl content. The degree of acetylation (DA) is usually calculated by measuring the integral of the carbonyl or methyl group divided by the integral of all the carbon atoms in the backbone.

In this study, the degree of acetylation was evaluated from the relative integrals of methyl group compared to the carbon integrals of the polysaccharidic backbone. The degree of acetylation of chitosan used was found as 22%.

### 4.5.3 Rheological test on Chitosan solution

Chitosan solution flow behaviour was characterized by rheological tests and a proper working range of viscosity, in respect to the microfabrication process, was determined.

Shear viscosity over a chosen frequency range between 1 and 100 rad/s was measured.

Figure 4.34 shows the resulted graphs; in particular average complex viscosity is reported in Figure 3.34 A and solvent evaporation was evaluated comparing the viscosity variations after three following tests, Figure 3.34 B. Table 4.8 reports the numerical values of viscosities at specific frequencies. In respect of chitosan solution, a significant evaporation was not expected since boiling point of water and acetic acid (118°C) are quite high. Chitosan solution showed a complex viscosity that remains almost constant (Newtonian behaviour) over the selected frequency range. Chitosan solution at the chosen solution concentration is therefore very stable, because the viscosity does not depend on the imposed frequency and the solvent evaporation can be neglected. For this reason chitosan solution yields to reproducible tissue engineering scaffolds.

Part 1: scaffold production by microfabrication

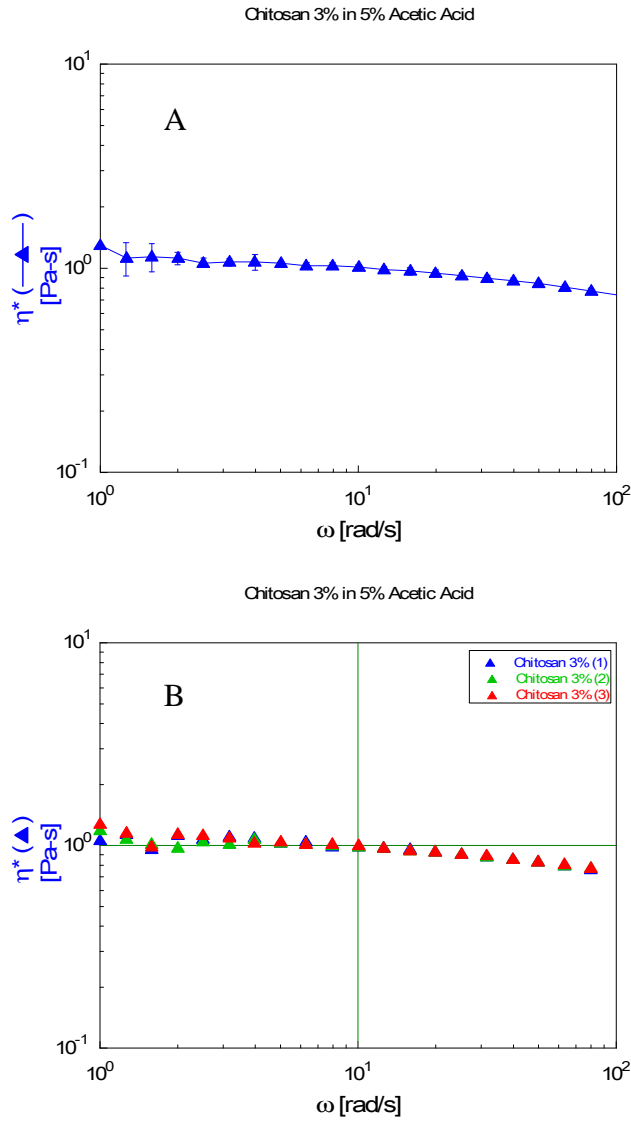


Figure 4.34. Complex viscosity plotted over frequency. (A) average viscosity (B) solvent evaporation evaluation

Table 4.8. Viscosity values of Chitosan solution at chosen frequency values

Test frequency [rad/sec]	Viscosity [Pas]
1	1.28
10	1.00
100	0.74

#### 4.5.4 Differential scanning calorimetry (DSC)

Differential scanning calorimetry analysis (DSC) was performed on the base chitosan powder and on the microfabricated scaffold to evidence material transitions and evaluate any possible modification of polymer due to the process.

Cast film was analysed as well as control.

DSC thermograms of chitosan powder, film and microfabricated scaffolds are presented in Figure 4.35.

Table 4.9 reports the evaluated values related to material transitions obtained by DSC analysis.

The graphs evidence a broad endothermic peak close to 100°C, attributed to evaporation of residual water or solvent, eliminated during the first heating scan.

The exothermic peak at approximately 300°C, according with previous studies<sup>44,45</sup> was due to the degradation of the main chain.

Glass transition temperature of chitosan is not clearly detectable from the graphs even if a weak signal can be observed at around 200°C, especially in chitosan film sample. In general Tg in chitosan is a subject of controversy. Being a natural polymer some properties like crystallinity, molecular weight, deacetylation degree can show wide variations according to the source and/or method of extraction and will influence the Tg.

Considering the starting heat of evaporation of pure water and acetic acid, 2257 J/g and 402 J/g respectively, the resulting heat of evaporation of 5% v/v acetic acid solution is 2164 J/g. From the integral of endothermic



evaporation peaks in the first runs the amount of water (in powder) or solvent (film and microfabricated scaffold) evaporated is calculated and the degradation exothermic peak is normalized to the actual mass involved during transformation.

Some differences between powder, film and scaffold related to the degradation process were detected; in particular degradation in chitosan powder occurred at higher temperature and bigger amount of material was involved.

Since film and scaffold showed a similar behaviour, it is possible to state that there was not a significant degradation associated to the microfabrication process.

For our purposes we are not interested in knowing specifically the kinetic of degradation happening to the polymer at high temperatures and which would require additional analysis. Conversely identifying any possible alteration occurring to the material due to the microfabrication process is of main interest in this work.

Part 1: scaffold production by microfabrication

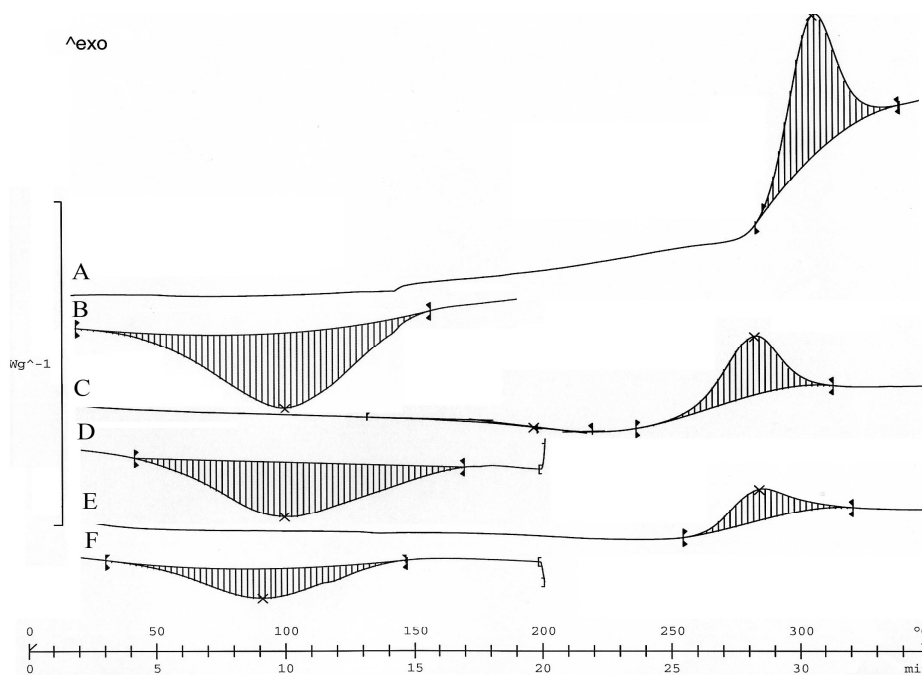


Figure 4.35. Thermographs of Chitosan powder first run (B) and second run (A). Chitosan film first run (D) and second run (C). Chitosan microfabricated scaffold first run (F) and second run (E)

Table 4.9. Transformations main values after DSC analysis of Chitosan powder, film and microfabricated scaffold

+	<b>Powder</b>		<b>Film</b>		<b>Scaffold</b>	
	<b>Initial weight [mg]</b>	9.6	10.3	5.5		
<b>Run</b>	1 <sup>st</sup>	2 <sup>nd</sup>	1 <sup>st</sup>	2 <sup>nd</sup>	1 <sup>st</sup>	2 <sup>nd</sup>
<b>Onset Temperature [°C]</b>	48	290	52	261	50	266
<b>Integral [mJ]</b>	1828	1222	2091	872	767	425
<b>Evaporated mass [mg]</b>	0.8		0.96		0.35	
<b>Normalized integral [J/g]</b>		139		93		83

#### **4.5.5 Attenuated total reflection infrared spectroscopy (ATR-FTIR)**

Infrared Spectroscopy analyses were performed on chitosan powder, cast film and microfabricated scaffold to evidence possible modifications due to the process.

ATR spectra of chitosan film, powder and microfabricated scaffold are given in Figure 4.36.

The spectra are comparable and no considerable differences can be observed.

The absorption bands observed at 1580 and 1645  $\text{cm}^{-1}$  are due to the  $-\text{NH}$  bending vibration in amine groups and the stretching vibration of  $\text{C}=\text{O}$  amide bond, respectively. The absorption at about 1645  $\text{cm}^{-1}$  is typical of non-deacetylated bonds of chitosan. The broad peak at 2860  $\text{cm}^{-1}$  may be attributed to C-H stretching vibrations and -H stretching linked to cyclic ring. The peak at 3300  $\text{cm}^{-1}$  is due to OH linked to polymer.

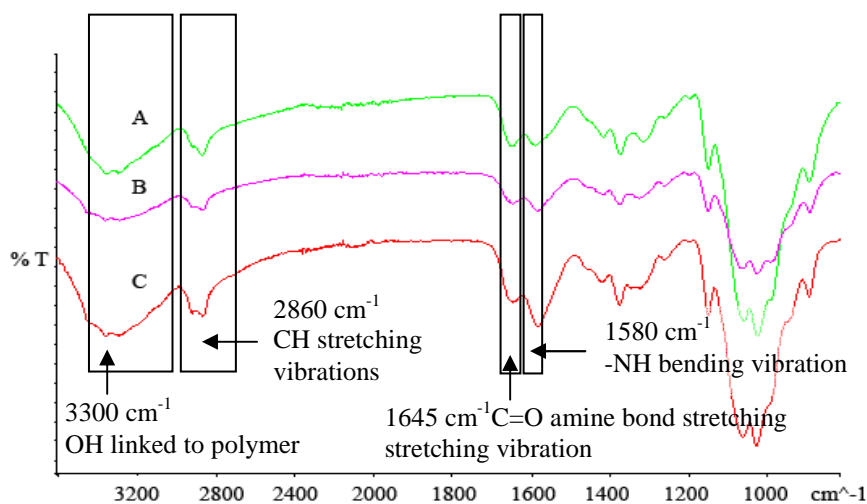


Figure 4.36. ATR spectra of chitosan a) powder, b) film and c) microfabricated scaffold

#### 4.5.6 Dynamic mechanical thermal analysis (DMTA)

The dynamic-mechanical thermal analysis (DMTA) of polymeric materials in general is of great interest resulting from its great sensitivity in detecting transitions and changes of internal molecular mobility and in probing a phase structure and morphology of polymers.

DMTA thermographs reveals relaxation phenomena through peaks in loss factor curve. The main of them are known as  $\alpha$  and  $\beta$  relaxation. The  $\beta$  relaxation has been assigned to the local mode of relaxation in the amorphous phase. The  $\alpha$  relaxation related to the glass transition of the amorphous phase is controlled by both intra- and intermolecular interactions. It is accompanied by a distinct decrease of the storage modulus  $E'$  with increasing temperature and the presence of  $E''$  peak.

DMTA was performed on chitosan scaffold and cast film, as comparison, to evidence the main material transitions.

Storage modulus ( $E'$ ) and loss factor ( $\tan \delta$ ) curves as a function of temperature of chitosan film and scaffold are given in Figure 4.37.

In particular the transition at about  $-18^{\circ}\text{C}$  could be attributed to  $\beta$  relaxation, representing a local motions of side groups in chitosan, while the peak at  $150^{\circ}\text{C} - 178^{\circ}\text{C}$  was related to  $\alpha$  relaxation, which is  $T_g$  of chitosan.

DMTA analysis usually shows  $T_g$  transitions much more evident if compared to DSC analysis due to drastic drop of  $E'$ . Furthermore in our specific case a slower heating rate ( $3^{\circ}\text{C}/\text{min}$ ) during DMTA analysis caused a lower  $T_g$ . When heating rate is faster there is not enough time for the polymer to dissipate heat energy along the polymer chains and  $T_g$  is observed at higher temperature.

Storage modulus showed a minimum value at  $40^{\circ}\text{C}$ . This can be explained as a structural reorganization of packing of chitosan molecules due to an increase of residual water mobility, volume expansion and change of hydrogen bond strength.

As expected in the case of chitosan scaffold the modulus was lower than the film since the scaffold has a porous weaker structure.

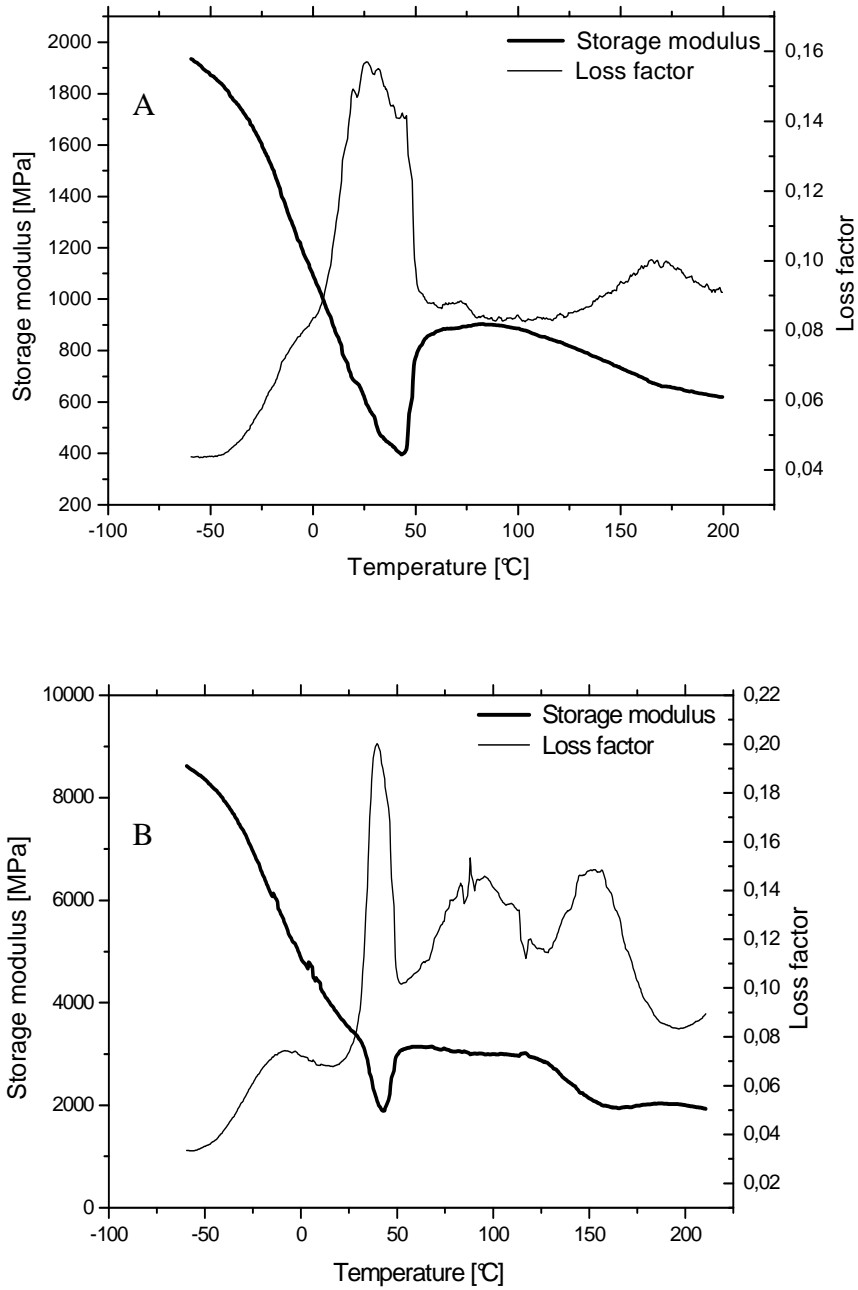


Figure 4.37. DMTA thermographs of chitosan scaffold (A) and cast film (B)

---

### **4.5.7 Preliminary *in vitro* culture studies**

After stabilization with NaOH treatment, the produced chitosan scaffold underwent to preliminary *in vitro* culture studies.

Cancerous osteoblasts (MG63) and fibroblast (MRC5) cell lines were seeded on the microfabricated chitosan scaffolds.

Two different time points were chosen: 4 and 10 days.

SEM imaging evaluated scaffold and cell morphology as well as cell attachment and growing.

Figure 4.38 and Figure 4.39 show SEM imaging of scaffolds after chosen time points of *in vitro* osteoblasts and fibroblasts cell culture.

It can be observed how scaffolds maintained their shape during cell culture.

Cells could spread, attach and grow on the microfabricated scaffolds confirming the biocompatibility character of the material; moreover pores were easily invaded by cells.

In general, as previously observed for synthetic polymer scaffolds, osteoblasts grew faster than fibroblasts.

---

Part 1: scaffold production by microfabrication

---

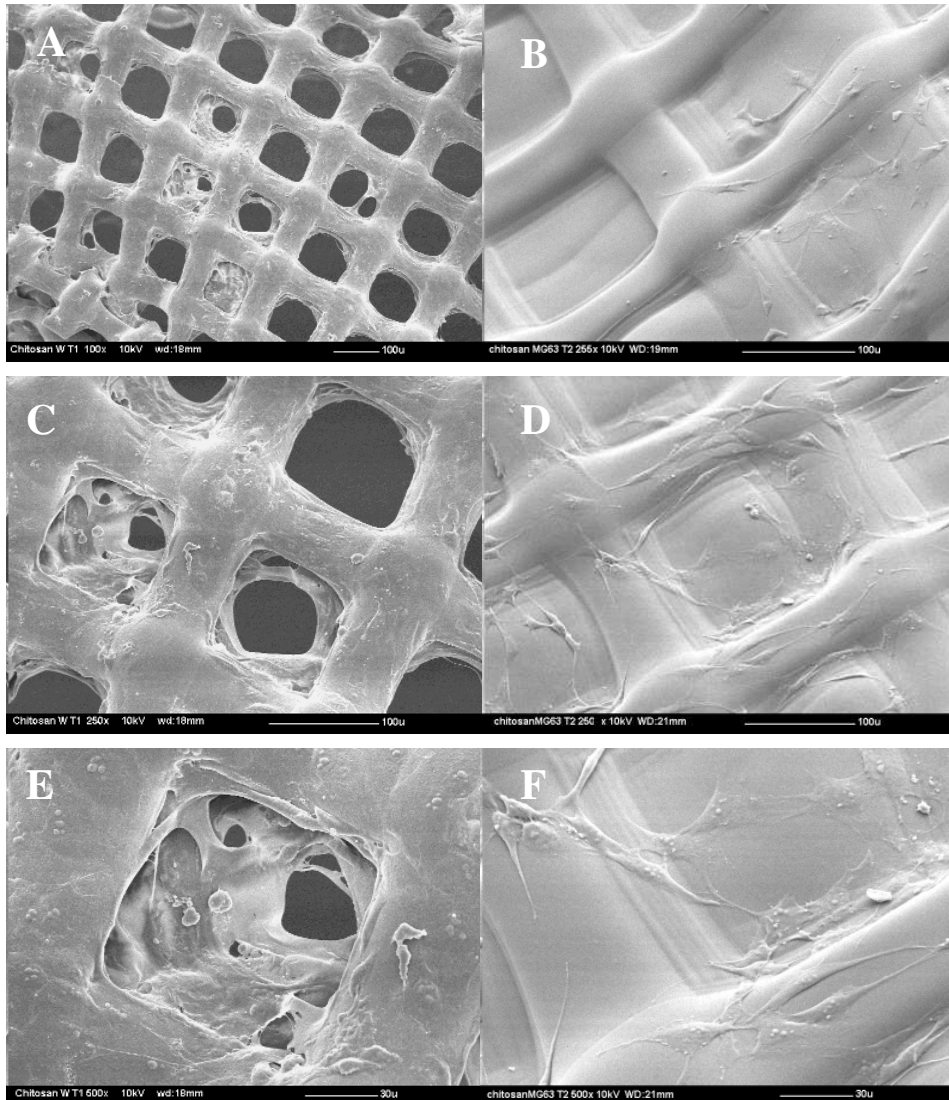


Figure 4.38. SEM imaging of chitosan microfabricated scaffold after 4 days (A, C, E) and 10 days (B, D, F) cell seeding with MG63 cell line. A, B, C, D, E, F different magnifications

As shown in Figure 4.38 (B, D, F) some chitosan scaffolds didn't show a porous structure. The firsts layers could sometime spread entirely on the substrate and the following layers formed on this first chitosan film. The



---

Part 1: scaffold production by microfabrication

---

reason for this difference could be attributed to variations in environmental conditions such as temperature or air humidity.

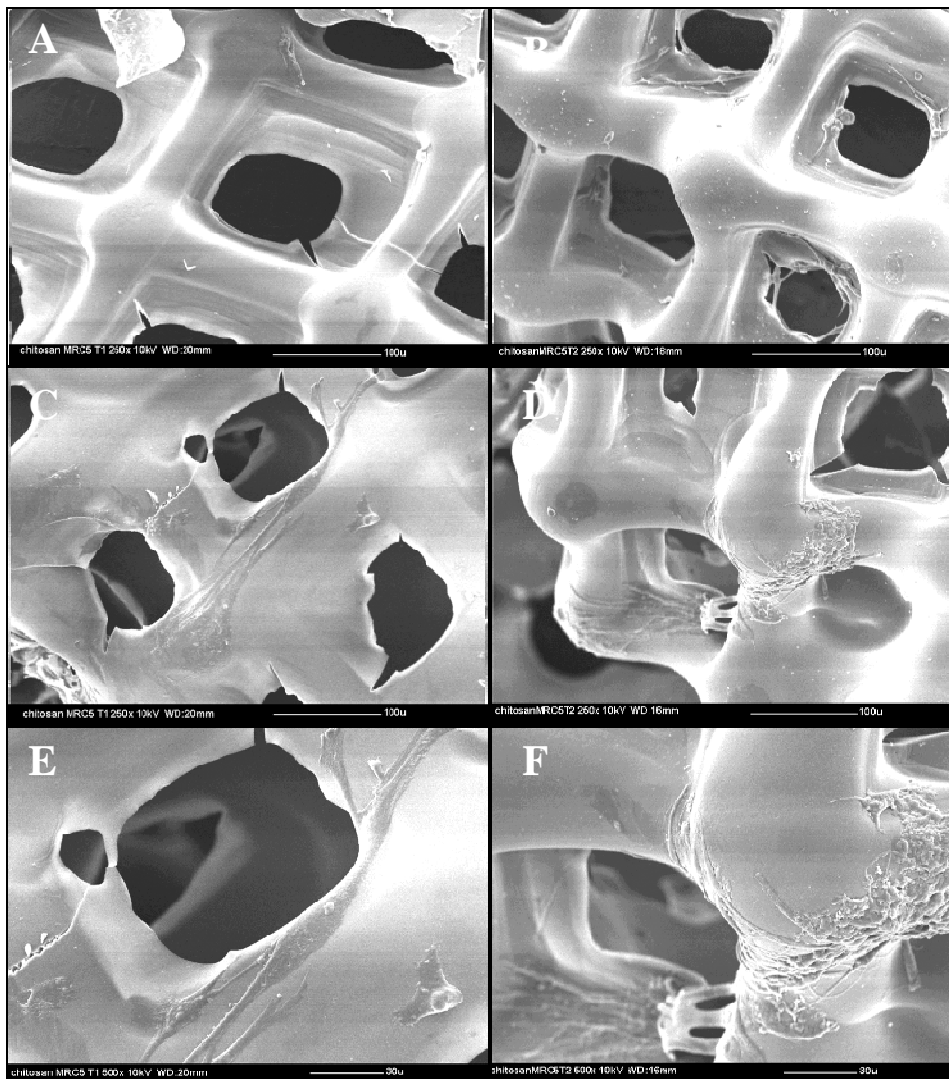


Figure 4.39. SEM imaging of chitosan microfabricated scaffold after 4 days (A, C, E) and 10 days (B, D, F) cell seeding with fibroblasts MRC5 cell line. A, B, C, D, E, F different magnifications

#### **4.6 Results and Discussion: microfabrication of chitosan ACP scaffolds**

Amorphous calcium phosphate (ACP) is the precursor of hydroxyapatite in bone mineral<sup>46</sup>. The important release of  $\text{Ca}^{2+}$  and  $\text{PO}_4$  ions associated to ACP is favorable to apatite formation.

Methacrylate-based composites with ACP demonstrated how this material could promote the recovery of mineral deficiencies in tooth structures being able to in vitro remineralize carious enamel lesions<sup>47</sup>.

The formation of “non-crystalline” calcium phosphate is a kinetic phenomenon<sup>48</sup>. The rapid mixing of the reaction solutions creates strong interactions between  $\text{Ca}^{2+}$  and  $\text{HPO}_4^{2-}$  ions, leading to irregular coordination complexes large enough in phase to separate from the solution. The following temperature-dependent transformation into apatite indicates that this initial phase is isothermally metastable with respect to the more ordered apatite configuration. The conversion mechanism of ACP to apatite is auto-catalytic: the interfacial surfaces of the emerging crystalline phase act as sites for heterogeneous nucleation, thereby accelerating the rate of conversion. Besides, the amorphous phase remains stable indefinitely if kept dry since water is fundamental in the nucleation process.

Pyrophosphate  $\text{P}^2\text{O}_7^{4-}$  ions were also used to stabilize ACP material to retard the conversion to apatite in dental applications<sup>23</sup>.

Thinking at the osteoinductive character of ACP particles, their combination with chitosan was investigated to produce microfabricated scaffolds with osteoconductive properties for bone tissue regeneration.

---

### Part 1: scaffold production by microfabrication

---

Rheological tests were used to evaluate viscosity changes between pure chitosan and chitosan filled with ACP, to identify the optimal viscosity range values to use inside the RP system.

Washing the produced scaffold by NaOH was fundamental to expose the particles to the surface, to put them directly in contact with the biological environmental. EDS analysis together with LV-SEM imaging confirmed the effectiveness of the washing process.

Using osteoblasts cell line MG63 preliminary in vitro culture studies were performed; cell morphology, attachment and growth were evaluated by SEM analyses.

Finally AFM imaging was used to measure the final particles size and their distribution in the chitosan matrix.

#### 4.6.1 Microfabricated scaffold

Chitosan scaffold filled with ACP particles having a well ordered structures were microfabricated as films 100 $\mu$ m thick containing 100 microns square pores (Figure 4.40).

80 overlapped layers composed the resulting scaffolds.

The selected process parameters to develop the scaffolds were fixed according to the ones used during pure chitosan scaffolds production.

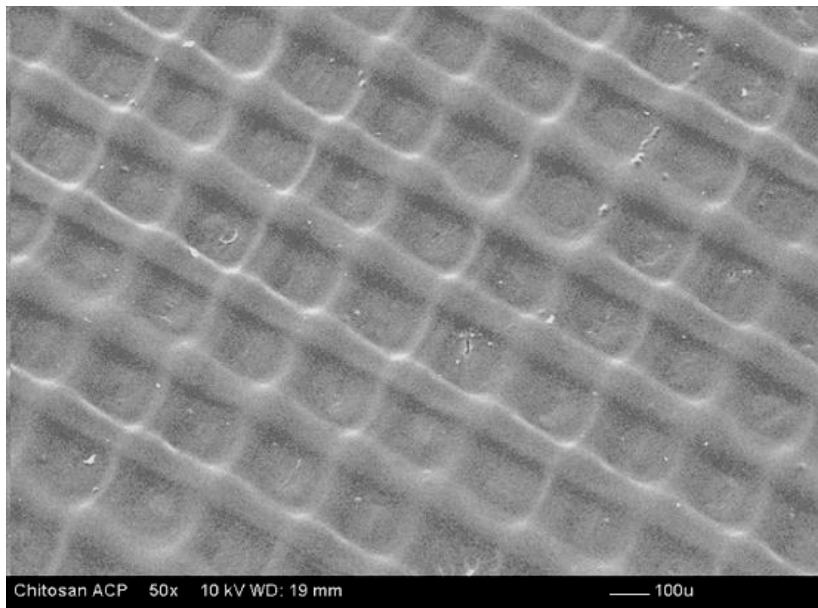


Figure 4.40. SEM images of Chitosan filled with ACP microfabricated scaffold

#### 4.6.2 Rheological tests

Evaluation of viscosity changes between pure chitosan solution and chitosan solution filled with ACP particles was performed by rheological tests.

Complex viscosity trends as a function of frequency are plotted in Figure 4.41.

Both the solutions show the typical polymer solution behavior; being non-Newtonian fluids the viscosity decreases with frequency. In the detail, the viscosity of a particle loaded suspension resulted to be lower than the viscosity of unloaded solution: in fact, the complex viscosity measured at the frequency value of 10 rad/sec (that is in the Newtonian region) for plain chitosan solution was 1.00 Pas while for the chitosan/ACP solution was 0.48 Pas, that is a reduction of 52%.

The viscosity of a suspension should increase for dilute concentration following the Einstein's theory <sup>49</sup>. In our case the viscosity decreased, and this is just due to the lower chitosan concentration in the suspension.

In fact, the suspension contained ACP-chitosan 0.4%-2.6% while the solution was at 3% chitosan. This choice was made to maintain constant the total amount of solid material in the solution (i.e. 3wt%) in order to produce microfabricated scaffolds with the same amount of material. Nevertheless, the viscosity reduction is quite high and could not be entirely attributed to the reduced polymer concentration, but to imprecise interactions between the partially dissolved filler and the polymer chain.

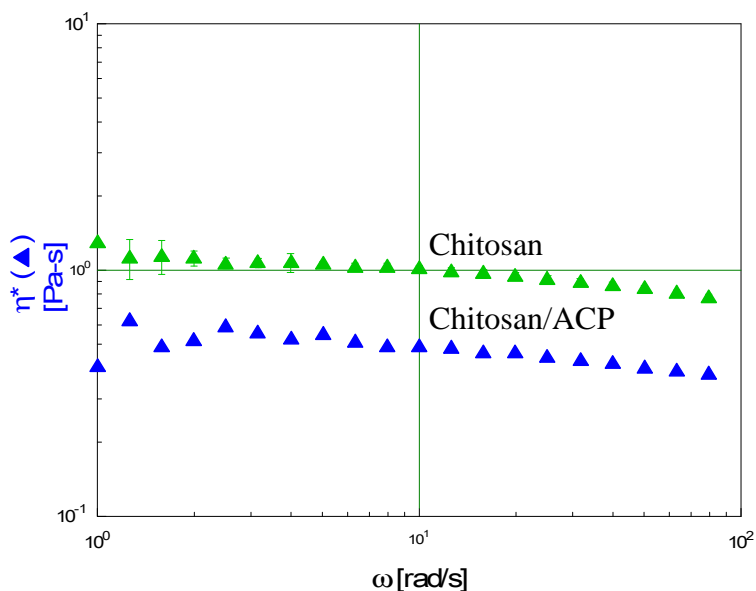


Figure 4.41. Comparison between viscosity of pure Chitosan solution and Chitosan filled with ACP particles solution

### 4.6.3 Thermogravimetric analysis (TGA)

Thermogravimetric analysis (TGA) was performed on pure chitosan, chitosan filled with ACP particles (composite) and ACP particles.

Figure 4.42 shows the thermographs resulted from thermal analysis test.

As expected, the ceramic phase evidence a limited weight loss, i.e. about 10% at 800°C. In detail, ACP presented the humidity water release at about 100°C (that corresponded to about 3%), a progressive weight loss between 200 and 400°C related to dehydroxylation phenomena and, finally, a sharp weight loss between 400 and 600°C related to the condensation of hydrogenophosphate ions<sup>50,51</sup>. On the contrary, chitosan evidenced a sharp weight loss at about 290°C that corresponds to degradation phenomena in

good agreement with DSC analysis (see chapter 4.5.4). Moreover, chitosan evidenced a sharp weight loss of 8% at about 110°C due to the loss of the adsorbed water.

Chitosan ACP composites were characterized by the absence of the weight drop related to the release of the absorbed water. Moreover, the degradation phenomena at about 290°C related to the polymeric phase (i.e. the chitosan) was still present, but in a broader temperature range. In fact, even if the maximum intensity of the phenomena is at 290°C in both the cases, the onset moved down from 270 to 200°C. This fact is in agreement with the existence of some unclarified interactions between the polymer and the ACP.

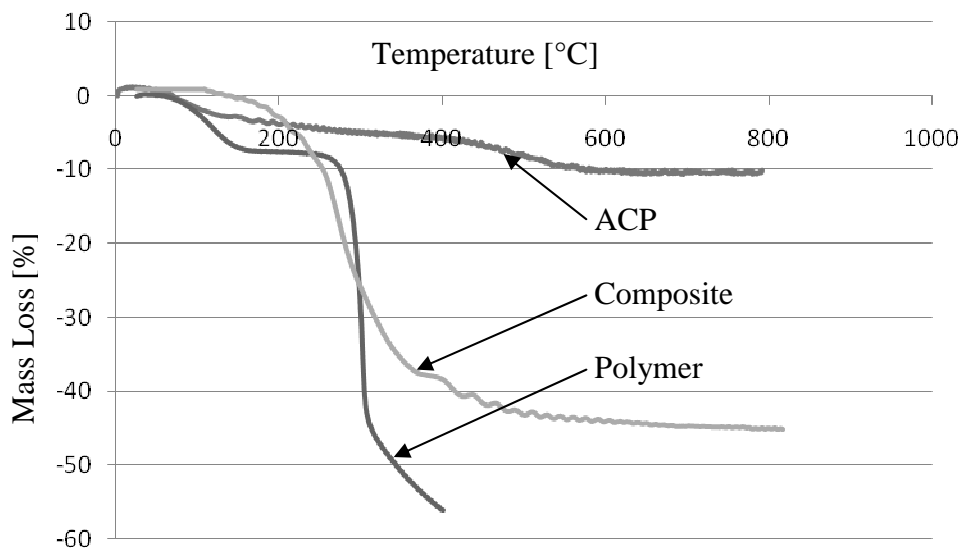


Figure 4.42. TGA thermograph related to pure chitosan, chitosan filled with ACP and pure ACP particles

#### 4.6.4 Preliminary in vitro culture studies

Human osteosarcoma derived osteoblasts cell line MG63 were cultured on microfabricated chitosan/ACP. The seeded scaffolds were observed by SEM analysis after two different time points (4, 10 days) (see Figure 4.43 and Figure 4.44).

Initially, osteoblasts spread preferentially on the top part of the scaffold, then migration in the pores region could be observed: cells were able to extend filopodia inside the pores.

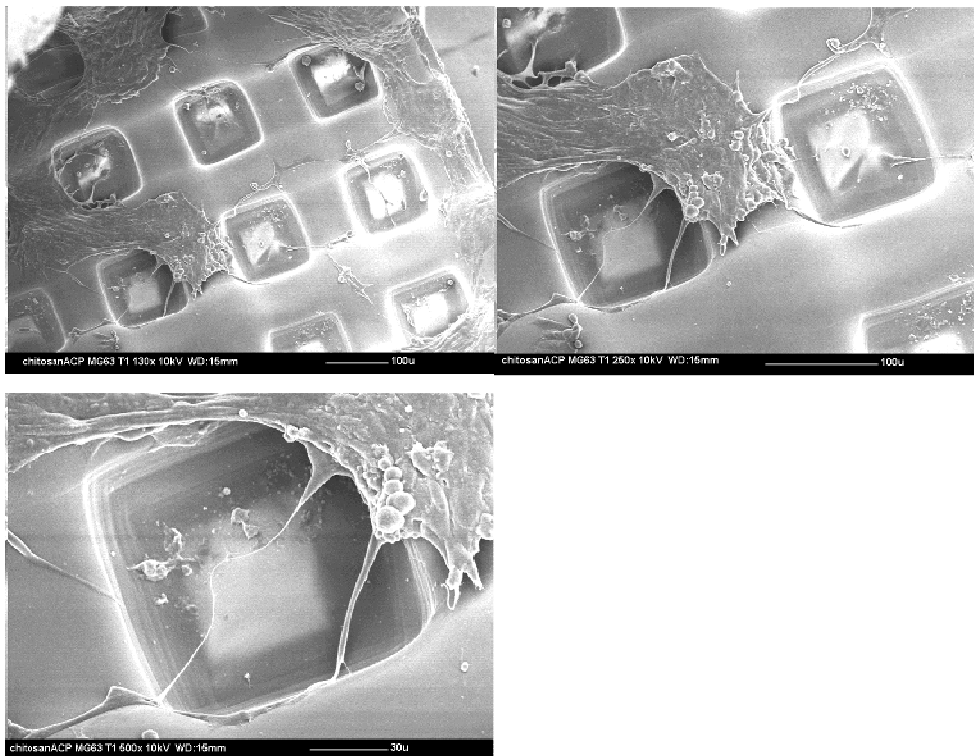


Figure 4.43. SEM images of Chitosan filled with ACP microfabricated scaffolds after 4 days cell seeding with MG63



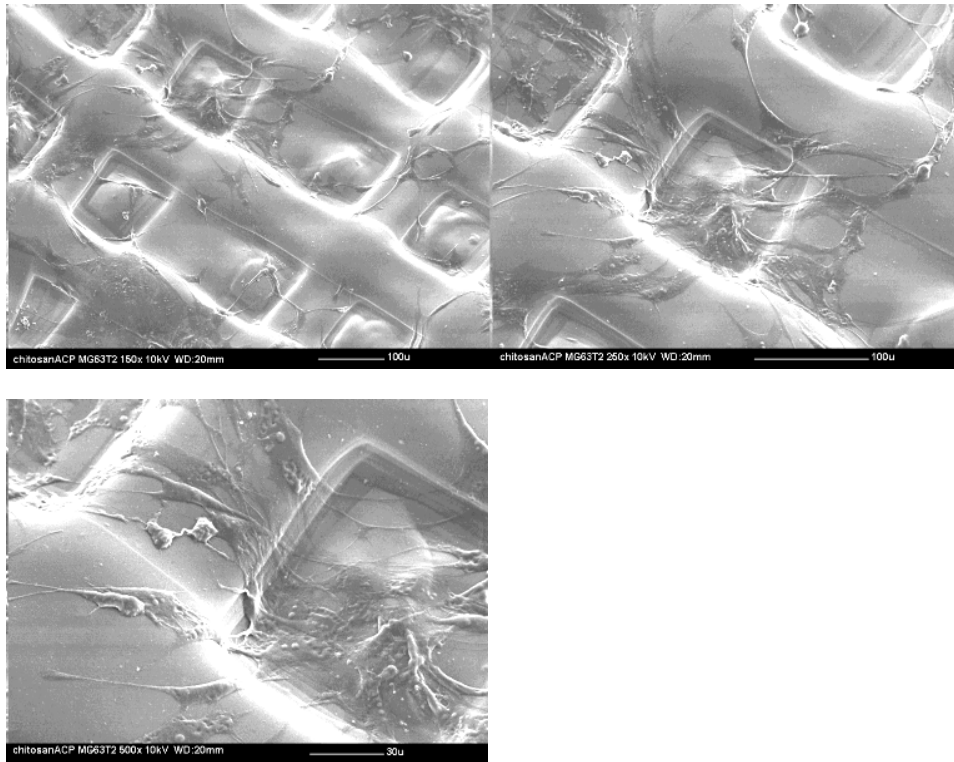


Figure 4.44. SEM images of Chitosan filled with ACP microfabricated scaffolds after 10 days cell seeding with MG63

#### 4.6.5 Energy dispersive spectroscopy (EDS)

Energy dispersive spectroscopy (EDS, EDAX) was used to identify elemental composition of chitosan/ACP scaffold surfaces, before and after washing with NaOH.

The aim of the analysis was to reveal the effectiveness of washing samples with NaOH in order to expose ACP particles to the surface, thus improving the osteoinductive character of the scaffold.

The surface analysis was conducted in combination with environmental scanning electron microscopy (LV-SEM) imaging.

During microfabrication process the ACP particles are trapped inside the chitosan matrix for surface energy implications.

NaOH washing removed the outside chitosan layer so exposing some ACP particles.

Figure 4.46 and Figure 4.48 show the EDS spectra of chitosan/ACP scaffolds, non-washed and washed with NaOH, respectively. Tables reporting the weigh fraction of the detected element composition on the surface, related to each spectrum, revealed that washed samples contained on the surface higher quantities of phosphate and calcium than non-washed samples. In the specific case the phosphate and calcium content of non-washed sample is 1.21 and 3.00 wt%, respectively, while, in the case of washed samples the values increases to 2.90 and 5.46 wt%.

Generally the depth of the analysis in the sample is dependent on the applied voltage<sup>52,53</sup> but still superficial; in our case , this semi-quantitative analysis confirms the efficacy of NaOH washing to expose higher quantities of calcium phosphate to the surface.

Figure 4.45 and Figure 4.47 are the associated LV-SEM imaging.

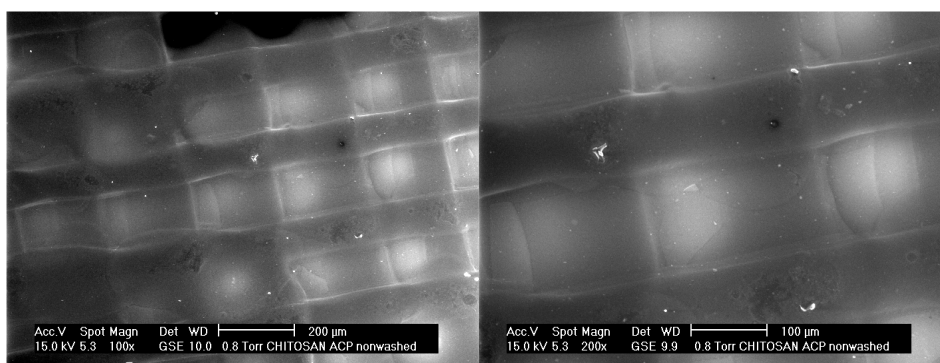
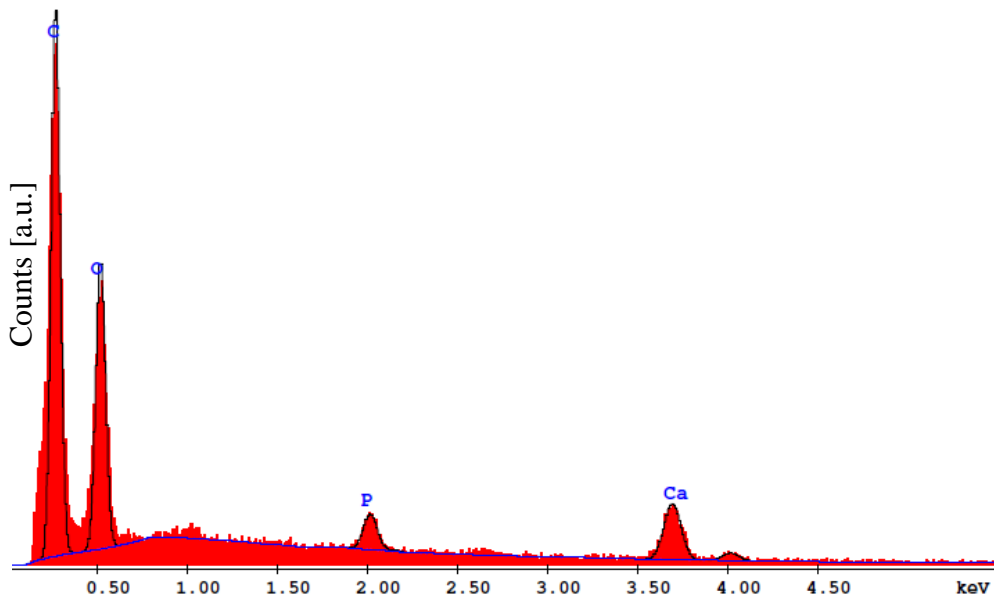


Figure 4.45. E-SEM imaging of chitosan filled with ACP particles before NaOH washing treatment

---

Part 1: scaffold production by microfabrication



EDAX ZAF Quantification (Standardless)  
 Element Normalized  
 SEC Table : Default

Element	Wt %	At %	K-Ratio	Z	A	F
C K	57.18	65.32	0.3151	1.0097	0.5455	1.0004
O K	38.62	33.12	0.0758	0.9929	0.1976	1.0000
P K	1.21	0.54	0.0101	0.9137	0.9179	1.0013
CaK	3.00	1.03	0.0284	0.9217	1.0294	1.0000
Total	100.00	100.00				

Figure 4.46. EDS spectra and semi-quantitative analysis of chitosan/ACP scaffold surface non-washed by NaOH

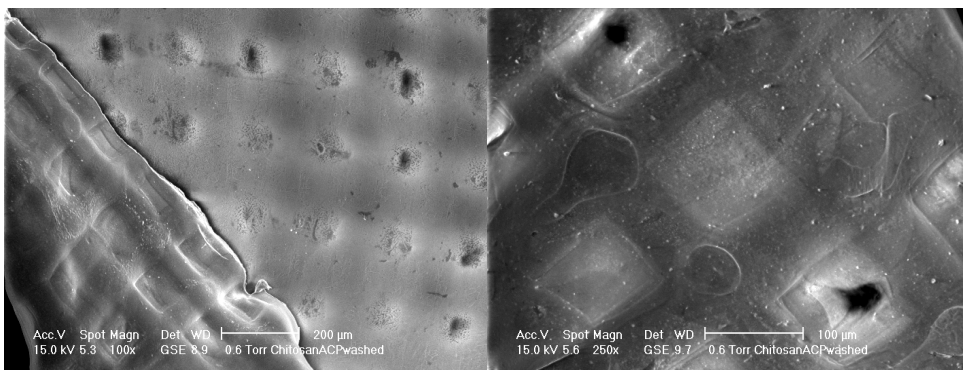
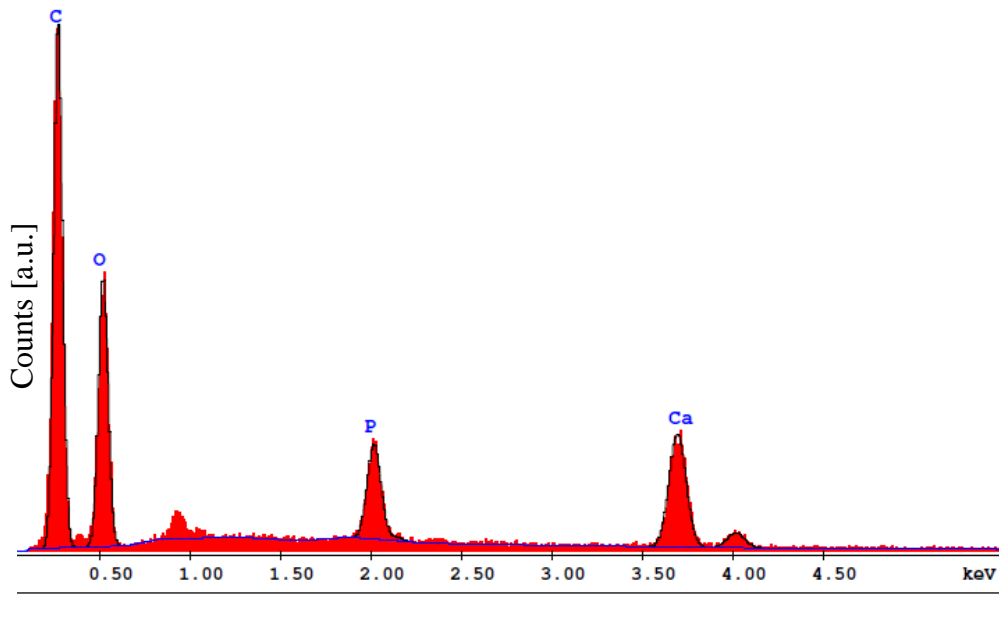


Figure 4.47. E-SEM imaging of chitosan filled with ACP particles after NaOH washing treatment



EDAX ZAF Quantification (Standardless)  
Element Normalized  
SEC Table : Default

Element	Wt %	At %	K-Ratio	Z	A	F
C K	56.64	66.11	0.2739	1.0125	0.4775	1.0003
O K	35.00	30.67	0.0640	0.9956	0.1837	1.0000
P K	2.90	1.31	0.0245	0.9165	0.9192	1.0022
CaK	5.46	1.91	0.0517	0.9244	1.0241	1.0000
Total	100.00	100.00				

Figure 4.48. EDS spectra and semi-quantitative analysis of chitosan/ACP scaffold surface washed by NaOH

Figure 4.49 shows the overlapped EDS spectra of washed and non-washed scaffold.

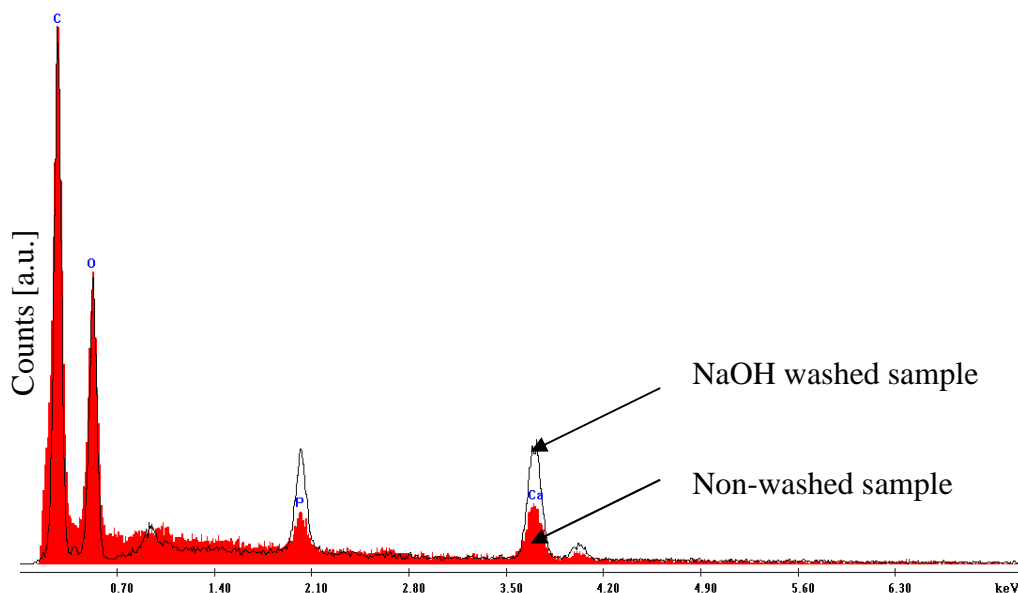


Figure 4.49. EDS overlapped spectra of chitosan/ACP scaffold washed and non washed

#### 4.6.6 Atomic Force Microscopy

Atomic force microscopy (AFM) analysis was performed on scaffold surface after NaOH washing treatment to analyze the topography of the surface and to measure surface exposed ACP particle size.

Evaluation of possible reductions in dimensions due to a combination of an erosion mechanism together with ACP dissolution was considered.

Figure 4.50 and Figure 4.51 show the topography of the scaffold surface. To better evidence the particles a Prewitt vertical filter was applied.

Figure 4.52 is a three dimensional view of the previous surface.

---

Part 1: scaffold production by microfabrication

---

Measurement of the particle size was also performed and Figure 4.53 and Figure 4.54 show the topography of the surface analyzed and the surface height profile, respectively.

The biggest visible particles, had a size of about 600 nm. A reduction of the particles size is thus evidenced if compared with the starting particle size.

Erosion and/or solubilization followed by recrystallization are the possible phenomena responsible for the reduction of this dimension.

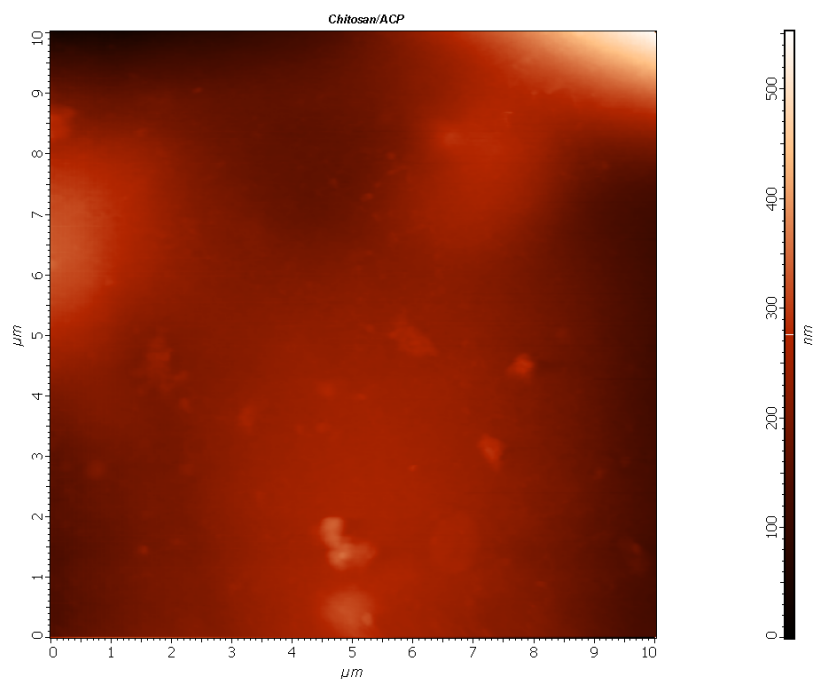


Figure 4.50. AFM imaging of chitosan/ACP scaffold surface

Part 1: scaffold production by microfabrication

---

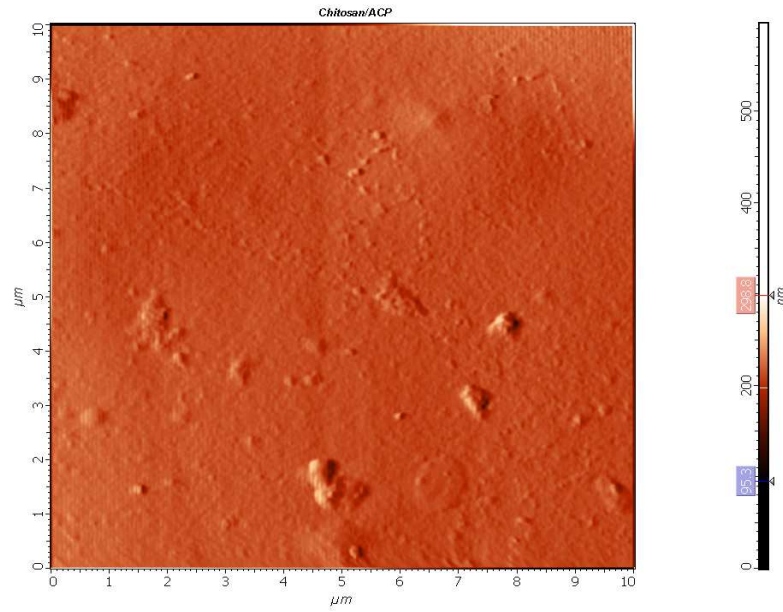


Figure 4.51. AFM imaging of chitosan/ACP scaffold surface. Prewitt vertical filter applied.

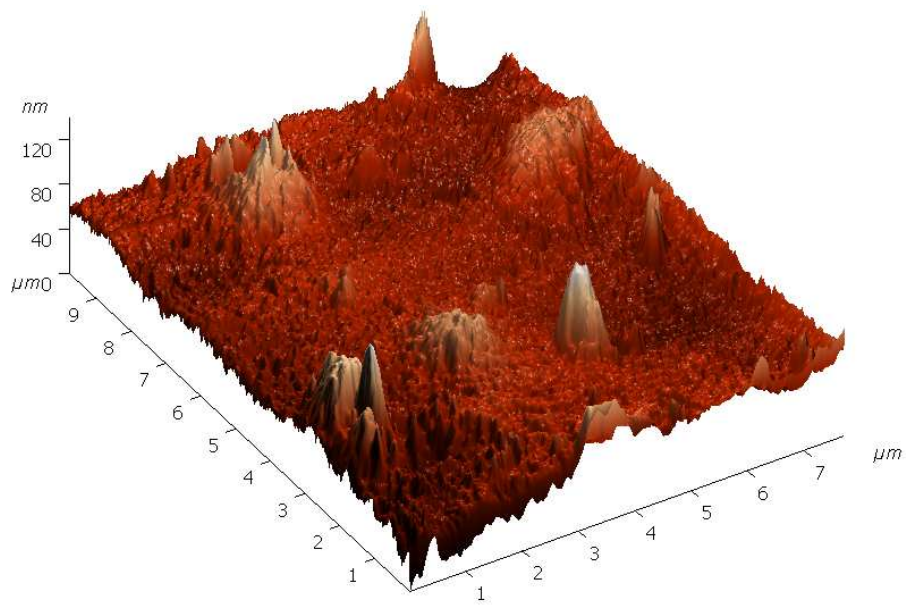


Figure 4.52. Three dimensional view of a 10 x 10  $\mu\text{m}$  square area analysed by AFM of a chitosan/ACP scaffold surface washed with NaOH

---

Part 1: scaffold production by microfabrication

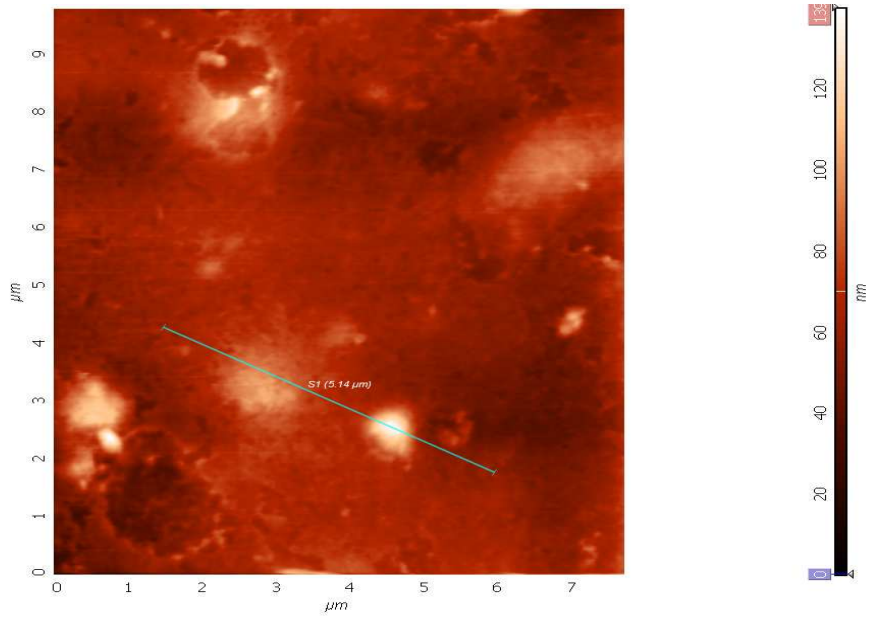


Figure 4.53. Topography of chitosan/ACP scaffold surface. The line indicates the selected area for the profile analysis

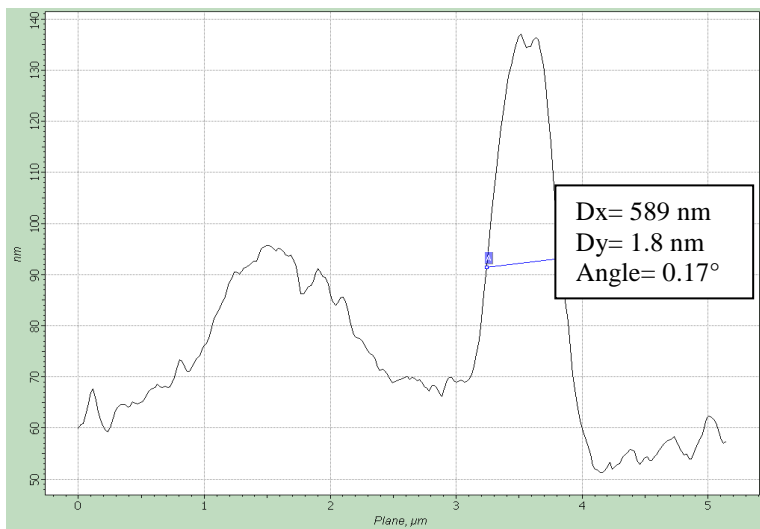


Figure 4.54. Surface height profile



## **5 PART 2: fused deposition modelling scaffold for human osteoblasts cell cultures**

### **5.1 Abstract**

Human osteoblasts, isolated from the tibial sponge bone, were seeded on medical-grade polycaprolactone-tricalcium phosphate (mPCL-TCP 80:20) and poly(D, L lactic acid)- tricalcium phosphate (PDLLA-TCP 90:10) scaffolds produced by fused deposition modelling (FMD) technique.

Scanning electron and confocal microscopy was used to characterize the cell-substrate interaction over different time points.

In addition, once the cells had reached the confluent stage, osteogenic media was used during cell culture to induce matrix formation. The newly formed matrix could provide a physical support forming an osteoblast sheet layer that was used to wrap the scaffold.

Cells viability was evaluated by fluorescein diacetate (FDA)/ propidium iodide (PI) staining.

The extent of cell proliferation was examined by PicoGreen™ quantification assay through the calculated cell DNA amount profile.

## **5.2 Introduction**

In tissue engineering (TE) research area living cells, biologically active molecules and structural scaffolds are combined together to form a tissue engineering construct (TEC) and promote the repair and regeneration of tissues.

One of the main efforts of tissue engineering (TE) is related to the development of techniques that can be used to produce scaffolds working as structural supports for cell seeding, attachment, growing, proliferation and differentiation.

Among these, rapid prototyping (RP) systems are able to produce scaffolds having a well ordered and reproducible structure. Control over scaffold geometry and porosity distribution and size is also possible.

In particular, regarding bone tissue regeneration application, an increasing trend has been seen towards the fabrication of polymer –based composite materials to obtain matrices having increased osteoconductive properties.

Producing scaffolds by composite materials combining together polymer and ceramic phases nowadays is a followed strategy. In this way better mechanical properties are achieved; higher strength is obtain by the ceramic phase while toughness and plasticity is gained thanks to the polymeric phase. From a biological point of view composite materials provide a suitable microenvironment that mimic the host tissue's inorganic phase<sup>54,55</sup>.

## PART 2: fused deposition modelling scaffold for human osteoblasts cell cultures

---

In this study FDM scaffolds produced from mPCL-TCP and PDLA-TCP composites, developed for bone tissue regeneration, were cell seeded with human osteoblasts derived by tibial sponge bone.

The use of cell-sheet assisted the cell seeding procedure to overcome the low surface to volume ratio of these scaffolds.

Okano's group developed the use of single sheets of cultured corneal epithelial cells and multilayered cardiomyocytes sheets for engineering transplantable cornea and myocardial tissues using a smart culture plate technology<sup>56,57</sup>.

Morphology of the scaffolds, cells distribution and growing was revealed by confocal laser microscope (CLM) and scanning electron microscopy (SEM) imaging at different time points. Viability of cells was investigated by confocal laser imaging. A proliferation analysis was evidenced by PicoGreen<sup>TM</sup> quantitation assay.

## **5.3 Materials and Method**

### **5.3.1 FDM scaffolds**

Scaffolds of mPCL-TCP (80:20) and PDLA:TCP (90:10) with a lay-down pattern 0/60/120° produced via fused deposition modelling (FDM) technique were cut into pieces having a 80 mm<sup>2</sup> cross sectional surface area<sup>58</sup>.

### **5.3.2 Cell culture**

Osteoblasts were isolated (with patient consensus) from tibial sponge bone. The bone chip explants were placed in a tissue culture flask until osteoblast outgrowth was observed. Once 80% confluence had occurred, the cells were trypsinized two times.

All the FDM scaffolds were sterilized by immersion in 70% ethanol.

Cell culture was performed by seeding each scaffold with 50000 cells concentrated in a volume of 20 µl. After 2h of incubation, required for cell attachment, the medium was added to each well and changed three times per week. 16000 cells/cm<sup>2</sup> were seeded on the monolayer controls.

Five time points were chosen: 2, 9, 16, 30, 45 days. Till 16 days growing media α-MEM (1g/l glucose + glutamine) (Sigma Chemicals, Missouri, US) supplemented with 1% antibiotics (100 IU mL<sup>-1</sup> penicillin and 100µg mL<sup>-1</sup> streptomycin) and 10% Fetal Calf Serum (FCS) was used. After confluence, at day 16, culture media was changed and osteogenic induction was

## PART 2: fused deposition modelling scaffold for human osteoblasts cell cultures

---

conducted through the use of supplemented media containing 10 nM dexamethasone (Dex), 100 mM  $\beta$ -glycerophosphate ( $\beta$ -GP) and 50  $\mu\text{g mL}^{-1}$  ascorbic acid (AA). Media was changed every 3 days. At day 30 matrix formation was enough to obtain osteoblasts sheets that were easily detached from the well-plate and used to wrap the scaffolds.

Figure 5.1 shows the osteoblast sheet detached from the well plate thanks to the use of a plastic soft scraper.



Figure 5.1. Osteoblast cell sheet detaching from the 6 well-plate

### 5.3.3 Proliferation assays

To measure the extent of proliferation, cell DNA amount profile was calculated, at each time-points by PicoGreen<sup>TM</sup> quantification assay (Quant-iT<sup>TM</sup> PicoGreen<sup>®</sup> dsDNA - Invitrogen). At the pre-determined time-points, cell-scaffold constructs and monolayers were washed in PBS solution, then incubated in a enzymatic solution, 0.5 mg/ml Proteinase K in PBE overnight at 37°C to detach/lyse the cells on the scaffolds. The resulting cell suspensions were then collected and mixed with PicoGreen dye at 1:1

volume ratio. The mixtures were read using a spectrophotometer for fluorescence at 520 nm with excitation wavelength of 485 nm.

#### **5.3.4 Scanning electron microscopy (SEM)**

Morphological observations were performed with optical microscopy and scanning electron microscopy (SEM) (Quanta 200 Scanning Electron Microscope – FE – operating mode: low vacuum, gaseous secondary electron GSE detector).

Before imaging, biological samples were fixed by using a glutaraldehyde solution (2.5% glutaraldehyde in cacodylic buffer solution, 0.1 M, PH=7.2) to preserve the structure of living tissues. Then the samples were dehydrated by dipping in a series of aqueous ethanol solutions at increasing concentrations. Prior to SEM imaging, samples were sputter coated (Biorad SC500, Hemel Hempstead, UK) with a thin layer of gold in argon atmosphere (1,4 mA at  $5 \times 10^{-7}$  for 1 min).

### **5.3.5 Cell staining and confocal laser microscopy imaging**

Evaluation of cell attachment and growing on the seeded scaffolds was performed by confocal laser microscopy (CLM) (Leica SP5, Germany) after rhodamine phalloidin and DAPI staining according to the manufacturers' protocol (Molecular Probes Inc., Oregon, USA – Product codes: R415 and D1306 respectively). Fixation with a formaldehyde solution (4% formaldehyde in PBS solution) and permeabilization with TritonX (0.2% TritonX in PBS solution) was performed before staining.

Qualitative cell viability was assessed using fluorescein diacetate–propidium iodide (FDA–PI) staining, following the manufacturers' protocol (Molecular Probes Inc., Oregon, USA – Product codes: F1303 and P1304MP respectively).

## 5.4 Results and Discussion

### 5.4.1 Optical imaging

Optical microscope imaging were taken at each time point to evidence the bridging mechanism used by osteoblasts to grow at the corners of the pores. This mechanism is evident when cells reach a certain level of confluence on the scaffold surface: in this experiment from day 16 as showed in Figure 5.2 and Figure 5.3.

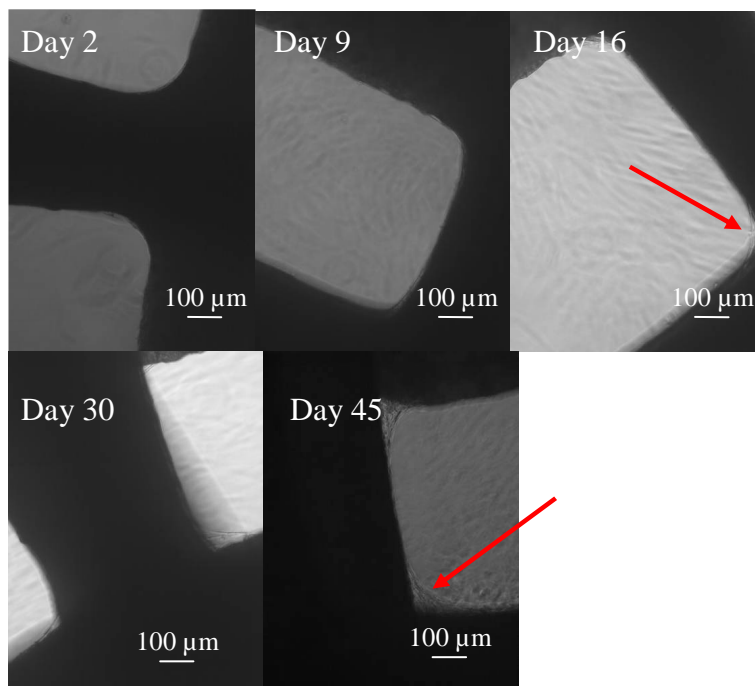


Figure 5.2. Optical microscope images of mPCL:TCP scaffolds. The arrow indicates the bridging mechanism that cells use to grow in the corner of pores



PART 2: fused deposition modelling scaffold for human osteoblasts cell cultures

---

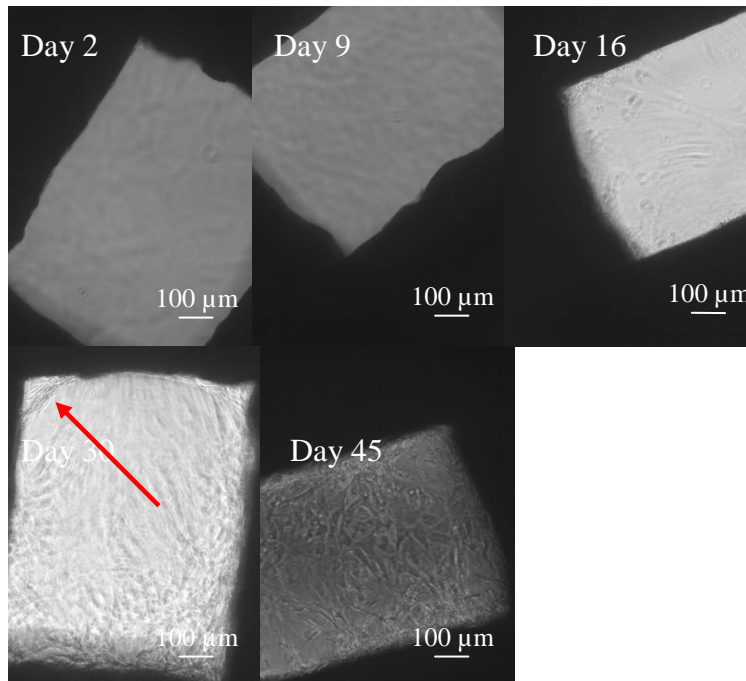


Figure 5.3. Optical microscope images of PDLLA:TCP scaffolds. The arrow indicates the bridging mechanism that cells use to grow in the corner of pores

### **5.4.2 Confocal laser imaging: Phalloidin rhodamine and Dapi staining**

Cells structure was evidenced by confocal laser microscopy (CLM) after Phalloidin rhodamine and Dapi staining.

In particular Phalloidin rhodamine stained the cell cytoskeleton resulted in red fluorescence while Dapi stained the cell nuclei resulted in blue fluorescence.

Both the materials were tested over the predetermined time points.

Figure 5.4 and Figure 5.6 show the CLM imaging for the mPCL:TCP and PDLLA: TCP materials respectively.

Figure 5.5 and Figure 5.7 illustrate cell morphologies at higher magnifications.

Transmitted images are also reported (smaller images) to better evidence the scaffold structure.

From the images no pronounced differences can be noticed between the two materials.

Cells could spread over the scaffolds uniformly starting from the polymeric matrix, and then filling the pores, by a bridging mechanism, starting from the corners of the matrix.

The arrows in Figure 5.4 and Figure 5.6 underline the growth of the cells from the corner of the scaffold.

PART 2: fused deposition modelling scaffold for human osteoblasts cell cultures

---

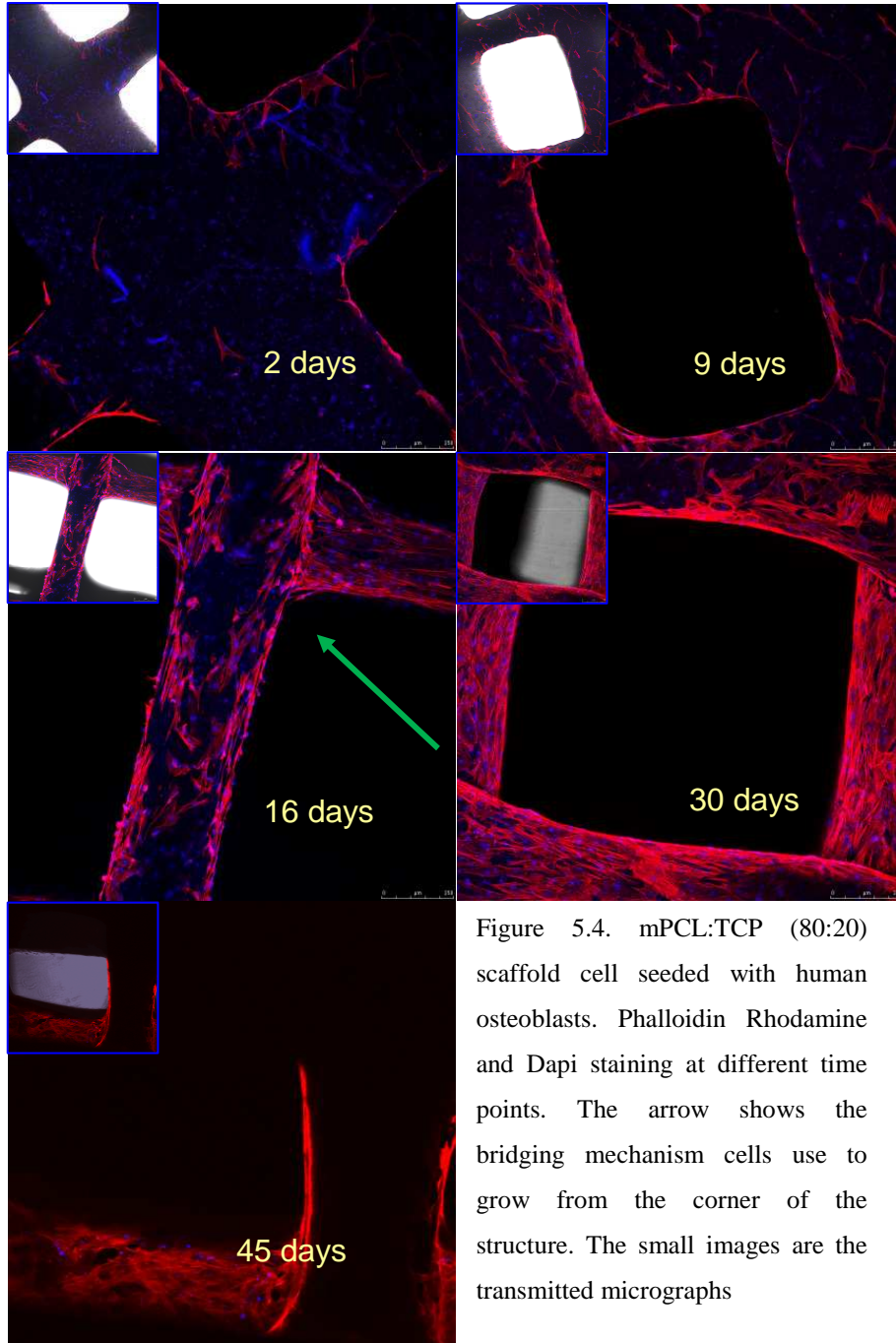


Figure 5.4. mPCL:TCP (80:20) scaffold cell seeded with human osteoblasts. Phalloidin Rhodamine and Dapi staining at different time points. The arrow shows the bridging mechanism cells use to grow from the corner of the structure. The small images are the transmitted micrographs

PART 2: fused deposition modelling scaffold for human osteoblasts cell cultures

---

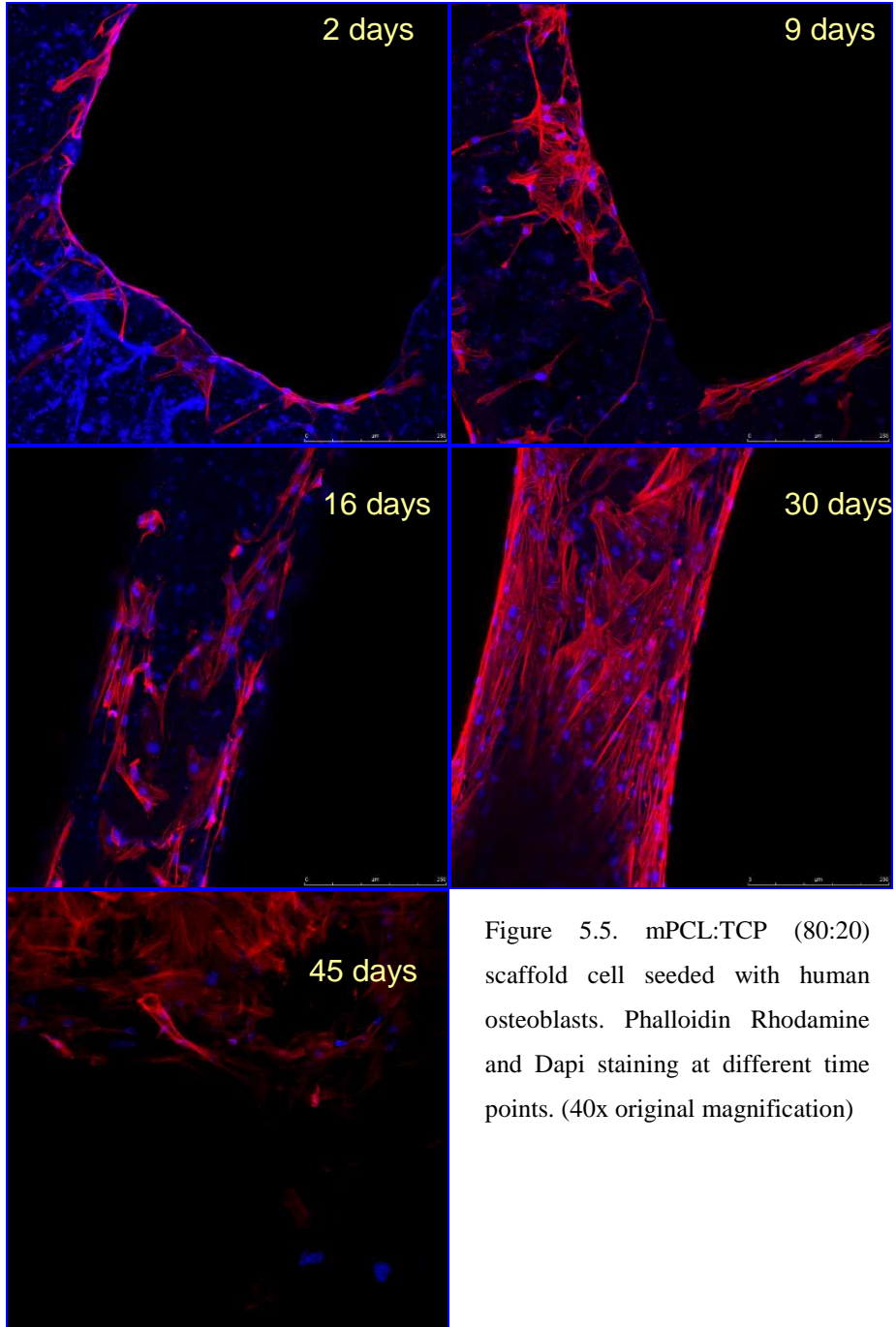


Figure 5.5. mPCL:TCP (80:20) scaffold cell seeded with human osteoblasts. Phalloidin Rhodamine and Dapi staining at different time points. (40x original magnification)

PART 2: fused deposition modelling scaffold for human osteoblasts cell cultures

---

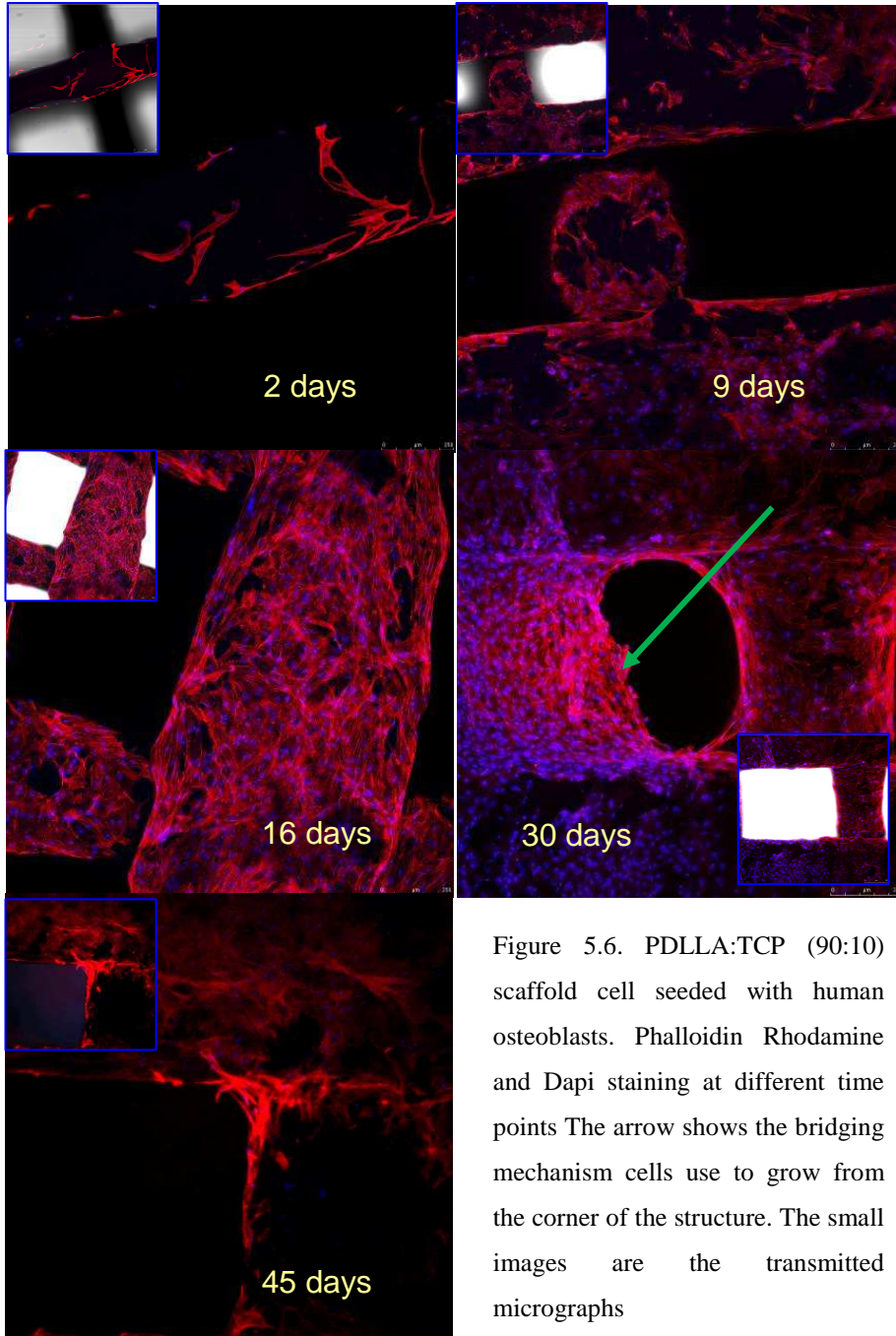


Figure 5.6. PDLA:TCP (90:10) scaffold cell seeded with human osteoblasts. Phalloidin Rhodamine and Dapi staining at different time points The arrow shows the bridging mechanism cells use to grow from the corner of the structure. The small images are the transmitted micrographs



PART 2: fused deposition modelling scaffold for human osteoblasts cell cultures

---

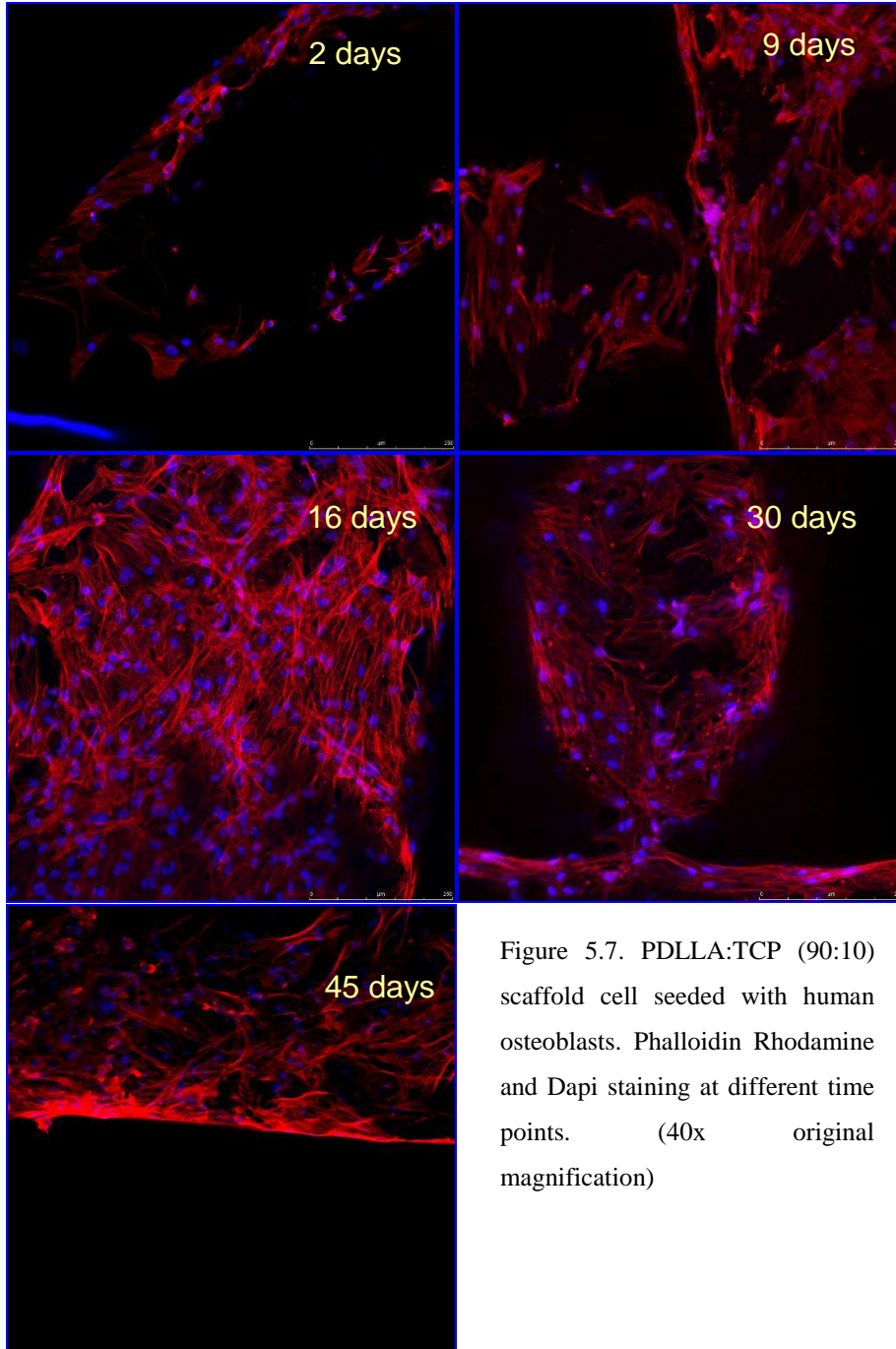


Figure 5.7. PDLA:TCP (90:10) scaffold cell seeded with human osteoblasts. Phalloidin Rhodamine and Dapi staining at different time points. (40x original magnification)

### **5.4.3 Confocal laser imaging: fluorescein diacetate–propidium iodide (FDA–PI)**

Osteoblast viability was evaluated by confocal laser microscopy (CLM) after fluorescein diacetate-propidium iodide (FDA-PI) staining. In fact, FDA stains viable cells green while PI stains necrotic and apoptotic cells red. The assay was done according to previously predetermined protocols.

Osteoblasts seeded over the two FDM scaffold materials were monitored for the chosen period of time. Every time point was examined.

Figure 5.8 and Figure 5.9 show the CLM imaging after staining of mPCL:TCP and PDLA:TCP, respectively. The transmitted images are also reported (small images) to better evidence the scaffold structure.

In both the materials viable cell number increased with time but at day 45 a reduction of viable cells was viewed.

This was most likely due to the high cell density at day 45.

PART 2: fused deposition modelling scaffold for human osteoblasts cell cultures

---

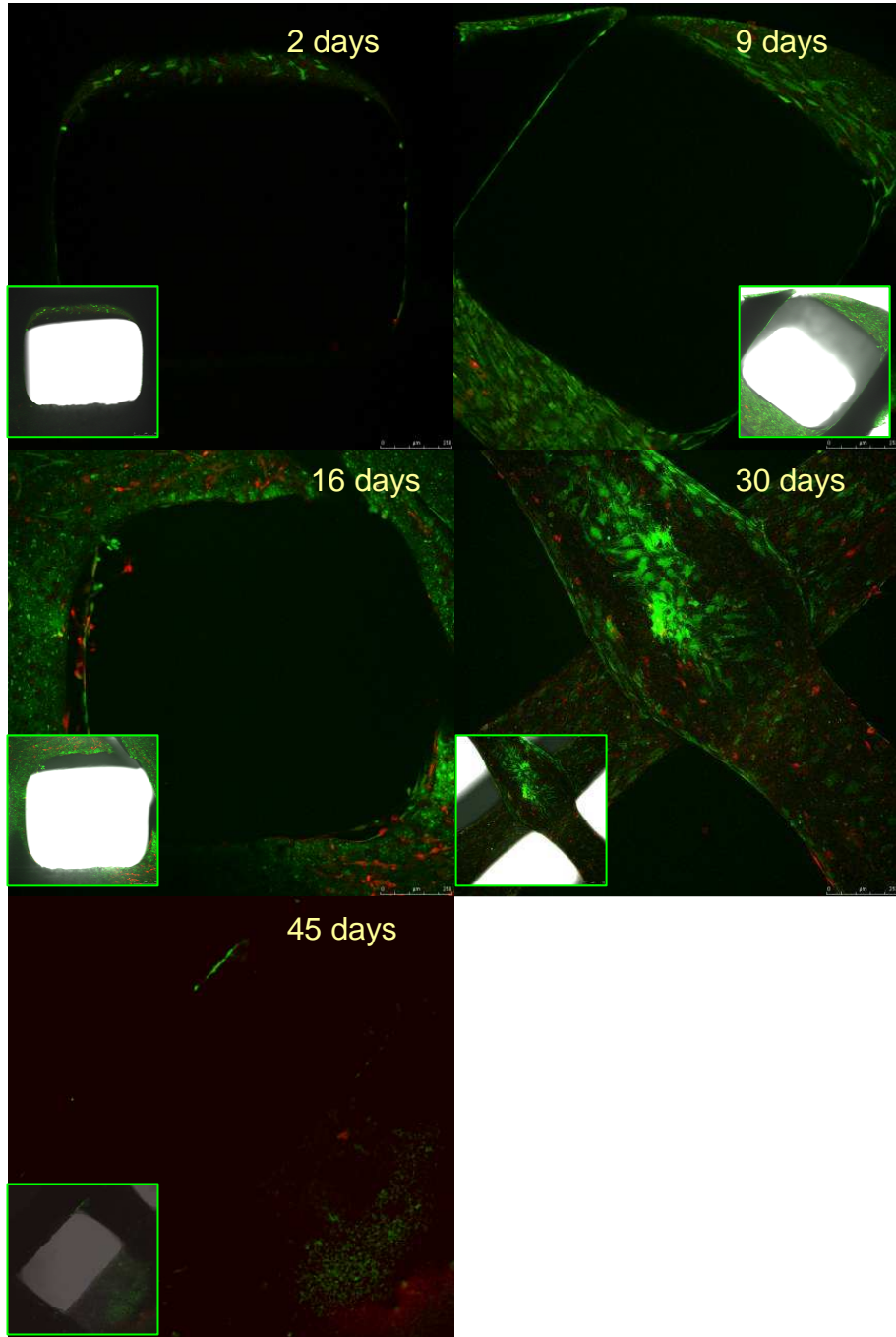


Figure 5.8. mPCL:TCP (80:20) scaffold cell seeded with human osteoblasts. fluorescein diacetate-propidium iodide (FDA-PI). The small images are the transmitted micrographs

---



PART 2: fused deposition modelling scaffold for human osteoblasts cell cultures

---

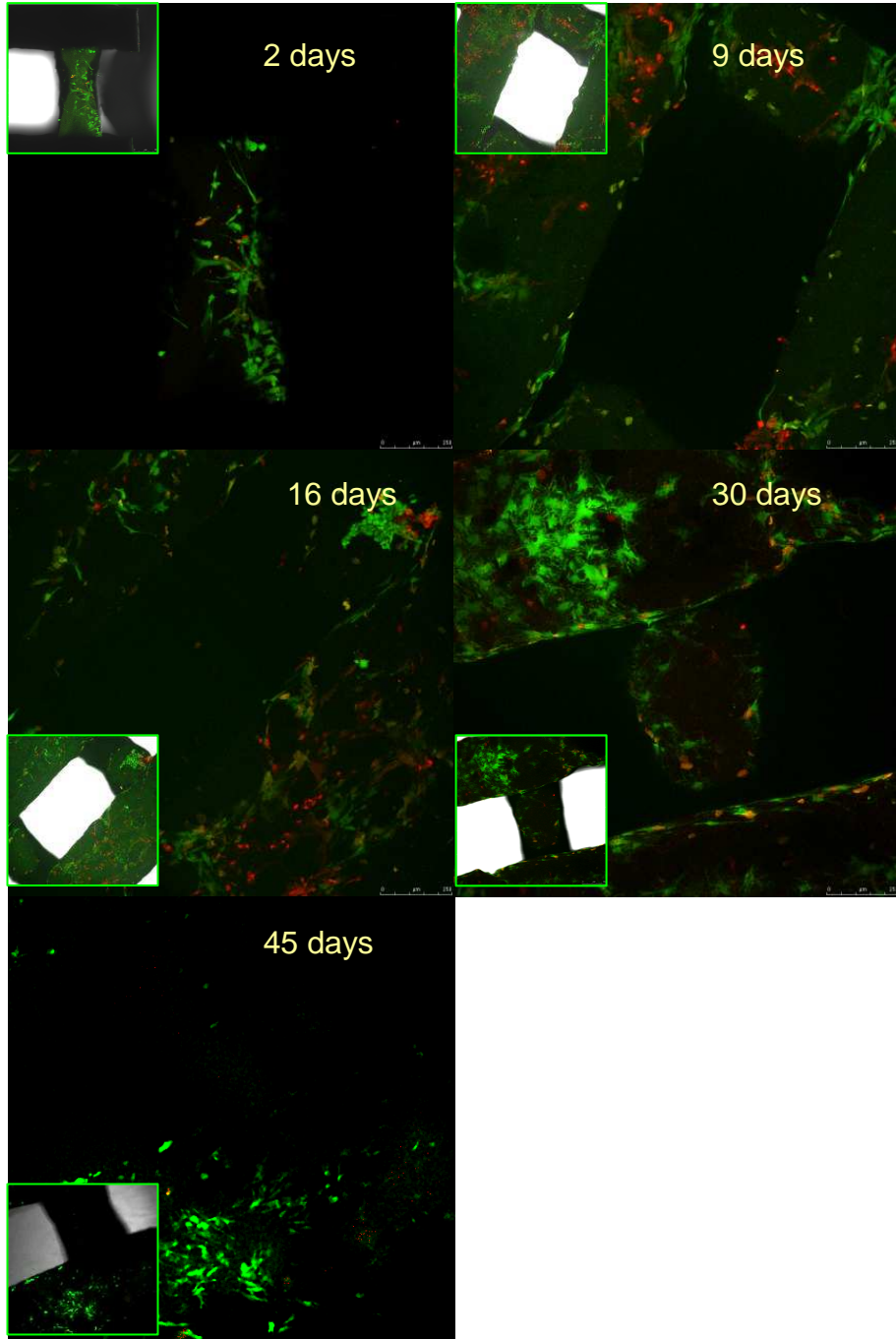


Figure 5.9. PDLLA:TCP (90:10) scaffold cell seeded with human osteoblasts. fluorescein diacetate-propidium iodide (FDA-PI). The small images are the transmitted micrographs

---

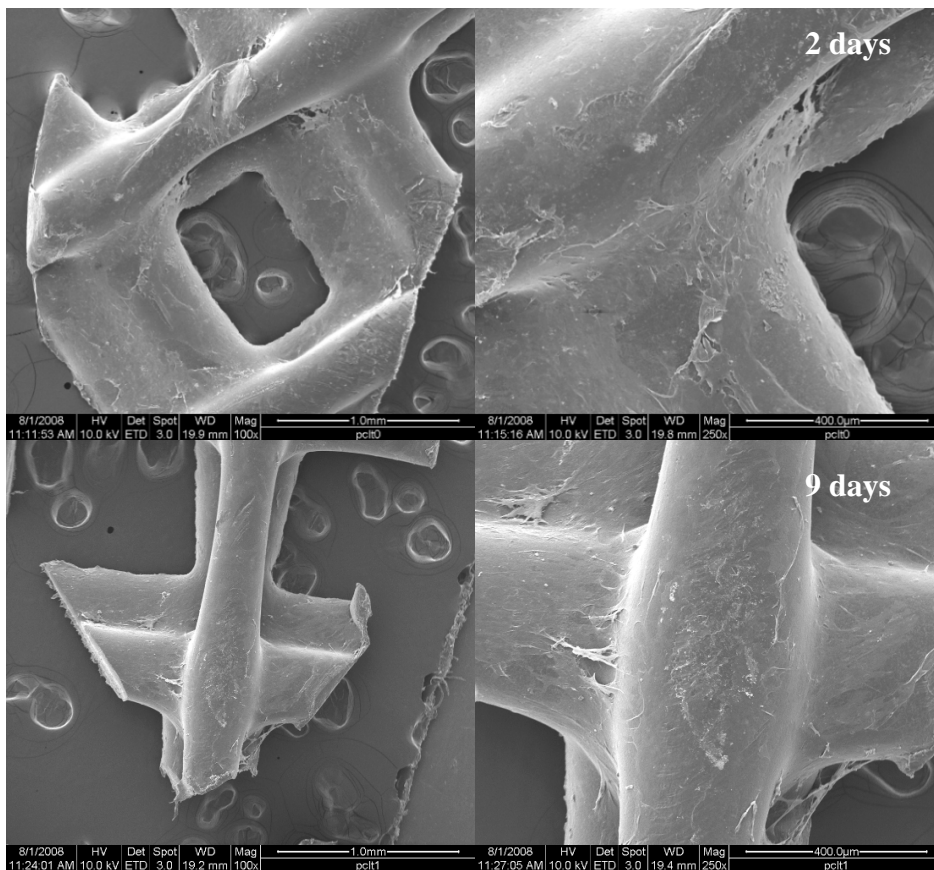
PART 2: fused deposition modelling scaffold for human osteoblasts cell cultures

---

### 5.4.4 Scanning Electron Microscopy (SEM)

Cell adhesion and growth behavior was evidenced by scanning electron microscopy (SEM) imaging.

Figure 5.10 and Figure 5.11 show the SEM imaging for mPCL:TCP (80:20) and PDLLA:TCP (90:10), respectively, at the prefixed time points. Different magnifications are reported.



PART 2: fused deposition modelling scaffold for human osteoblasts cell cultures

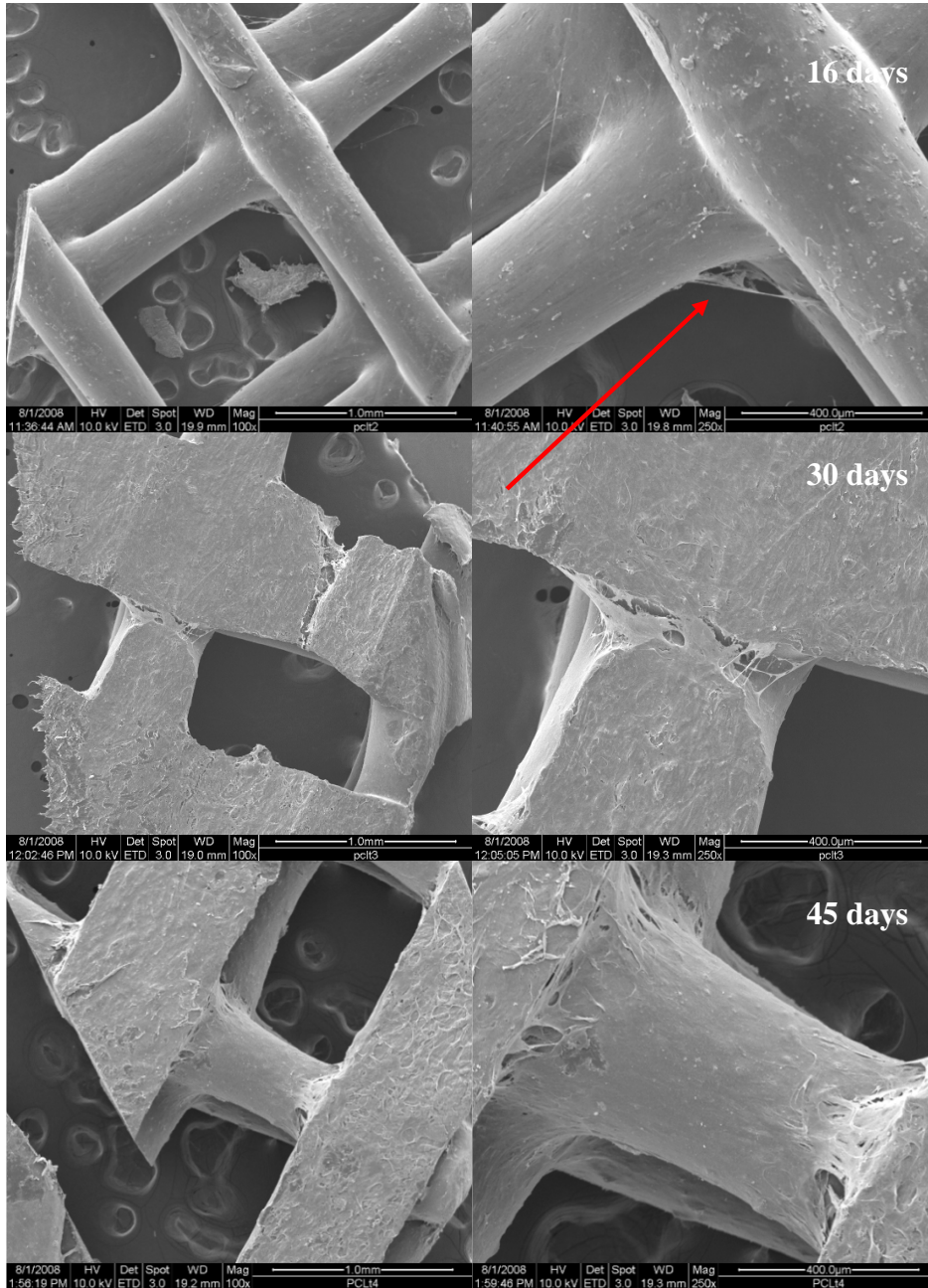
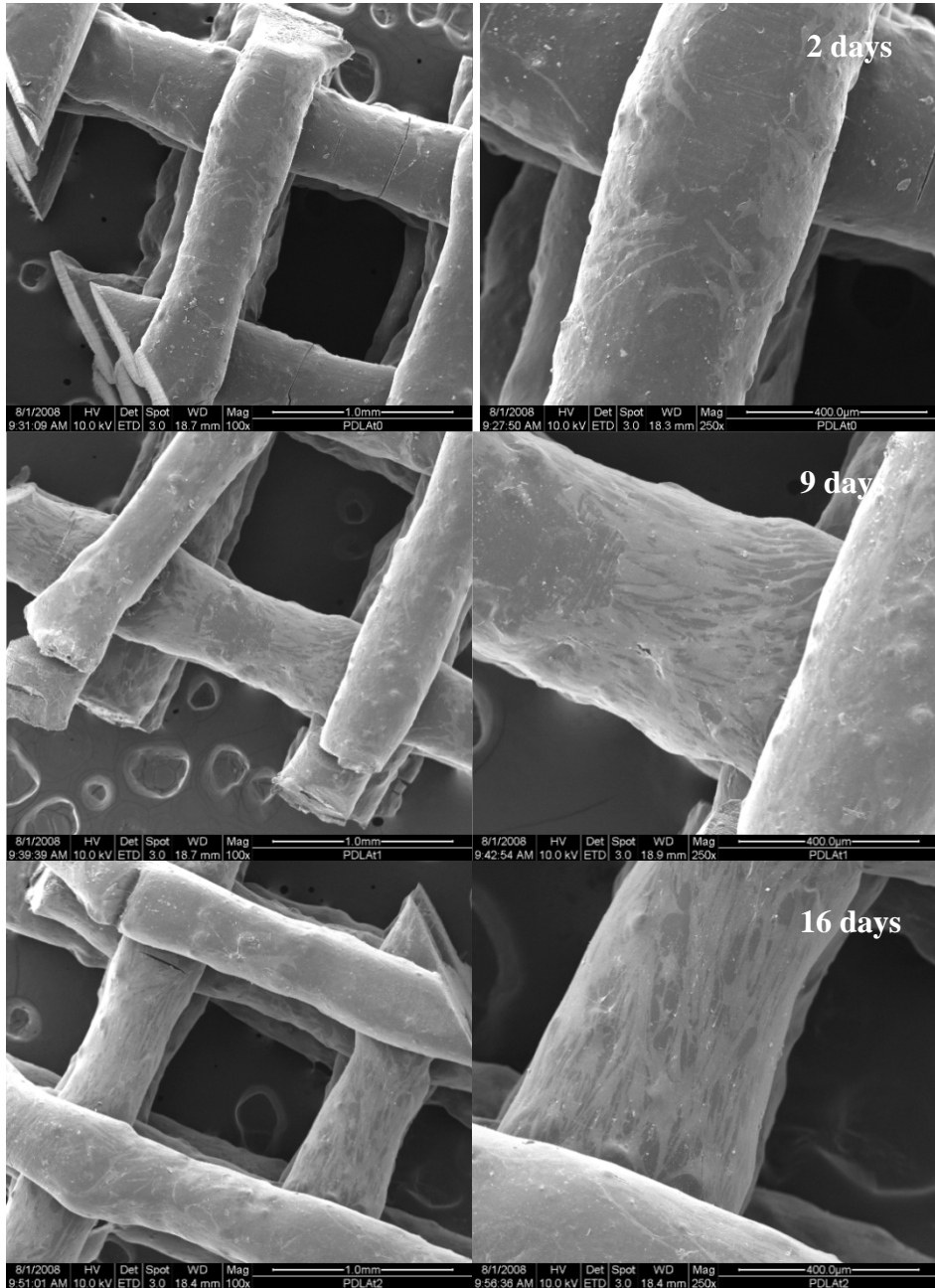


Figure 5.10. SEM imaging of mPCL:TCP (80:20) scaffold cell seeded with human osteoblasts at different time points. The arrow indicates cells bridging mechanism at the matrix corners

PART 2: fused deposition modelling scaffold for human osteoblasts cell cultures

---



PART 2: fused deposition modelling scaffold for human osteoblasts cell cultures

---

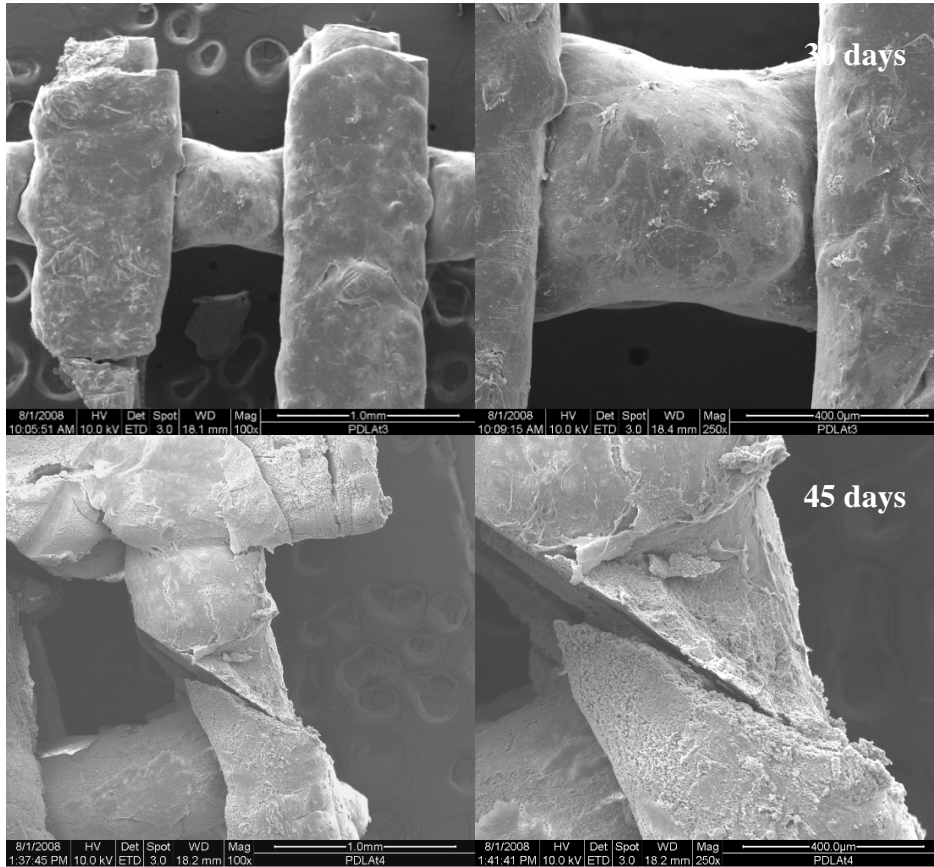


Figure 5.11. SEM imaging of PDLA:TCP (90:10) scaffold cell seeded with human osteoblasts at different time points

### 5.4.5 Proliferation Assay – PicoGreen™

To measure the extent of proliferation, cell DNA amount profile was calculated, at each time-points by PicoGreen™ quantification assay.

Figure 5.12 represents the trends of DNA amount profile measured over the predetermined time points. DNA amount profile for monolayer cell culture is reported as well.

From the graph it is possible to say that there was an increase of DNA amount during the first two weeks. Then a plateau is visible for both the materials.

This trend is expected and confirms the morphological evaluations previously showed by CLM and SEM imaging (chapters 5.4.2, 5.4.3 and 5.4.4). During matrix formation, after day 16, cells don't grow significantly.

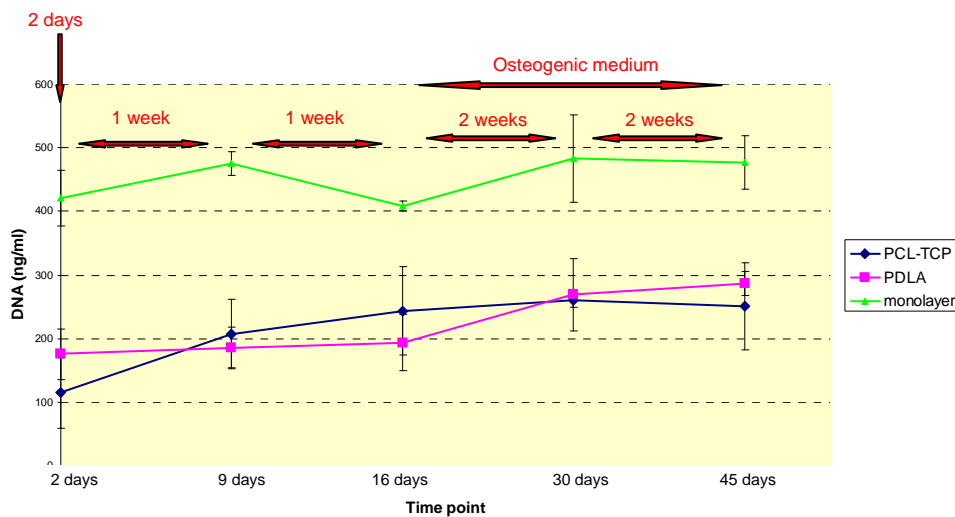


Figure 5.12. DNA amount profile as a function of culturing time

## 6 Conclusions

Tissue engineering, involving the use of living cells and extracellular components from either synthetic and natural polymers, aims to regenerate tissues and restore or replace deteriorating or aging biological structures.

The research work revolves around the use of a novel rapid prototyping technique to produce ordered scaffolding supports with a micrometric resolution.

Microfabrication system was developed and used in combination with synthetic, PDLA and PLGA, and natural, chitosan, polymeric solutions.

The reproducibility of the technique was achieved combining together proper process parameters and solution viscosities. Material characterization tests were used to assess possible material modifications due to the process and establish polymer solution viscosity working ranges suitable for obtaining well ordered microfabricated scaffolds.

Thinking at the osteoinductive character of ACP particles the combination with chitosan was evaluated to microfabricate scaffolds for bone tissue regeneration application. Superficial analyses revealed the effectiveness of NaOH treatment to expose the ceramic phase to the biological environment. Preliminary biological tests allowed to evaluate cells attachment and penetration. In particular different scaffold morphologies with micrometric structures were produced and cells behaviour was examined.

The second part of the work dealt with human osteoblasts cell culture on fused deposition modelling scaffolds for bone repair and restoration. This rapid prototyping technique makes use of thermoplastic polymers which are extruded on a platform; the final 3D scaffolds result to have higher

## Conclusions

---

porosities compared to microfabrication; thus oriented toward different applications. Cells morphology, viability and proliferation were examined.

The possibility to have a system able to fabricate reproducible scaffolds with a micro-resolution represents a big potential for tissue engineering applications. Future microfabrication develops could comprehend the design of scaffolds having gradient of porosity, thus varying specifically inside the same structure. This could offer a great advantage in those applications where porosity is not necessarily constant among the whole structure.

Furthermore a challenging objective is to develop the microfabrication system for organ or tissue printing, a novel concept in which cells and hydrogel matrices are spatially organized into layered hybrid constructs, with controlled architecture and defined cellular placement.



## 7 Bibliography Chapter 4 and 5

1. Langer, R. & Vacanti, J. P. *Tissue Engineering* (Science, 1993).
2. Salgado, A. J., Coutinho, O. P. & Reis, R. Bone Tissue Engineering: State of the Art and Future Trends. *Macromolecular Bioscience* **4**, 743-765 (2004).
3. Hutmacher, D. W. Scaffolds in tissue engineering bone and cartilage. *Biomaterials* **21**, 2529-2543 (2000).
4. Chen, G., Ushida, T. & Tateishi, T. Development of biodegradable porous scaffolds for tissue engineering. *Materials Science and Engineering: C* **17**, 63-69 (2001).
5. Mikos, A. G. & Temenoff, J. S. Formation of highly porous biodegradable scaffolds for tissue engineering. *Electron. J. Biotechnol.* **3**, 23-24 (2000).
6. Comb, J. W., Priedeman, W. R. & Turley, P. W. in *Proc. of the Solid Freeform Fabrication Symposium* (ed. Marcus, H. L. e. a.) 42-49 (1994).
7. Hutmacher, D. W., Sittinger, M. & Risbud, M. V. Scaffold-based tissue engineering: rationale for computer-aided design and solid free-form fabrication systems. *Trends in Biotechnology* **22**, 354-362 (2004).
8. Leong, K. F., Cheah, C. M. & Chua, C. K. Solid freeform fabrication of three-dimensional scaffolds for engineering replacement tissues and organs. *Biomaterials* **24**, 2363-2378.

---

Bibliography Chapter 4 and 5

---

9. Vozzi, G., Flaim, C., Ahluwalia, A. & Bhatia, S. Fabrication of PLGA scaffolds using soft lithography and microsyringe deposition. *Biomaterials* **24**, 2533-2540 (2003).
10. Vozzi, G., Flaim, C. J., Bianchi, F., Ahluwalia, A. & Bhatia, S. Microfabricated PLGA scaffolds: a comparative study for application to tissue engineering. *Materials Science and Engineering: C* **20**, 43-47 (2002).
11. Ghosh, S., Viana, J. C., Reis, R. L. & Mano, J. F. Development of porous lamellar poly(l-lactic acid) scaffolds by conventional injection molding process. *Acta Biomaterialia* **4**, 887-896 (2008).
12. Mikos, A. G. et al. Preparation and characterization of poly(L-lactic acid) foams. *Polymer* **35**, 1068-1077 (1994).
13. Mooney, D. J., Baldwin, D. F., P., S. N., Vacanti, J. P. & Langer, R. Novel approach to fabricate porous sponges of poly(D,L-lactic-co-glycolic acid) without the use of organic solvents. *Biomaterials* **17**, 1417-1422 (1996).
14. Yang, F. et al. Poly(l,l-lactide-co-glycolide)/tricalcium phosphate composite scaffold and its various changes during degradation in vitro. *Polymer Degradation and Stability* **91**, 3065-3073 (2006).
15. Athanasiou, K. A., Niederauer, G. G. & Agrawal, C. M. Sterilization, toxicity, biocompatibility and clinical applications of polylactic acid/ polyglycolic acid copolymers. *Biomaterials Polymer Scaffolding and Hard Tissue Engineering* **17**, 93-102 (1996).
16. Di Martino, A., Sittering, M. & Risbud, M. V. Chitosan: A versatile biopolymer for orthopaedic tissue-engineering. *Biomaterials* **26**, 5983-5990 (2005).

17. Geing, L. et al. Direct writing of chitosan scaffolds using a robotic system. *Rapid Prototyping Journal* **11**, 90-97 (2005).
18. Madihally, S. V. & Matthew, H. W. T. Porous chitosan scaffolds for tissue engineering. *Biomaterials* **20**, 1133-1142 (1999).
19. Chun, H. J., Kim, G. W. & Kim, C. H. Fabrication of porous chitosan scaffold in order to improve biocompatibility. *Journal of Physics and Chemistry of Solids* **69**, 1573-1576 (2008).
20. Hsu, S. H. et al. Chitosan as Scaffold Materials: Effects of Molecular Weight and Degree of Deacetylation. *Journal of Polymer Research* **11**, 141-147 (2004).
21. Lavertu, M. et al. A validated <sup>1</sup>H NMR method for the determination of the degree of deacetylation of chitosan. *Pharmaceutical Biomedical Analysis* **32**, 1149-1158 (2003).
22. Zhou, H. Y. et al. Effect of molecular weight and degree of chitosan deacetylation on the preparation and characteristics of chitosan thermosensitive hydrogel as a delivery system. *Carbohydrate Polymers* **73**, 265-273 (2008).
23. Skrtic, D., Antonucci, J. M., Eanes, E. D. & Eidelman, N. Dental composites based on hybrid and surface-modified amorphous calcium phosphates. *Biomaterials* **25**, 1141-1150 (2004).
24. Gupta, B. R. *Applied Rheology In Polymer Processing* (2005).
25. Petrie, C. J. S. Extensional viscosity: A critical discussion. *Journal of Non-Newtonian Fluid Mechanics Extensional Flow* **137**, 15-23 (2006).
26. Garlotta, D. A Literature Review of Poly(Lactic Acid). *Journal of Polymers and the Environment* **9**, 63-84 (2002).

---

Bibliography Chapter 4 and 5

---

27. Ram, A. & Kadim, A. Shear degradation of polymer solutions. *Journal of Applied Polymer Science* **14**, 2145-2156 (1970).
28. Vazquez, M., Schmalzing, D., Matsudaira, P., Ehrlich, D. & Mckinley, G. Shear-induced degradation of linear polyacrylamide solutions during pre-electrophoretic loading. *Analytical chemistry* **73**, 3035-3044 (2001).
29. Zhang, X., Espiritu, M., Bilyk, A. & Kurniawan, L. Morphological behaviour of poly(lactic acid) during hydrolytic degradation. *Polymer Degradation and Stability* **93**, 1964-1970 (2008).
30. Ho, K. G., Pometto, A. L. & N, H. P. Effects of Temperature and Relative Humidity on Polylactic Acid Plastic Degradation. *Journal of Environmental Polymer Degradation* **7**, 83-92 (1999).
31. Li, S. & McCarthy, S. Further investigations on the hydrolytic degradation of poly(DL-lactide). *Biomaterials* **20**, 35-44 (1999).
32. Reich, G. Ultrasound-induced degradation of PLA and PLGA during microsphere processing: influence of formulation variables. *Journal of Pharmaceutics and Biopharmaceutics* **45**, 165-171 (1998).
33. Grizzi, I., Garreau, H., Li, S. & Vert, M. Hydrolytic degradation of devices based on poly(DL-lactic acid) size-dependence. *Biomaterials* **16**, 305-311 (1995).
34. Lostocco, M. R. & Huang, S. J. The hydrolysis of poly(lactic acid)/poly(hexamethylene succinate) blends. *Polymer Degradation and Stability* **61**, 225-230 (1998).
35. Flick, E. W. *Industrial Solvents Handbook* (William Andrew Inc., 1988).

36. Zheng, W. & Simon, S. L. Polystyrene freeze-dried from dilute solution: Tg depression and residual solvent effects. *Polymer* **47**, 3520-3527 (2006).
37. Belfiore, L. A. in *Physical Properties of Macromolecules* (Wiley, New York, 2009).
38. Pluta, M. Morphology and properties of polylactide modified by thermal treatment, filling with layered silicates and plasticization. *Polymer* **45**, 8239-8251 (2004).
39. Pluta, M. & Galeski, A. Plastic Deformation of Amorphous Poly(l/dl-lactide): Structure Evolution and Physical Properties. *Biomacromolecules* **8**, 1836-1843 (2007).
40. Pluta, M., Jeszka, J. K. & Boiteux, G. Polylactide/montmorillonite nanocomposites: Structure, dielectric, viscoelastic and thermal properties. *European Polymer Journal* **43**, 2819-2835 (2007).
41. Pluta, M., Murariu, M., Da Silva Ferreira, A. & Alexandre, M. Polylactide Compositions. II. Correlation Between Morphology and Main Properties of PLA/Calcium Sulfate Composites. *Journal of Polymer Science* **45**, 2770-2780 (2007).
42. Geng, L. et al. Direct writing of chitosan scaffolds using a robotic system. *Rapid Prototyping Journal* **11**, 90-97 (2005).
43. Duarte, M. L., Ferreira, M. C., Marvão, M. R. & Rocha, J. Determination of the degree of acetylation of chitin materials by <sup>13</sup>C CP/MAS NMR spectroscopy. *Biological Macromolecules* **28**, 359-363 (2001).
44. Mucha, M. & Pawlak, A. Thermal analysis of chitosan and its blends. *Thermochimica Acta* **427**, 69-76 (2005).

---

Bibliography Chapter 4 and 5

---

45. Neto, C. G. T. et al. Thermal Analysis of Chitosan Based Networks. *Carbohydrate Polymers* **62**, 97-103 (2005).
46. Glimcher, M. J., Bonar, L. C., Grynblas, M. D., Landis, W. J. & Roufosse, A. H. Recent studies of bone mineral: is the amorphous calcium phosphate theory valid? *Journal of Crystal Growth* **53**, 100-119 (1981).
47. Skrtic, D., Hailer, A. W., Takagi, S., Antonucci, J. M. & Eanes, E. D. Quantitative Assessment of the Efficacy of Amorphous Calcium Phosphate/Methacrylate Composites in Remineralizing Caries-like Lesions Artificially Produced in Bovine Enamel. *Journal of Dental Research* **75**, 1679-1686 (1996).
48. Eanes, E. D., Gillessen, I. H. & Posner, A. S. Intermediate states in the precipitation of hydroxyapatite. *Nature* **5008**, 365-367 (1965).
49. Belfiore, L. A. in *Physical Properties of Macromolecules* (Wiley, New York, 2009).
50. Jiang, D., Premachandra, G. S., Johnston, C. & Hem, S. L. Structure and adsorption properties of commercial calcium phosphate adjuvant. *Vaccine* **23**, 693-698.
51. Destainville, A., Champion, E., Bernache, A. D. & Laborde, E. Synthesis, characterization and thermal behavior of apatitic tricalcium phosphate. *Materials Chemistry and Physics* **80**, 269-277 (2003).
52. Chan, D. K., Misquitta, S. F., Ying, J. F., Martner, C. C. & Hermsmeier, B. D. Chemical Depth Profiling on Submicron Regions: a Combined Focused Ion Beam/Scanning Electron Microscope Approach. *Surf. Interface Anal.* **27**, 199-203 (1999).

---

Bibliography Chapter 4 and 5

---

53. Zehringer, R. & Hauert, R. Depth profile analysis of the C/Si interface: comparison of destructive and nondestructive techniques. *Surface Science* **262**, 21-24 (1992).
54. Zhou, Y. et al. Combined marrow stromal cell-sheet techniques and high-strength biodegradable composite scaffolds for engineered functional bone grafts. *Biomaterials* **28**, 814-824 (2007).
55. Karageorgiou, V. & Kaplan, D. Porosity of 3D biomaterial scaffolds and osteogenesis. *Biomaterials* **26**, 5474-5491 (2005).
56. Shimizu, T. et al. Polysurgery of cell sheet grafts overcomes diffusion limits to produce thick, vascularized myocardial tissues. *FASEB J* (2006).
57. Nishida, K. et al. Corneal reconstruction with tissue-engineered cell sheets composed of autologous oral mucosal epithelium. *N Engl J Med* **351**, 1187-1196 (2004).
58. Zhou, Y., Hutmacher, D. W., Varawan, S. L. & Lim, T. M. Effect of Collagen-I Modified Composites on Proliferation and Differentiation of human Alveolar Osteoblasts. *Aust. J. Chem* **59**, 571-578 (2006).

## 8 Acknowledgements

This thesis work, which is part of the Integrated PhD Programme of the EU Expertissues NoE, has been accomplished thanks to the cooperation of different research groups.

Most of the work has been carried out at the laboratories of the Department of Materials Engineering and Industrial Technologies, University of Trento. It was a pleasure for me working together with Prof. Claudio Migliaresi and his group and I would like to express gratitude to all the people of the laboratory. In particular I desire to thank Prof. Claudio Migliaresi, Dr. Antonella Motta and Dr. Devid Maniglio for their assistance, guidance and unconditional support.

Different people cooperated directly to the work. A special thank is for all with whom I have sheared everyday work and friendship: Eva, Mariangela, Erika, Alessia, Cristina, Dario, Giuseppe (directly involved in the development of the microfabrication system), Enrico, Massimo, Christian, Fabio, Walter, Lorenzo, Andrea, Luca and Alfredo.

In particular I really appreciated all the time Matteo has dedicated to help me from the beginning of the work, always and unconditionally.

I really enjoyed working together with Tugba Endogan, From METU – BIOMAT, Department of Polymer Science and Technology, Ankara



---

## Acknowledgements

---

(Turkey). She collaborated with me at the development of natural base microfabricated scaffolds.

Finally part of this work was performed in collaboration with Prof. Dietmar W. Hutmacher at the HIBI, Queensland University of Technology, Brisbane (Australia) who supervised me during the last period of my research. He offered me a good opportunity and a precious contribution to the improvement of the present work. I would like to thank also Shirly Sieh who have spent patiently most of her time teaching me new techniques functional to the work.

I wish to thank Expertissues NoE for its financial support and the chance to attend the following courses and congresses:

- TERMIS-EU 2008, 22<sup>nd</sup> – 26<sup>th</sup> July 2008, Porto (Portugal), Oral Presentation: "*Production of PDLA and PLGA scaffolds by microfabrication and electrospinning techniques*"  
E. Carletti, T. Endogan, A. Motta, D. Maniglio, V. Hasirci, N. Hasirci, C. Migliaresi
- 5th Marie Curie Cutting Edge 2008: synthesis and applications of self-assembling materials at nano-scale, 14<sup>th</sup> – 18<sup>th</sup> April 2008, Madeira (Portugal), Poster Presentation: "*Microfabricated Chitosan/Amorphous Calcium Phosphate Composite scaffolds: production and characterization*"  
F. Z. Volpato, E. Carletti, T. Endogan, C. Migliaresi
- TICME 2007 - 1<sup>st</sup> Meeting: Advances in Polymers, Composites and Biomaterials, 16<sup>th</sup> – 19<sup>th</sup> December 2007, Trento (Italy), Poster Presentation: "*Microfabrication of Chitosan and PDLA Scaffolds*"  
E. Carletti, T. Endogan, E. Bella, A. Motta, D. Maniglio, V. Hasirci, N. Hasirci, C. Migliaresi
- 4<sup>th</sup> Marie Curie Cutting Edge inVENTS: biocompatibility evaluation and biological behaviour of polymeric biomaterials, 9<sup>th</sup> – 13<sup>rd</sup> October 2007, Alvor, Algarve (Portugal), Oral Presentation: "*Preparation and Characterization of Microfabricated Chitosan Scaffolds*"  
E. Carletti, T. Endogan, C. Migliaresi, A. Motta, D. Maniglio, V. Hasirci, N. Hasirci

## Acknowledgements

---

- 4<sup>th</sup> European Symposium on Biopolymers ESBP 2007, 2<sup>nd</sup> – 4<sup>th</sup> October 2007, Kusadasi (Turkey), Poster Presentation: *"Microfabrication of Chitosan and PLGA Scaffold for Tissue Engineering"*  
T. Endogan, E. Carletti, A. Motta, D. Maniglio, V. Hasirci, N. Hasirci, C. Migliaresi
- Expertissues Training Course: Cell-biomaterial Interfaces: from theory to practice, 17<sup>th</sup> -20<sup>th</sup> October 2006, Prague (Czech Republic), Poster Presentation: *"3D scaffold for tissue engineering produced by microfabrication technology: work in progress"*  
E. Carletti, D. Maniglio, C. Migliaresi

Finally, a special thank is for my lovely family, my parents Pietro and Editta and my sister Valentina for their precious support.



UNIVERSITY  
OF TRENTO - Italy

